UNIVERSITY OF CALIFORNIA, SAN DIEGO

Assembly and function of non-centrosomal microtubule arrays

A dissertation submitted in partial satisfaction of the
requirements for the degree
Doctor of Philosophy

in

Biomedical Sciences

by

Shaohe Wang

Committee in charge:

Professor Karen Oegema, Chair
Professor Timothy Bigby
Professor Andrew Chisholm
Professor Don Cleveland
Professor Arshad Desai

2014

The dissertation of Shaohe Wang is approved, and it is acceptable in quality and form for publication on microfilm and electronically:

_____

_____

_____

_____

_____

Chair

University of California, San Diego

2014

DEDICATION

To my parents Liangsan WANG and Mingyun LI.

To my dear wife Di WU.

EPIGRAPH

Life is not about waiting for the storm to pass,

it is about learning to dance in the rain.

TABLE OF CONTENTS

LIST OF ABBREVIATIONS

DMSO	Dimethyl sulfoxide
DNA	Deoxyribonucleic acid
dsRNA	Double-stranded RNA
GAP	GTPase activating protein
GDP	Guanosine 5'-diphosphate
GTP	Guanosine 5'-triphosphate
MosDEL	Mos1 transposon mediated deletion
MosSCI	Mos1 transposon mediated single copy insertion
MT	Microtubule
MTOC	Microtubule organizing centers
RNA	Ribonucleic acid
RNAi	RNA interferece
ts	Temperature sensitive
γ-TuRC	γ-Tubulin ring complex
γ-TuSC	γ-Tubulin small complex

LIST OF FIGURES

LIST OF TABLES

ACKNOWLEDGEMENTS

I would first like to thank my wife, Di, who has given me unconditional support throughout my years as a graduate student. We live on the opposite side of the earth, but we manage to video chat almost everyday. Her smile and voice are always the most precious reward for my little success and the best cure when I get frustrated.

I would also like to thank my advisor Karen, who is both a great scientist and a great mentor. I have been amazed and influenced by her curiosity, creativity and persistence. I admire her as a pure scientist who is curious about anything new and interesting, even if it has nothing to do with her own research. She is extremely helpful to provide brilliant ideas when I — and other members in the lab — get stuck. She is willing to tackle the most difficult problem as long as it is interesting. Most importantly, she is very good at pointing out my weakness and push me to do my best.

Arshad is a great co-mentor of mine. I think the OD lab members will all agree with me that Arshad knows everything. He has an amazing memory that allows him to know very well with all the literature in the field. He is undoubtedly an expert in microtubules, which is of great help to me. He is obsessed with microscopy and I have learned a whole lot from him.

I would like to thank my thesis committee members Andrew, Don and Tim. Andrew is a *C. elegans* genetist and developmental biologist who gave me many key

advices about both general project design and specific epidermis assays. Don and Tim also helped structure my major project and improve my data presentations.

I am so grateful to have Mark as my "scientific twin". We joined in the lab at the same time and quickly became buddies. We chat about science, about life and about everything. I would turn to Mark when I got another little complain about that background mutation, that hard-to-make transgene and that not-so-good presentation. He is also very good at pushing me to stay on top of things since I tend to procrastinate.

I would like to thank all OD lab members for all their great help. Specially, Becky taught me all the basics of *C. elegans*. Dhanya and Yao are the biochemists I bother all the time. Renat is the physicist in the lab who taught me to code with Python. Adina is such a sweet bay mate who always asks when I get a little sad.

Chapter 2, in part, is currently being prepared for submission for publication. Wang, Shaohe; Desai, Arshad; Oegema, Karen. The dissertation author was the primary investigator and author of this material.

Chapter 3, in part, is currently being prepared for submission for publication. Quintin, Sophie; Wang, Shaohe; Pontabry, Julien; Bender, Ambre; Oegema, Karen; Labouesse, Michel. The dissertation author was one of the primary investigators and the second author of this material.

VITA

2008 B. S. in Biological Sciences, Tsinghua University, Beijing, China

2014 Ph. D. in Biomedical Sciences, University of California, San Diego

PUBLICATIONS

Li, X., Jia, S., **Wang, S.**, Wang, Y., & Meng, A. (2009). Mta3-NuRD complex is a master regulator for initiation of primitive hematopoiesis in vertebrate embryos. *Blood*, 114(27), 546472.

Green, R., Kao, H.L., Audhya, A., Arur, S., Mayers, J., Fridolfsson, H., Schulman, M., Schloissnig, S., Niessen, S., Laband, K., **Wang, S.**, Starr, D., Hyman, A.A., Desai, A., Schedl, T., Gunsalus, K. C., Piano, F., & Oegema, K. (2011). A high-resolution *C. elegans* essential gene network based on phenotypic profiling of a complex tissue. *Cell*, 145(3), 47082.

Green, R., Mayers, J. R., **Wang, S.**, Lewellyn, L., Desai, A., Audhya, A., & Oegema, K. (2013). The midbody ring scaffolds the abscission machinery in the absence of midbody microtubules. *J. Cell Biol.*, 203(3), 50520.

ABSTRACT OF THE DISSERTATION

Assembly and function of non-centrosomal microtubule arrays

by

Shaohe Wang

Doctor of Philosophy in Biomedical Sciences

University of California, San Diego, 2014

Professor Karen Oegema, Chair

In contrast to the radial microtubule arrays organized by centrosomes in dividing cells, many differentiated cells assemble non-centrosomal microtubule arrays adapted for specific cellular functions, including nuclear positioning and migration, maintenance of tissue architecture and intracellular transportation. In an RNAi screen in *C. elegans*, we identified NOCA-1 as a novel protein that does not contribute to centrosome-driven embryonic cell divisions but is required to form microtubule arrays in the germline that are essential for organismal fertility. In this

dissertation, I focused on NOCA-1 to study the assembly mechanism and cellular function of non-centrosomal microtubule arrays.

The *noca-1* gene encodes 8 isoforms expressed in a variety of tissues. Two distinct long isoforms control assembly of microtubule arrays in the germline and embryonic epidermis, respectively. In contrast, a short isoform functions in parallel to the microtubule minus end-binding protein Patronin (PTRN-1) to control assembly of microtubule arrays in the post-embryonic epidermis. Evidence for the redundant activity of NOCA-1 and PTRN-1 includes synthetic lethality and early larval stage dye permeability of *noca-1*Δ*;ptrn-1*Δ double mutants, both of which are rescued by selectively expressing PTRN-1 in the post-embryonic epidermis. In support of the genetic interaction, NOCA-1 co-sediments with taxol-stabilized microtubules from worm lysates and purified recombinant NOCA-1, like PTRN-1, binds to microtubule ends in a microtubule-anchoring assay. We conclude that NOCA-1 represents a new class of microtubule end-binding proteins with essential functions of its own, as well as parallel functions with Patronin, in the assembly of non-centrosomal microtubule arrays in multiple *C. elegans* tissues.

Non-centrosomal microtubule arrays in embryonic epidermis contribute to elongation, the process that converts the oval-shaped embryo into an elongated worm. By using two different means of disrupting microtubules, we showed that disrupting microtubules alone does not affect elongation. However, when actomyosin contractility is compromised by a partial loss-of-function mutant of *let-502* (a Rho kinase), disrupting microtubules results in elongation arrests and causes

embryonic lethality. Intact microtubules and normal LET-502 activity are reqruied for E-cadherin clustering at adherens junctions and the maturation of hemidesmosomes, possibly explaining the elongation defects we observed. We conclude that microtubules in the embryonic epidermis contribute to elongation, but only is required when actomyosin contractility is reduced.

Chapter 1

Introduction

Microtubules (MTs) are conserved protein polymers that play many important roles in eukaryotic cells. The building blocks of MT polymers are heterodimers of α-tubulin and β-tubulin, both of which are highly conserved among all eukaryotes (Little *et al.*, 1981). Together with actin and intermediate filaments, MTs make up the cytoskeleton providing mechanical strength for the cell. MTs are often assembled into higher order arrays to fulfill their functions. In dividing cells, MTs are assembled by centrosomes into a dynamic array, known as the mitotic spindle, to segregate chromosomes and orient the division plane. In differentiated cells, MTs are assembled — usually independent of centrosomes — into relatively stable arrays to position nuclei and organelles, provide transportation tracks and also serve as primary structure components of cilia and flagella (Desai and Mitchison, 1997).

The non-centrosomal MT arrays in differentiated cells are the subjects of

this dissertation. Both the assembly mechanism and the cellular function of these arrays will be discussed. In this chapter, a general introduction of MTs and MT arrays is given. In the next chapter, I will focus on the study of NOCA-1, a novel MT end binding protein, to elucidate the assembly and function of non-centrosomal MT arrays in *C. elegans* tissues. The third chapter will be a case study on the function of epidermal non-centrosomal arrays during *C. elegans* embryonic elongation. In the last chapter, the major conclusions will be summarized and the implications and future directions will be discussed.

1.1 MT structure and properties

MTs are hollow tubes measured 25 nm in diameter (Desai and Mitchison, 1997). Inside a MT, α/β-tubulin dimers interact head-to-tail to form linear protofilaments, which interact laterally to get the tube structure (Figure 1.1). The majority of self-assembled MTs from purified tubulin have 14 protofilaments, while MTs in vivo and MTs nucleated from centrosomes and axonemes in vitro mostly have 13 protofilaments (Desai and Mitchison, 1997). In theory, adjacent protofilaments could interact laterally either through α-β monomer interactions (A-lattice) or through α-α and β-β monomer interactions (B-lattice). Ultrastructural analysis has established that MTs mainly adopt the B-lattice (Mandelkow *et al.*, 1986; Song and Mandelkow, 1993; Kikkawa *et al.*, 1994; Song and Mandelkow, 1995). In this conformation, at least one A-lattice seam has to be present to allow registration

of the protofilaments (Figure 1.1). The function of the A-lattice seam is currently unclear.

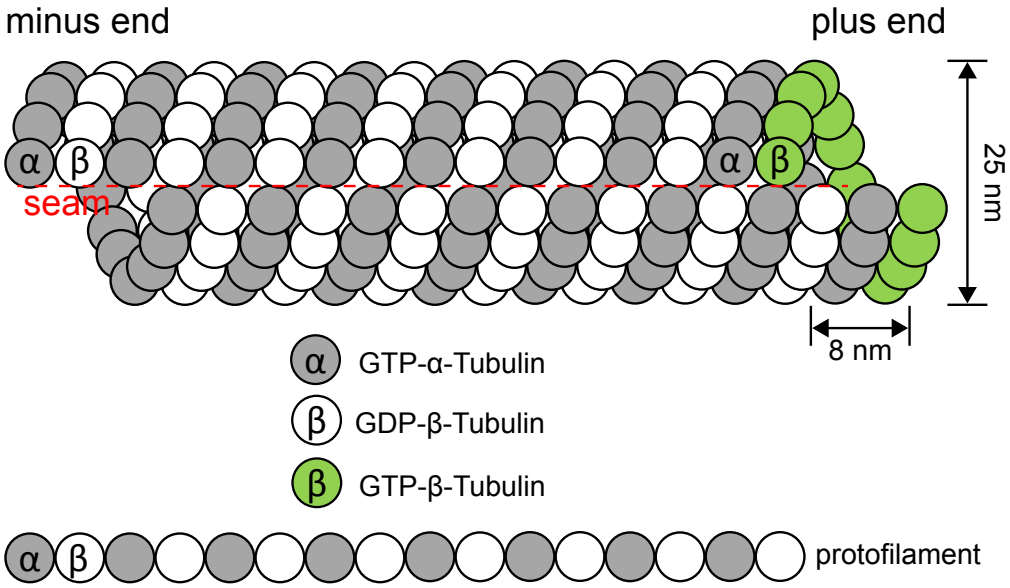

Figure 1.1: Microtubule structure.
Microtubules (MTs) are hollow tubes with an outer diameter of 25 nm. The building blocks of MTs are α/β-tubulin dimers, which interact head-to-tail to form protofilaments. 10-15 protofilaments interact laterally to form a closed tube. Shown here is a MT containing 13 protofilaments. Due to the head-to-tail interaction of α/β-tubulin dimers, MT has intrinsic polarity with α-tubulins exposed at the minus ends and β-tubulins exposed at the plus ends. Both α-tubulin and β-tubulin bind to GTP, but only the β-tubulin bound GTP can exchange with free GTP in solution. During polymerization, the β-tubulin bound GTP hydrolyzes to be GDP. Thus, most β-tubulins in the MT lattice is GDP bound. However, a very thin layer (<100 subunits) of GTP bound β-tubulin is present at the plus ends (Desai and Mitchison, 1997). This GTP cap is thought to stabilize MTs.

MTs are physically very stiff. The persistence length quantifies the polymer stiffness and gets larger as a polymer gets more stiff. For a MT, the persistence length is as large as 5200 μm, meaning that MTs are rigid over cellular dimensions (Gittes *et al.*, 1993). This property is well suited for the MT function of providing mechanical strength for cells. For comparison, the persistence length of an actin

filament is only ∼17.7 μm (Gittes *et al.*, 1993).

MTs are dynamic polymers. Early cytologists appreciated the dynamics of MTs when they noticed that organizations of the "spindle fibres" or "aster rays" change rapidly over time (Desai and Mitchison, 1997). Later, the components of MTs — α/β-tubulin dimers — were purified based on its affinity with colchicine, a drug that inhibits mitosis (Weisenberg *et al.*, 1968). The same work also showed that each tubulin dimer co-purify with two GTP molecules, one of which exchanges rapidly with free GTP in solution. Further studies showed that the β-tubulin bound GTP hydrolyzes during MT polymerization (Weisenberg *et al.*, 1976). In 1984, Mitchison and Kirshner made the interesting observation that individual MT ends could switch between polymerization and depolymerization, a non-equilibrium state they termed as "dynamic instability" (Mitchison and Kirschner, 1984). This unique property of the MTs allows rapid remodeling of the MT arrays and faster exploration of cellular space (Holy and Leibler, 1994).

MTs are intrinsically polarized. All protofilaments in the same MT are orientated in the same direction, so that the two ends of MTs are exposed with either α- or β-tubulins, termed as minus and plus ends respectively (Figure 1.1). Different chemical properties of the two ends result in different behaviors including different rates of polymerization and depolymerization: plus ends always grow faster than minus ends under the same condition. In vitro, both ends exhibit dynamic instability; e.g. they can grow, shrink and switch between the two states, although the rates and transition frequencies are slightly different. In vivo, however, plus

ends become dramatically more dynamic while the minus ends are mostly stabilized. In cells or cell extracts, the growth rate of plus ends is 5 to 60 fold higher than that of pure tubulin at a similar concentration (from $\sim$1 μm/min in vitro, to 5–60 μm/min in various cells; Desai and Mitchison, 1997; Srayko *et al.*, 2005; Zanic *et al.*, 2013). The catastrophe frequency of plus ends also goes up 20–30 fold from in vitro to in vivo (Simon *et al.*, 1992; Zanic *et al.*, 2013). In contrast, the minus ends in cells almost never polymerize; they are either stable or quickly depolymerize (Dammermann *et al.*, 2003). Thus, the plus and minus ends of MTs seem to be specialized for distinct functions in living cells.

MTs are nucleated polymers. De novo MT formation from purified tubulin has to go through a kinetically slow process to form a nucleus, which then allows relatively fast growth of the polymer. The nucleus of spontaneously nucleated MTs likely has 10-14 tubulin dimers (Fygenson and Flyvbjerg, 1995). The kinetic barrier of MT nucleation is a perfect handle for the cells to control where and when MTs are generated. The key regulator of MT nucleation is γ-tubulin, which was discovered by Oakley and Oakley (1989) in a study of genetic suppressors of heat-sensitive β-tubulin mutant in *Aspergillus nidulans* (Oakley and Morris, 1981; Oakley and Oakley, 1989). In all studied examples, γ-tubulin localizes to the MT nucleation structures, such as centrosomes in dividing cells and apical surface of epithelial cells (Figure 1.2C and D). Perturbation of γ-tubulin invariably inhibits MT nucleation (Hannak *et al.*, 2002; Green *et al.*, 2011). Purified γ-tubulin-containing protein complexes (γTuRC, γ-Tubulin Ring Complex; Fig-

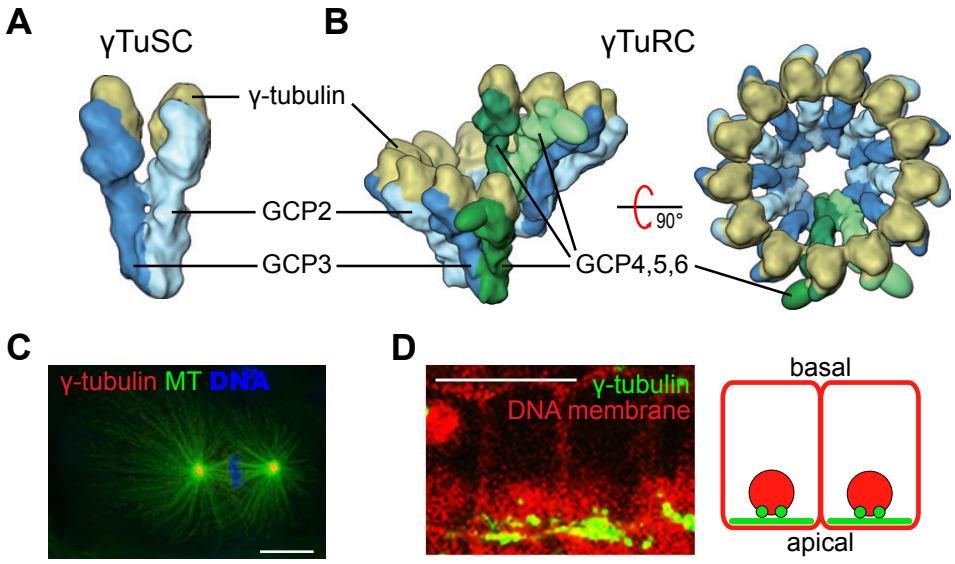

Figure 1.2: MT nuleation is mediated by γTuRC.
(A) Diagram of the γTuSC, a Y-shaped complex composed of γ-tubulin, GCP2 and GCP3.
(B) Diagram of the γTuRC, a ring-shaped complex composed of several γTuSC and γTuSC-like complex.
(C) Immunofluorescence image of the first division of *C. elegans* embryo at metaphase stage. Note that γ-tubulin localizes to the centrosomes, where MTs are focused at. Scale bar: 10μm.
(D) Left: spinning disk confocal image of the E16 primordium (intestine epithelial cells) in a developing *C. elegans* embryo expressing histone::mCherry and membrane::mCherry. Right: diagram of the epithelial cells. Note that γ-tubulin loclaizes to the apical surface. Scale bar: 10μm.
Images in (A) and (B) are from Figure 5 of Kollman *et al.* (2011) with modifications; immunofluorescence image in (C) is courtesy of Valeria Viscardi, a former postdoc from our lab; image in (D) is from Figure 1 of Feldman and Priess (2012) with modifications.

ure 1.2B) from both *Xenopus* egg extracts and *Drosophila* embryo extracts can stimulate MT nucleation in vitro (Zheng *et al.*, 1995; Oegema *et al.*, 1999). The γTuRC is composed of γTuSC, a more tightly bound γ-tubulin small complex (Figure 1.2A; Oegema *et al.*, 1999). Recently, the cryoEM structure of the budding yeast γTuSC revealed a 13-fold symmetry that resembles the 13-protofiliment MTs, suggesting a templating model for MT nucleation (Kollman *et al.*, 2010).

1.2 Centrosomal MT arrays

Centrosomes are organelles thought to be the primary microtubule organizing centers (MTOC; Figure 1.3A) in animal cells. Each centrosome has two perpendicularly orientated centrioles surrounded by a protein matrix called pericentriolar material (PCM), which contains γTuRC, thus the MT nucleation activity. Centrioles are short cylindrical structures with 9-fold symmetry, containing 9 triplet, doublet or singlet MTs depending on species (Bettencourt-Dias and Glover, 2007). In addition to their role of recruiting PCM in centrosomes, centrioles can become basal bodies that direct cilia and flagella formation. For more information on the biogenesis and function of centrosomes, see Bettencourt-Dias and Glover (2007) for a review.

Centrosome-based radial MT array formation illustrates the importance of localized MT nucleation and minus end anchoring. During cell divisions, numerous MTs are nucleated from centrosomes, forming radial MT arrays with minus ends

anchored at the vicinity of centrosomes and plus ends towards the cell cortex and chromosomes. The two centrosome-based arrays together form the bi-polar spindle which segregates the chromosomes and positions the division plane. During interphase, there is only one radial MT array centered at the centrosome that is usually adjacent to the nuclear envelope. Besides, centrosome-based radial MT arrays are also present in migratory differentiated cells such as neutrophils (Bartolini and Gundersen, 2006).

Localized MT nucleation requires centrosome recruitment of the MT nucleator γ-TuRC. A number of proteins have been implicated in the γ-TuRC recruitment. Depletion of the PCM matrix protein pericentrin in mammalian cells or mutating the PCM matrix protein SPD-5 in *C.elegans* both abolish the centrosomal localization of γ-tubulin (Hamill *et al.*, 2002; Takahashi *et al.*, 2002; Zimmerman *et al.*, 2004b). In the case of pericentrin, it appears to recruit γ-tubulin through interactions with the γ-TuSC components GCP2 and GCP3 (note that kendrin is pericentrin; Takahashi *et al.*, 2002; Flory and Davis, 2003; Zimmerman *et al.*, 2004b). Other centrosomal proteins including CG-NAP and CP309 may act in a similar way as pericentrin (Takahashi *et al.*, 2002; Kawaguchi and Zheng, 2004). GCP-WD/NEDD1, on the other hand, appears to recruit the γ-TuRC through a direct interaction with γ-tubulin (Haren *et al.*, 2006; Lüders *et al.*, 2006; Manning *et al.*, 2010). In fact, GCP-WD/NEDD1 was considered to be a γ-TuRC component that mediates its interaction with the centrosome (Lüders *et al.*, 2006). Ninein is thought to recruit γ-TuRC to the centrosome through interaction between its

N-terminal domain and γ-tubulin (Delgehyr *et al.*, 2005; Mogensen *et al.*, 2000). Another player in recruiting γ-TuRC to the centrosome is mto1p in fission yeast and its related protein centrosomin in *Drosophila*. Both mto1p and centrosomin are required for γ-tubulin localization to the spindle pole body (the yeast equivalent of centrosome) or centrosome and both proteins can pull down γ-tubulin (Megraw *et al.*, 1999; Terada *et al.*, 2003; Sawin *et al.*, 2004).

It is less clear that how MT minus ends are anchored to the centrosomes. The MT nucleation complex γ-TuRC is able to cap the minus ends and block polymerization (Zheng *et al.*, 1995), making it a good candidate for capping the minus ends at the centrosome. However, nucleation and anchoring of MTs at the centrosomes seem to be independent of each other (Dammermann *et al.*, 2003). In mouse fibroblast cells, both mother and daughter centrioles have similar nucleating activity, but MTs are focused specifically at the mother centrioles where ninein preferentially localizes to (Mogensen *et al.*, 2000). Expressing the ninein C-terminus removes endogenous ninein and the γ-TuRC from the centrosome and causes defects in MT anchoring (Delgehyr *et al.*, 2005). Although proposed to be a MT anchoring protein, ninein has not been shown to directly cap the MT minus ends. MT anchoring to the centrosomes also requires dynein/dynactin activity, Cep135, PCM-1 and EB1, although these requirements could be indirect (Quintyne *et al.*, 1999; Askham and Vaughan, 2002; Dammermann and Merdes, 2002; Ohta *et al.*, 2002; Kim *et al.*, 2004; Guo *et al.*, 2006).

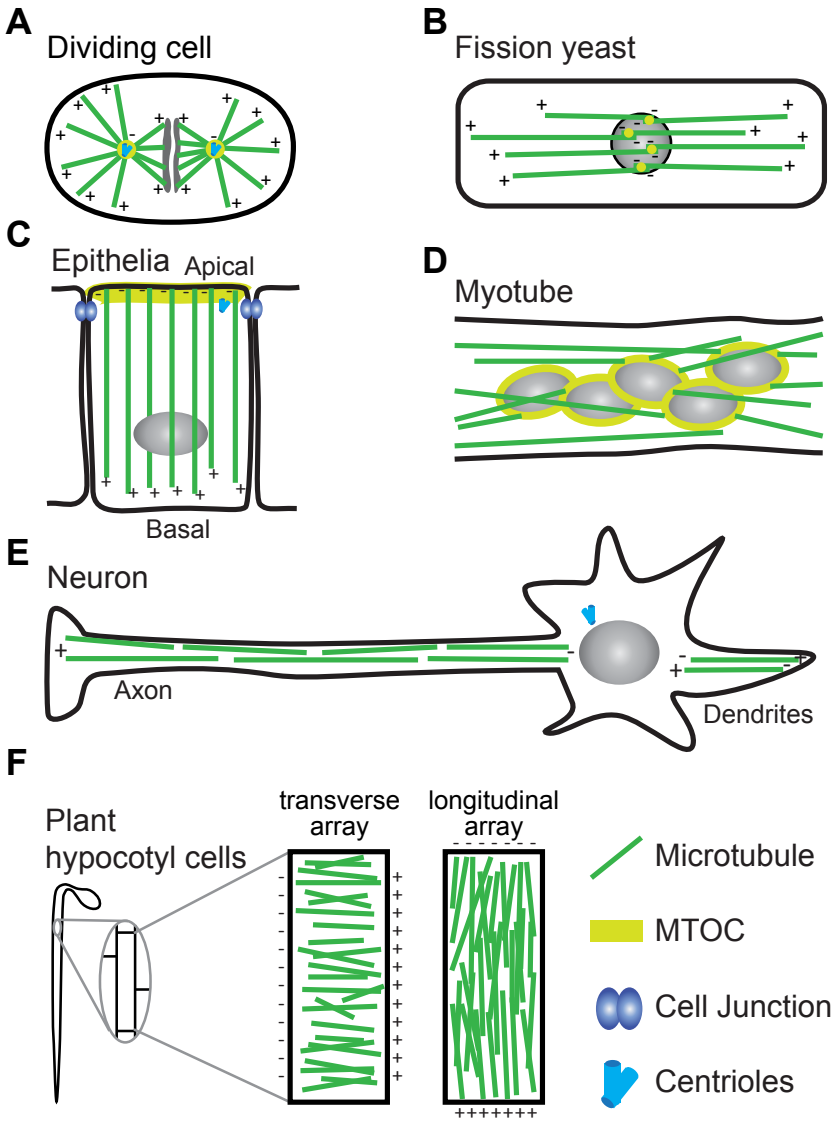

Figure 1.3: MT arrays in dividing and differentiated cells.
Note that the centrosome organized MT array in dividing cell (A) is radial, while non-centrosomal MT arrays are linear (B-F).

1.3 Non-centrosomal MT arrays

Non-centrosomal MT arrays in dividing cells and cilia/flagella are not discussed here. In dividing cells, non-centrosomal arrays contribute to spindle formation in both meiosis and mitosis. Female meiosis in animal cells relies solely on centrosome-independent mechanisms to organize the meiotic spindle (Bartolini and Gundersen, 2006). Plant cells have no centrosomes, thus, the mitotic spindle has to be organized independent of centrosomes. Even mitosis in some animal cells can occur rather normally in the absence of centrosomes (Khodjakov *et al.*, 2000; Bonaccorsi *et al.*, 2000; Megraw *et al.*, 2001; Basto *et al.*, 2006; Mahoney *et al.*, 2006). For mechanisms concerning centrosome-independent organization of radial MT arrays, readers are directed to Meunier and Vernos (2012) for a review. Non-centrosomal MT arrays in cilia and flagella are special cases since they depend on the centriole-like organelles termed as basal bodies (Bartolini and Gundersen, 2006). For more information on cilia and flagella, see Jana *et al.* (2014) for a review.

This dissertation focuses on the linear non-centrosomal MT arrays in non-dividing cells. In fission yeast and differentiated animal cells such as epithelial cells, neurons and myotubes, MT arrays are parallel and orientated along the polarity axis (Figure 1.3B-E). In plant cells, the cortical MT arrays could be orientated either transversely or longitudinally at the cell surface (Figure 1.3F; Dixit *et al.*, 2006). All of these non-centrosomal arrays are linear and not focused at the cen-

trosomes (Figure 1.3; Bartolini and Gundersen, 2006).

1.3.1 MT polarity in non-centrosomal arrays

Two different assays have been used to determine the MT polarity in non-centrosomal arrays. Early studies in various epithelial cells and neurons employed the classic hook decoration assay (Heidemann and McIntosh, 1980). In this assay, exogenous tubulins were polymerized from existing MT walls, forming one or several curved tubulin sheets. Cross sections of such preparations were then examined using EM, where clockwise decorated hook indicates plus end toward the observer and counterclockwise indicates minus (Heidemann and McIntosh, 1980).

Later studies capitalized on live cell imaging of fluorescence labeled EB1 (End Binding protein 1) family proteins to determine the MT polarity. EB1 proteins specifically track the growing MT ends in vitro, but do not distinguish plus and minus ends (Akhmanova and Steinmetz, 2008). Interpretations of EB1 tracking the growing *plus* ends in vivo largely came back to the early observations that MT minus ends do not polymerize in cells (Dammermann *et al.*, 2003). In those studies, the polarities of free MT ends were determined by either comparing the dynamic behavior of ends with centrosome-emitting MT plus ends (Yvon and Wadsworth, 1997), or simple assumption that the more dynamic ends are plus ends (Waterman-Storer and Salmon, 1997; Vorobjev *et al.*, 1997). Thus, care should be taken when claiming MT polarity in a certain cell type. Nevertheless, EB1 based imaging results were consistent with established knowledge of MT polarity in both

centrosomes and differentiated cells, justifying their use to determine MT polarity (Stepanova *et al.*, 2003; Srayko *et al.*, 2005).

The interphase MT arrays in fission yeast run along the long axis of cells. Each cell has 3 to 5 MT bundles, where MTs in each bundle are thought to be antiparallel and have their plus ends toward the cell tip (Figure 1.3B Drummond and Cross, 2000; Tran *et al.*, 2001). The two ends of MT bundles were both thought to be plus ends because they both have comparable growth and shrinkage rates with plus ends dynamics in vitro and in some cells (Drummond and Cross, 2000; Tran *et al.*, 2001). Consistent with this proposed MT organization, the cell tips have enriched localization of Tip1p, a CLIP170-like protein thought to localize at the MT plus ends (Brunner and Nurse, 2000; Akhmanova and Steinmetz, 2010).

Epithelial cells generally have parallel MT arrays along the apicobasal axis, where minus ends point to the apical surface (Figure 1.3C). A range of epithelial cells, including fish retinal pigment epithelial cells (Troutt and Burnside, 1988), canine kidney epithelial cells MDCK (Bacallao *et al.*, 1989), *Drosophila* wing epidermis (Mogensen *et al.*, 1989), Sertoli cells in rat testis (Redenbach and Vogl, 1991) and human intestine epithelial cells Caco-2 (Meads and Schroer, 1995), have been examined using the hook decoration method and in all cases the MT minus ends are uniformly orientated towards the apical side. However, exceptions do exist. In the dorsal epidermis of developing *C. elegans* embryos, MTs are not oriented along the apicobasal axis, but rather along the long axis of cells with plus ends towards the same direction of nuclear migration, as indicated by live imaging

of EB1-GFP (Figure 1.3; Fridolfsson and Starr, 2010).

Defferentiated myotubes have linear MT arrays along the major cell axis (Figure 1.3D). It is generally assumed that minus ends are close to the nuclear envelope where the MT nucleation factors are localized (Tassin *et al.*, 1985). A study used EB1 imaging to show that the MTs in the myotubes are antiparallel (Pizon *et al.*, 2005).

Neurons have linear non-centrosomal MT arrays in their axons and dendrites (Figure 1.3E). A typical neuron has one long process called the axon and several short processes called dendrites. In vertebrate neurons, hook decoration assays have shown that most MTs in axons have their minus ends towards the cell body, while MTs in dendrites have mixed polarities (Burton and Paige, 1981; Heidemann *et al.*, 1981; Baas *et al.*, 1987, 1988; Troutt and Burnside, 1988). There is some difference in invertebrate neurons. Using EB1 based imaging, it was shown that MTs in the axons of *Drosophila* neurons have similar MT polarity as in vertebrates. However, MTs in the dendrites of *Drosophila* neurons have a rather uniform polarity with their plus ends towards the cell body, unlike the mixed polarity described in vertebrate neurons (Stone *et al.*, 2008).

The cortical MT arrays in plant hypocotyl cells can be oriented either transversely or longitudinally (Figure 1.3F Yuan *et al.*, 1994; Sugimoto *et al.*, 2000; Ehrhardt and Shaw, 2006). Fast growing cells have transversely oriented cortical arrays, which transition to be longitudinally oriented when cells stop growing (Sugimoto *et al.*, 2000; Ehrhardt and Shaw, 2006). In both types of arrays, MTs

are mostly oriented in the same direction as visualized by low-level expressed EB1-GFP (Dixit *et al.*, 2006).

1.3.2 Function of non-centrosomal MT arrays

Non-centrosomal MT arrays are important for nuclear positioning and tissue maintenance in several cell types. In fission yeast, the nuclei are positioned by pushing force generated by MT polymerization (Tran *et al.*, 2001). In the multinuclear fungus *Aspergillus nidulans*, mutants in the MT motor protein dynein caused severe nuclear positioning defects, indicating a role of MT arrays in these cells (Xiang *et al.*, 1994). In the syncytial germline of *C. elegans*, the nuclei are normally kept in their membrane compartments through interactions with MTs (Zhou *et al.*, 2009). Disrupting MT itself or the nucleus-MT linkage in *C. elegans* germline causes nuclear mis-positioning, which leads to complete sterility due to a catastrophic disruption of the tissue architecture featured by multi-nucleation and vesiculation (Zhou *et al.*, 2009; Green *et al.*, 2011). It appears that syncytial tissues are more susceptible to nuclei positioning defects, since mis-positioned nuclei in syncytial tissues have more potential to disrupt the overall tissue architecture.

Non-centrosomal MT arrays help establish or maintain the cellular polarity. In fission yeast, mutants of MT regulators bend or have irregular cell shape with additional growth point besides the two cell tips (reviewed in Hagan, 1998; Chang, 2001). Mutation of a kinesin-like protein Tea2p mislocalized a tip marker Tea1p, suggesting that MT based transportation may accumulate specific proteins to the

cell tip (Browning *et al.*, 2000; Mata and Nurse, 1997).

Non-centrosomal MT arrays commonly serve as transportation tracks. In epithelial cells, both plus end and minus end directed motors are implicated in apical transport, while only plus end directed kinesins are implicated in basolateral transport (Lafont *et al.*, 1994; Tai *et al.*, 1999; Noda *et al.*, 2001; Jaulin *et al.*, 2007). It appears that MTs are mainly facilitating rather than specifying the transport, since disrupting MTs reduces transportation efficiency but does not cause missorting for at least some cargoes (Grindstaff *et al.*, 1998). In neurons, specific proteins are transported between the cell body and processes (axons and dendrites). The long distance makes axonal transport rather challenging, but cells manage to use MT motors kinesins and cytoplasmic dynein to move cargoes away from or towards the cell bodies (reviewd in Hirokawa and Takemura, 2005). In differentiating muscle cells, MTs are required for transporting sarcomeric myosin, a major protein component of sarcomeres (Pizon *et al.*, 2005). In plant cells, MTs direct the deposition of cellulose microfibrils in the cell wall. Early observation that the organization of cellulose microfibrils was sensitive to colchicine led to the proposal that mitotic spindle is involved, since colchicine was best known to disrupt the spindle (Green, 1962). Soon after, the cortical MT arrays were described and these arrays were shown to co-align with the cellulose microfibrils in adjacent cell walls, suggesting that the cortical MT arrays are more likely to direct cellulose synthesis (Ledbetter, 1963). More recently, a functional YFP (Yellow Fluorescent Protein) fused cellulose synthase in *Arabidopsis* was visualized to move

along the cortical MT tracks, indicating a relatively direct mechanism of MTs guiding cellulose synthesis in the cell wall (Paredez *et al.*, 2006).

1.3.3 Array assembly: generating MTs

In order to assemble non-centrosomal arrays, MTs need to be first generated by either γ-TuRC-dependent MT nucleation, or by MT severing enzymes (discussed below), and then be stabilized and/or anchored to certain cellular structures. As in centrosomal MT arrays, localized MT nulceation and minus end anchoring seem to be the key aspects of assembly mechanism.

In cells containing non-centrosomal MT arrays, the MT nucleating complex γ-TuC (γ-Tubulin Complex) is usually localized to non-centrosomal structures, but in many cases it is unclear how γ-tubulin get localized.

In fission yeast, γ-TuC localizes to three different MTOCs at different time of the cell cycle. During mitosis, γ-TuC localizes to the spindle pole body (SPB; the fission yeast equivalent of centrosomes) that organizes the mitotic spindle (reviewed in Hagan, 1998). From anaphase, an equitorial MTOC (eMTOC) was assembled at the cell equator and disassembled after cytokinesis (Heitz *et al.*, 2001). During interphase, γ-TuC are concentrated at several perinuclear dots that contain the MT nucleating activity (Tran *et al.*, 2001). One of these dots is the SPB and others are termed as iMTOCs (interphase MTOCs). A centrosomin related protein mto1p and its partner mto2p form a complex which recruits the γ-tubulin complex to iMTOCs (Sawin *et al.*, 2004; Venkatram *et al.*, 2004; Samejima *et al.*, 2008).

Besides, a J domain containing protein rsp1p interacts with the chaperon hsp70 and regulates the eMTOC disassembly (Zimmerman *et al.*, 2004a).

In epithelial cells, γ-tubulin localizes to the apical surface in many cases, but the fate of centrosomes differ by cell types. In mammalian epithelial cell lines Caco-2 (intestine) and WIF-B (hepatocyte), both centorsomal and non-centrosomal γ-tubulin can be detected by immunofluorescence, but MDCK (kidney) cells appear to have only centrosomal γ-tubulin staining (Meads and Schroer, 1995). In developing organisms, however, γ-tubulin and the MT nucleation activity are frequently released from centrosomes and re-localize to the apical surface (Jankovics and Brunner, 2006; Brodu *et al.*, 2010; Fridolfsson and Starr, 2010; Feldman and Priess, 2012). In *Drosophila* tracheal cells, the γ-TuRC first releases from the centriole in a spastin (a MT severing enzyme, see below) dependent manner, then gets anchored to the apical surface through a transmembrane protein Piopio (Brodu *et al.*, 2010). However, it is worth pointing out that Piopio is an extracellular matrix protein, whose majority is outside in the lumen (Bökel *et al.*, 2005). Whether the short cytoplasmic tail of Piopio acts directly to recruit γ-TuRC remains unclear. In developing *C. elegans* intestine, a direct hand-off of γ-TuRC from the centrosomes to the apical surface was observed and this hand-off depends on cenrosome itself and the polarity protein PAR-3 (Feldman and Priess, 2012). Interestingly, the PCM proteins TAC-1 and AIR-1, but not the PCM matrix protein SPD-5, also become enriched at the apical surface during differentiation (Feldman and Priess, 2012).

In myotubes, the MT nucleation activity re-distribute to the entire nuclear envelope from centrosomes during differentiation (Tassin *et al.*, 1985), but it is unclear how this relocalization occurs.

In neurons, γ-tubulin was reported to localize only to the centrosomes and not capping the MT minus ends in axons and dendrites (Baas and Joshi, 1992). Based on this observation, MTs were proposed to be nucleated from the centrosomes and then transported. There were some debates on whether MT polymers or tubulin subunits are transported (Baas and Brown, 1997; Hirokawa *et al.*, 1997; Terada *et al.*, 2000). Regardless of the transport, accumulating evidence argues against centrosomes as the MT nucleating structure in neurons. First, flies that lose centrioles during development have a generally normal nervous system (Basto *et al.*, 2006). Second, centosomes in rodent hippocampal neurons lose their MT nucleation activity during development and axons still grow upon laser ablation of centrosomes (Stiess *et al.*, 2010). Recently, the Golgi outposts in *Drosophila* dendritic arborization neurons are found to contain γ-tubulin and CP309 and directly nucleate MTs (Ori-McKenney *et al.*, 2012).

In plant cells, γ-tubulin is involved in both the establishment and remodeling of cortical MT arrays. During initiation of cortical MT arrays in both tobacco BY-2 cells and plant hypocotyl cells, the γ-TuRC localizes to random dots at the cortex to nucleate MTs (Lindeboom *et al.*, 2013a). However, not all of the new MTs are marked with a GFP fused γ-TuRC marker, suggesting there may be a γ-TuRC independent way to generate MTs (Lindeboom *et al.*, 2013a). Another

study on tobacco BY-2 cells shows that γ-tubulin is recruited to existing MT lattice to nucleate more MTs (Murata *et al.*, 2005). A MT based MT nucleation was also demonstrated during *Drosophila* spindle formation, where an Augmin complex recruits the γ-TuRC to existing MTs and nucleates new MTs, much like the Arp2/3 complex for actin filements (Goshima *et al.*, 2008). During the reorientation of cortical MT arrays from transverse to longitudinal arrays (Figure 1.3F), recruitment of γ-TuRC to existing MTs nucleate MTs at a certain angle, which appears to initiate the reorientation process (Lindeboom *et al.*, 2013b).

MT severing is another way of generating MTs. Katanin, spastin and fidgetin are the three described MT severing enzymes, all of which are members of the AAA ATPase (reviewed in Roll-Mecak and McNally, 2010). The *Drosophila* spastin has been crystallized and the structure work combined with light and X-ray scattering in solution suggested an intriguing model that the spastin hexamer pulls off the tubulin tail to disassemble tubulin subunits (Roll-Mecak and Vale, 2008). In vivo, MT severing has been involved in generating short MTs for meiotic spindle in *C. elegans*, depolymerizing MTs from both ends during mitosis in *Drosophila* S2 cells, debranching branched MTs in cortical MT arrays in *Arabidopsis*, assembling and disassembling cilia and flagella and generating MTs for axon elongation and branching (reviewed in Roll-Mecak and McNally, 2010).

MT severing plays an important role in non-centrosomal MT array formation, presumably by generating more MTs by exposing more MT ends. Spastin was identified as the most mutated gene in a neurodegenerative disease hereditary

spastic paraplegia (Hazan *et al.*, 1999). Like its family member Katanin, purified spastin can sever and disassemble MTs (Roll-Mecak and Vale, 2005). When overexpressed in tissue culture cells or in vivo, spastin indeed disassembles MTs (Errico *et al.*, 2002; Sherwood *et al.*, 2004; Trotta *et al.*, 2004). This MT disassembly function of spastin puzzled some researchers when they observed that spastin null mutant flies have fewer MT bundles in the axons at neuromuscular junctions (Sherwood *et al.*, 2004), making them to propose that spastin may sever MTs generated in the cell body to facilitate their transport. Meanwhile, Trotta *et al.* (2004) proposed that spastin positively regulate synapse formation by promoting MT dynamics. Interestingly, katanin seems to increase the MT density by making short MTs in *C. elegans* meiotic spindle (McNally *et al.*, 2006). A parallel hypothesis was then generalized to explain the less dense MTs observed in neuron processes (Roll-Mecak and Vale, 2006). A recent study in plant cortical MT array re-orientation elegantly illustrated this idea. The re-orientation is a rapid process when plant cortical arrays transiton from being transverse to longitudinal (Figure 1.3F). During this process, katanin is recruited to the MT crossover points, where newly growing MTs cross with existing ones, and selectively cut the new MTs to generate more plus ends growing in the same direction as new ones (Lindeboom *et al.*, 2013b). This katanin-mediated severing contributes to the majority of newly formed longitudinal MTs (Lindeboom *et al.*, 2013b), explaining the re-orientation defects in katanin mutants.

1.3.4 Array assembly: stabilizing and anchoring MTs

In order to form functional MT arrays, newly formed MTs need to be stabilized and anchored to certain structures. Ninein and the newly identified CAMSAP protein family are implicated in MT anchoring.

Ninein was shown to anchor MTs to both centrosomal and non-centrosomal sites in mammalian cells (Mogensen *et al.*, 2000; Delgehyr *et al.*, 2005). Ninein appears to be conserved in vertebrates and absent from invertebrates. In mouse fibroblast cells, both mother and daughter centrioles in the centrosomes can nucleate MTs, but ninein preferentially localizes to the mother centrioles, where MTs are anchored at (Mogensen *et al.*, 2000). In mouse inner ear epithelial cells (cochlear cells), ninein localizes to both centrosomes and the apical surface, where MTs are anchored at (Mogensen *et al.*, 2000). In fact, During inner ear epithelial development, cytoplasmic ninein became localized to the non-centrosomal apical sites (Moss *et al.*, 2007). In cultured epithelial cells, endogenous ninein localizes to both centrosomes and cytoplasmic speckles (Moss *et al.*, 2007). The ninein speckles frequently co-localize with MTs and are found to move along the MTs (Moss *et al.*, 2007). Interestingly, ninein localizes to the cell junctions in living mouse epidermis and this junction localization depends on desmoplakin (Lechler and Fuchs, 2007). It is worth noting though, that ninein has not been biochemically characterized, so we still don't know whether it is a bona fide MT anchoring protein.

CAMSAPs are a new family of proteins that can cap and stabilize the MT

minus ends. This protein family is highly conserved among all eumetazoa,i.e. animals with differentiated tissues (Baines *et al.*, 2009). Invertebrates only have one CAMSAP, while vertebrates have three CAMSAPs in each species (Baines *et al.*, 2009). All CAMSAPs have a conserved CKK domain at the C-terminus that mediates the MT interaction (Baines *et al.*, 2009). Nezha/CAMSAP3 was first identified as a MT minus-end binding protein that tethers MTs to the zonula adherens in cultured epithelial cells through an interaction between Nezha and PLEKHA7 (Meng *et al.*, 2008). Later, the Drosophila homologue of CAMSAPs, Patronin, was shown in vitro to directly bind to and protect the MT minus ends from being depolymerized by kinesin-13 (Goodwin and Vale, 2010). The mammalian CAMSAPs were recently characterized in vitro, and some unique properties of them were identified (discussed below; Jiang *et al.*, 2014; Hendershott and Vale, 2014).

There are some interesting differences among the CAMSAPs and Patronin (Jiang *et al.*, 2014; Hendershott and Vale, 2014). First, CAMSAPs and *Dorsophila* Patronin affect the minus end dynamics differently. Binding of CAMSAP2, CAMSAP3 and Patronin dramatically slows down the minus end polymerization rate and stabilize the ends from being depolymerization by either kinesin-13 or breakage (Goodwin and Vale, 2010; Jiang *et al.*, 2014; Hendershott and Vale, 2014), but CAMSAP1 does not affect the minus end polymerization and does not confer stability (Jiang *et al.*, 2014). Second, CAMSAP2 and CAMSAP3 decorate a short MT stretch as they track the growing minus ends, while CAMSAP1 and Patronin only bind to the ends without forming stretches (Jiang *et al.*, 2014; Hendershott

and Vale, 2014). Third, CAMSAPs and Patronin use different domains to achieve minus end binding. CAMSAPs use their CKK domain for minus end binding, while an additional MBD domain in CAMSAP2 and CAMSAP3 is reqruied for MT stabilization. In contrast, Patronin uses a different domain containing the coiled coil region for minus end binding and its CKK domain for MT stabilization (Jiang *et al.*, 2014; Hendershott and Vale, 2014). Overall, the minus end regulation appears to be more complicated than simple capping and stabilization.

In vivo, CAMSAPs regulate non-centrosomal MTs that are involved in mitosis, cell polarity, cell migration and neurite growth. In *Drosophila* S2 cells, Patronin inhibition causes a short spindle phenotype (originally Patronin was named Ssp4 for short spindle 4; Goshima *et al.*, 2007). Patronin also has a role in *Drosophila* embryonic mitosis to switch from poleward flux to anaphase B elongation (Wang *et al.*, 2013). Depletion of CAMSAP2 from cultured epithelial cells leads to a Golgi reorientation defect indicative of polarity defects and reduces the cell migration ability in a monolayer wound healing assay (Jiang *et al.*, 2014). Recently, CAMSAPs are shown to regulate neurite growth. In both cultured neurons and rat primary neurons, CAMSAP1 is required for neurite growth and the binding of its CC1 region with spectrin is important (King *et al.*, 2014). In the nematode *C. elegans*, the CAMSAP homologue PTRN-1 localizes to punctates along the neurites and *ptrn-1* mutant worms have abnormal neurite morphology (Marcette *et al.*, 2014; Richardson *et al.*, 2014).

Chapter 2

NOCA-1 and PTRN-1 control non-centrosomal MT array assembly in *C. elegans* tissues

2.1 Summary

In contrast to the centrosomal microtubule arrays in dividing cells, many differentiated cells assemble non-centrosomal microtubule arrays adapted for specific cellular functions. From an RNAi screen in *C. elegans*, we identified NOCA-1 as a novel protein that does not contribute to centrosome-driven embryonic cell divisions but is required to form microtubule arrays in the germline that are essential for organismal fertility. The *noca-1* gene encodes 8 isoforms expressed in a variety of tissues. Two distinct long isoforms control assembly of microtubule

arrays in the germline and embryonic epidermis, respectively. In contrast, a short isoform functions in parallel to the microtubule minus end-binding protein Patronin (PTRN-1) to control assembly of microtubule arrays in the post-embryonic epidermis. Evidence for the redundant activity of NOCA-1 and PTRN-1 includes synthetic lethality and early larval stage dye permeability of *noca-1*Δ*;ptrn-1*Δ double mutants, both of which are rescued by selectively expressing PTRN-1 in the post-embryonic epidermis. In support of the genetic interaction, NOCA-1 co-sediments with taxol-stabilized microtubules from worm lysates and purified recombinant NOCA-1, like PTRN-1, binds to microtubule ends in a microtubule-anchoring assay. Live imaging of the epidermal syncytium where NOCA-1 and PTRN-1 function redundantly revealed an array of evenly spaced microtubule bundles that run circumferentially around the animal. This array, comprised of both stable and dynamic microtubules, is subtly affected in single *noca-1*Δ and *ptrn-1*Δ mutants but nearly completely eliminated in *noca-1*Δ*;ptrn-1*Δ worms, suggesting that this specialized non-centrosomal array supports epidermal integrity during animal growth. We conclude that NOCA-1 represents a new class of microtubule end-binding proteins with essential functions of its own, as well as parallel functions with Patronin, in the assembly of non-centrosomal microtubule arrays in multiple *C. elegans* tissues.

2.2 Introduction

MTs are often assembled into arrays to fulfill their diverse cellular functions. Dividing animal cells use centrosomes to assemble two radial MT arrays that form the bipolar mitotic spindle to segregate chromosomes. In contrast, fission yeast, differentiated animal cells and plant cells often assemble linear MT arrays (Bartolini and Gundersen, 2006). In the fission yeast *S. pombe*, three to five linear MT bundles attach to the nucleus and position the nucleus in the middle by balanced pushing force (Tran *et al.*, 2001). In epithelial cells, parallel MTs run along the apical-basal axis and direct memebrane trafficking (reviewd in Müsch, 2004; Nelson and Yeaman, 2001). In myotubes, MTs are originated from the nuclear periphery and transport myosin during sarcomere formation (Tassin *et al.*, 1985; Pizon *et al.*, 2005). In neurons, the linear MT arrays in the axons and dendrites support their unique shape and direct polarized organelle transport (reviewd in Hirokawa and Takemura, 2005). In growing plant hypocotyl cells, parallel MTs are transversely oriented in the cortical MT array to direct cellulose deposition to the cell wall (Paredez *et al.*, 2006). Therefore, non-centrosomal MT arrays play critical roles in many differentiated cells by providing structure support and serving as transportation tracks. Nevertheless, it remains unclear how non-centrosomal MT arrays are assembled.

To assemble non-centrosomal arrays, MTs need to be first generated and then be stabilized and anchored. MTs can be generated by γ-tubulin mediated nu-

cleation or by MT severing. γ-Tubulin functions in a ring-shaped protein complex γ-TuRC (γ-Tubulin Ring Complex) to control MT nucleation (Zheng *et al.*, 1995; Oegema *et al.*, 1999). γ-TuRC as well as the MT nucleation activity frequently re-locates to non-centrosomal sites in differentiated cells, such as the perinuclear iMOTC in fission yeast (Tran *et al.*, 2001), the apical surface in epithelial cells (Meads and Schroer, 1995; Jankovics and Brunner, 2006; Brodu *et al.*, 2010; Fridolfsson and Starr, 2010; Feldman and Priess, 2012), the nuclear envelope in myotubes (Tassin *et al.*, 1985), the Golgi outposts in neuronal processes (Ori-McKenney *et al.*, 2012) and the existing MT lattice in plant cells (Lindeboom *et al.*, 2013b). Therefore, it seems that MTs are generated by localized MT nucleations in many cases. On the other hand, MT severing contributes to MT generations in both neurons and plants, presumably by generating short "MT seeds" (Roll-Mecak and Vale, 2006). In neurons, the MT severing enzymes spastin and katanin are requried to generate MTs for axon elongation and branching (reviewed in Roll-Mecak and McNally, 2010). In plant hypocotyl cells, katanin mediates the reorientation of cortical MT arrays from being transverse to longitudinal (Lindeboom *et al.*, 2013b). During the reorientation, katanin is recruited to the MT crossover point, where newly growing MTs cross with existing MTs, and selectively cut the new MTs to generate more plus ends growing in the same direction as new ones (Lindeboom *et al.*, 2013b). Thus, MTs in non-centrosomal arrays are generated by localized MT nucleation or MT severing.

MT stabilization and anchoring require players other than the γ-TuRC,

although this MT nucleating complex can cap the minus ends and block polymerization (Zheng *et al.*, 1995). Ninein and CAMSAPs are involved in MT minus end anchoring. In mammalian cells, ninein has been shown to anchor MTs to both centrosomal and non-centrosomal sites (Mogensen *et al.*, 2000). In mouse epidermis, localization of ninein to cellular junctions is dependent on desmoplakin (Lechler and Fuchs, 2007). However, it remains unclear whether ninein directly binds to MTs due to the lack of in vitro study. CAMSAPs belong to a conserved protein family in eumetazoa and all CAMSAPs contain a CKK domain that binds to MTs (Baines *et al.*, 2009). All three CAMSAPs in human and the only CAMSAP homolog patronin in *Drosophila* can bind specifically to the MT minus ends, but they differ in abilities of reducing minus end dynamics (Jiang *et al.*, 2014; Hendershott and Vale, 2014). In cultured epithelial cells, Nezha/CAMSAP3 was shown to anchor MTs to the zonula adherens through an interaction between Nezha and PLEKHA7 (Meng *et al.*, 2008). In *C. elegans*, mutating the only CAMSAP homolog PTRN-1 affects the MT stability in neurites and results in abnormal neurite morphology (Marcette *et al.*, 2014; Richardson *et al.*, 2014). Therefore, MT minus end anchoring mediated by ninein or CAMSAPs is important for assembling non-centrosomal arrays.

In a RNAi screen in *C. elegans*, we identified NOCA-1 (NOn-Centrosomal Array-1) as a novel protein that specifically functions in MT formation in differentiated tissues (Green *et al.*, 2011). Depletion of NOCA-1, just like depletion of γ-tubulin, results in a catastrophic germline phenotype featured by multinu-

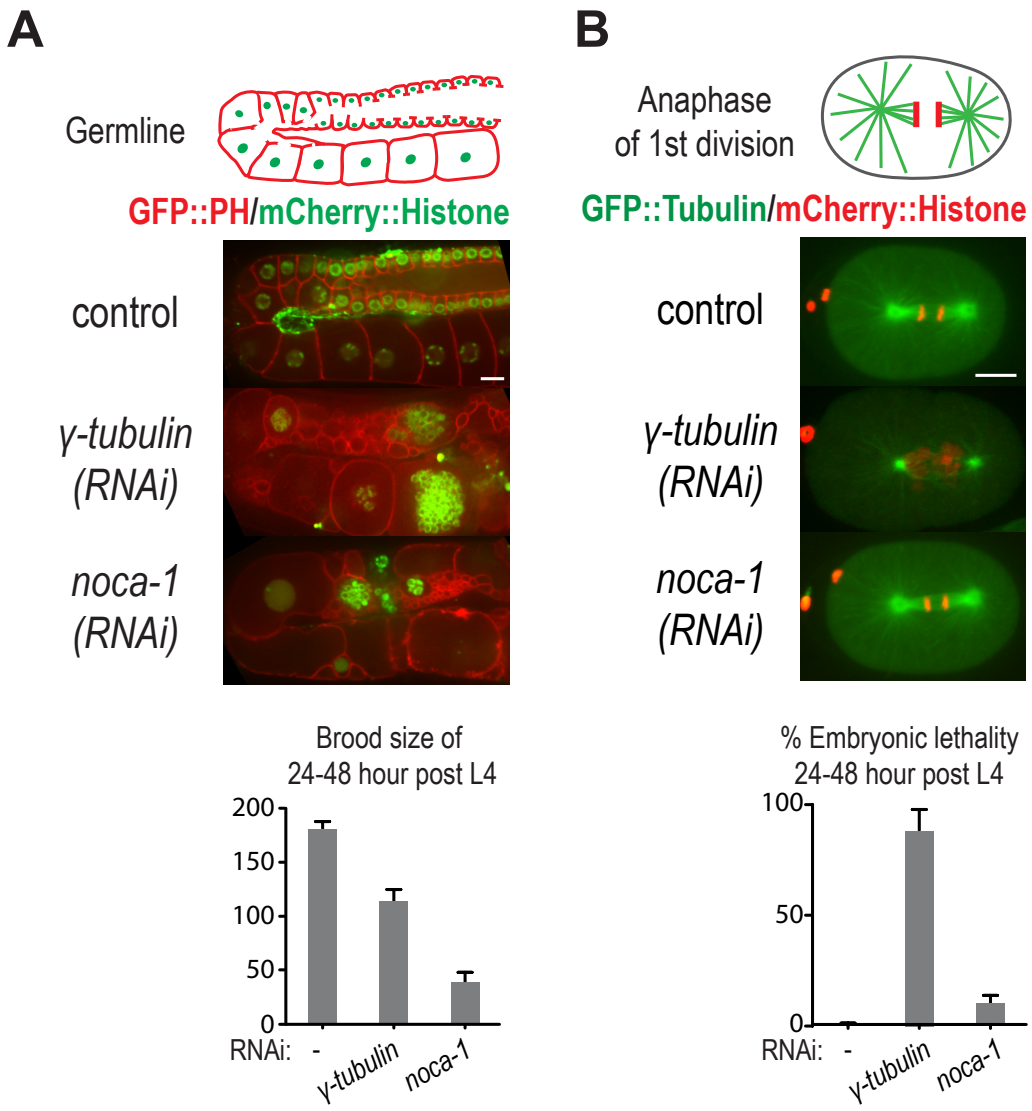

Figure 2.1: NOCA-1 specifically function in non-centrosomal MT array formation.
(A) Top: schematic and images of germlines expressing GFP::PH and mCherry::Histone. Bottom: plot of the brood size after depletion of γ-tubulin or NOCA-1.
(B) Top: schematic and images of dividing 1-cell embryos expressing GFP::Tubulin and mCherry::Histone. Bottom: plot of the embryonic lethality after depletion of γ-tubulin or NOCA-1.
Error bars are SEM of the brood size or percent lethality per worm. Scale bars, 10 μm.

cleation and vesiculation and causes sterility (Figure 2.1A; Green *et al.*, 2011). Additionally, NOCA-1 depletion reduces the number of growing MTs and causes nuclear migration defects in embryonic epidermis (Green *et al.*, 2011). However, unlike γ-tubulin, NOCA-1 is dispensable for centrosome driven embryonic divisions (Figure 2.1B). Therefore, NOCA-1 is a novel player functioning in non-centrosomal MT array formation, but the mechanism of NOCA-1 function is unknown.

Here, we show that NOCA-1 binds to the MT ends and controls MT array formation in multiple *C. elegans* tissues, either by itself, or together with PTRN-1, which is the only CAMSAP homolog in *C. elegans*. NOCA-1 has eight isoforms expressing in many tissues. Two of the long isoforms control MT array formation in the germline and embryonic epidermis, respectively. In contrast, a short isoform functions together with PTRN-1 to control assembly of MT arrays in post-embryonic epidermis. Mechanistically, both NOCA-1 and PTRN-1 co-sediment with taxol-stabilized MTs from worm lysates and purified NOCA-1 as well as PTRN-1 binds to MT ends in a MT anchoring assay. We propose that NOCA-1 represents a new class of MT end binding proteins with essential functions of its own, as well as parallel functions with Patronin, in the assembly of non-centrosomal microtubule arrays in multiple *C. elegans* tissues.

2.3 Results

2.3.1 NOCA-1 and PTRN-1 are genetically redundant for normal *C. elegans* development

We found that *noca-1*Δ and *ptrn-1*Δ were synthetic larval lethal (Figure 2.2A). Both NOCA-1 and PTRN-1 were previously implicated in MT array formation (Green *et al.*, 2011; Marcette *et al.*, 2014; Richardson *et al.*, 2014). Despite some other defects, *noca-1*Δ worms grew up to be morphologically normal adults (Figure 2.2A), indicating the organismal development was largely normal. PTRN-1 is the only CAMSAP homolog in *C. elegans* (Baines *et al.*, 2009) and *ptrn-1* mutants had abnormal neurites (Marcette *et al.*, 2014; Richardson *et al.*, 2014). However, we made a null *ptrn-1*Δ allele using MosDEL (Figure 2.3; Frøkjær-Jensen *et al.*, 2010) and found the mutant worms had no obvious phenotypes (Figure 2.2A). In sharp contrast, *noca-1*Δ*;ptrn-1*Δ double mutants grew much slower and about 60% of the worms died during the first three days of post-embryonic development (Figure 2.2A and B). Most deaths occurred during the L4 and early adult stages (Figure 2.2B). The 40% survivors were only half the size of wild type worms and they failed to move normally (unc, for uncoordinated; Figure 2.2A). Therefore, we conclude that NOCA-1 and PTRN-1 function redundantly to support the post-embryonic development of *C. elegans*.

We suspected the epidermal integrity of *noca-1*Δ*;ptrn-1*Δ double mutants was affected for two reasons. First, when the double mutants died, they were

often broken up with some internal tissues leaking out. Second, the double mutant worms were more susceptible to the coverslip compression when mounted onto the imaging slide. To test this idea, we examined the permeability of worms to a HOECHST DNA dye (Moribe *et al.*, 2004) and found that *noca-1*Δ*;ptrn-1*Δ worms became permeable from early larval stage (Figure 2.2C). The percentage of permeable worms increased as development went on (Figure 2.2C). In addition, the epithelial junction marked by DLG-1::GFP was defective in *noca-1*Δ*;ptrn-1*Δ double mutants (Figure 2.2D). The epidermis of adult *C. elegans* comprises one large syncytium covering the majority of its body area (hyp7), two lateral syncytia formed by fusion of seam cells and several other syncytia at the head and tail (Figure 2.2D; Chisholm and Hsiao, 2012). DLG-1::GFP marks the apical junctions between these syncytia. Normally, the seam junctions are connected to the head epidermis and appear to be two parallel lines running along the whole seam length (Figure 2.2D). In *noca-1*Δ*;ptrn-1*Δ double mutants, however, the seam junctions were disconnected from the head epidermis and also had broken points or abnormal branches (Figure 2.2D). Therefore, NOCA-1 and PTRN-1 are reqruied to maintain the epidermal integrity in post-embryonic worms.

Figure 2.2: NOCA-1 and PTRN-1 are genetically redundant for normal *C. elegans* development.
(A) Left: images of control and mutant worms at 72 hours post L1 recovery. Right: plots of the frequency of living worms at 72 hours post L1 stage for indicated genotypes. Error bars are SD of 3 to 5 independent experiments. n shows the total number of analyzed worms.
(B) Growth curve and death curve of worms with indicated genotypes. Error bars are SEM.
(C) Top: DIC and fluorescent images of worms after staining with Hoechst33258 DNA dye. Bottom: plot of percent permeable worms for indicated genotypes. Error bars are margin of error at 95% confidence.
(D) Left: schematic and images of worms expressing DLG-1::GFP. Right: plot of percent worms with indicated phenotypes. Error bars are margin of error at 95% confidence.
Scale bars, 10 μm unless specified.

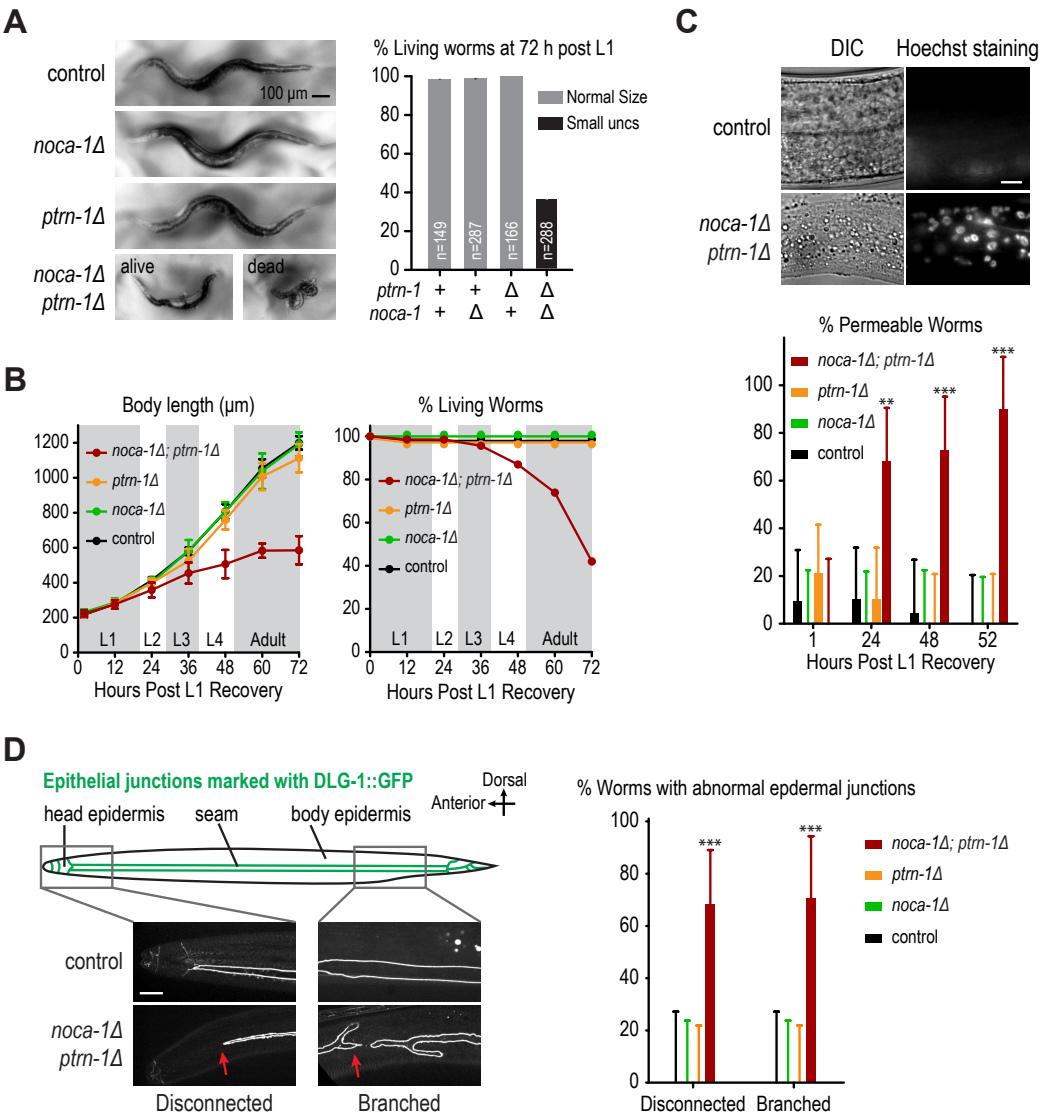
A
control
noca-1Δ
ptrn-1Δ
noca-1Δ ptrn-1Δ
100 µm
alive
dead
% Living worms at 72 h post L1
Normal Size
Small uncs
n=149
n=287
n=166
n=288
ptrn-1 + + Δ Δ
noca-1 + Δ + Δ
B
Body length (µm)
noca-1Δ; ptrn-1Δ
ptrn-1Δ
noca-1Δ
control
L1 L2 L3 L4 Adult
Hours Post L1 Recovery
% Living Worms
Hours Post L1 Recovery
C
DIC
Hoechst staining
control
noca-1Δ ptrn-1Δ
% Permeable Worms
noca-1Δ; ptrn-1Δ
ptrn-1Δ
noca-1Δ
control
Hours Post L1 Recovery
D
Epithelial junctions marked with DLG-1::GFP
Dorsal
Anterior
head epidermis
seam
body epidermis
control
noca-1Δ ptrn-1Δ
Disconnected
Branched
% Worms with abnormal epdermal junctions
noca-1Δ; ptrn-1Δ
ptrn-1Δ
noca-1Δ
control
Disconnected
Branched

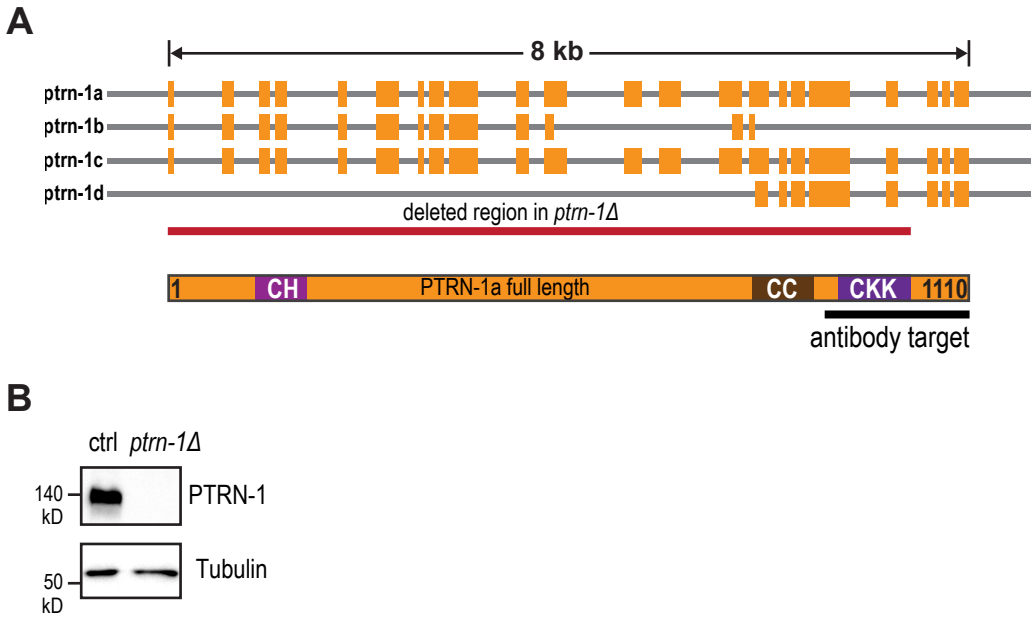

Figure 2.3: Validation of a null *ptrn-1*Δ allele by MosDEL.
(A) Schematic showing the PTRN-1 isoforms, deleted region in *ptrn-1*Δ and the PTRN-1 domain structure.
(B) Immunoblot using a polyclonal antibody targeting the C-terminal region of PTRN-1.

2.3.2 NOCA-1 and PTRN-1 control MT array assembly in the post-embryonic epidermis

The developmental defects in *noca-1*Δ*;ptrn-1*Δ worms could originate from one or several tissues. To determine whether NOCA-1 and PTRN-1 function in specific tissues, we used MosSCI (Frøkjær-Jensen *et al.*, 2008) to construct transgenic worms expressing PTRN-1 under a series of tissue-specific promoters and tested whether they can rescue the synthetic lethality of *noca-1*Δ*;ptrn-1*Δ worms. We found that expressing PTRN-1 only in the epidermis (Pdpy-7), but not neurons (Prgef-1) or pharynx and intestine (Ppha-4), could rescue both the lethality and unc phenotype of *noca-1*Δ*;ptrn-1*Δ worms (Figure 2.4A). Thus, NOCA-1 and PTRN-1 function specifically in the post-embryonic epidermis to support *C. elegans* development.

Because both NOCA-1 and PTRN-1 were involved in MT array formation in other contexts, we want to determine whether MT arrays in *noca-1*Δ*;ptrn-1*Δ worms were affected. Live imaging of GFP labeled MTs in the post-embryonic epidermis revealed a MT array of evenly spaced MT bundles that run circumferentially around the animal (Figure 2.4B). This MT array seemed to be at the very surface of cells, since the fluorescence signal decreased rapidly when the imaging focus moved inside (data not shown). Some MTs in the array were relatively stable, while others exhibited clear dynamics (Figure 2.5A). While this array was only subtly affected in single *noca-1*Δ and *ptrn-1*Δ mutants, it was nearly eliminated

in *noca-1*Δ*;ptrn-1*Δ double mutants (Figure 2.4C and D). Therefore, we conclude that NOCA-1 and PTRN-1 function redundantly to control MT array formation in the post-embryonic epidermis.

Interestingly, the MT dynamics was differently affected in *noca-1*Δ and *ptrn-1*Δ mutants. We quantified the MT dynamics by counting growth and shrinkage events that pass a line perpendicular to the MT arrays with the aid of kymographs. A MT growth event was indicated by the appearance of signal along the time axis (green arrowhead in Figure 2.4E), while the shrinkage event was indicated by the disappearance of signal (red arrowhead in Figure 2.4E). We found only half dynamic events (growth or shrinkage) in *noca-1*Δ single mutants and more than 50% of dynamic events in *ptrn-1*Δ mutants (Figure 2.4E). Thus, we conclude that inhibiting NOCA-1 and PTRN-1 have different effects in MT dynamics.

Figure 2.4: NOCA-1 and PTRN-1 control MT array assembly in the post-embryonic epidermis.
(A) Left: schematic of PTRN-1::GFP transgenes under tissue-specific promoters. Right: plot of the frequency of living worms at 72 hours post L1 stage for indicated genotypes. Error bars are SEM of 3 to 5 independent experiments. n shows the total number of analyzed worms.
(B) Schematic and images of MTs marked by TBB-2::GFP in the post-embryonic epidermis.
(C) Images of post-embryonic epidermis in worms with indicated genotypes.
(D) Left: schematic showing method to measure of the MT bundle density. Right: plot of the MT bundle density in worms with indicated genotypes. Error bars are SEM.
(E) Left: kymograph showing examples of MT shrinkage and MT growth. Right: plot of the frequency of indicated MT dynamic events, growth or shrinkage in worms with indicated genotypes.
Scale bars, 10 μm unless specified.

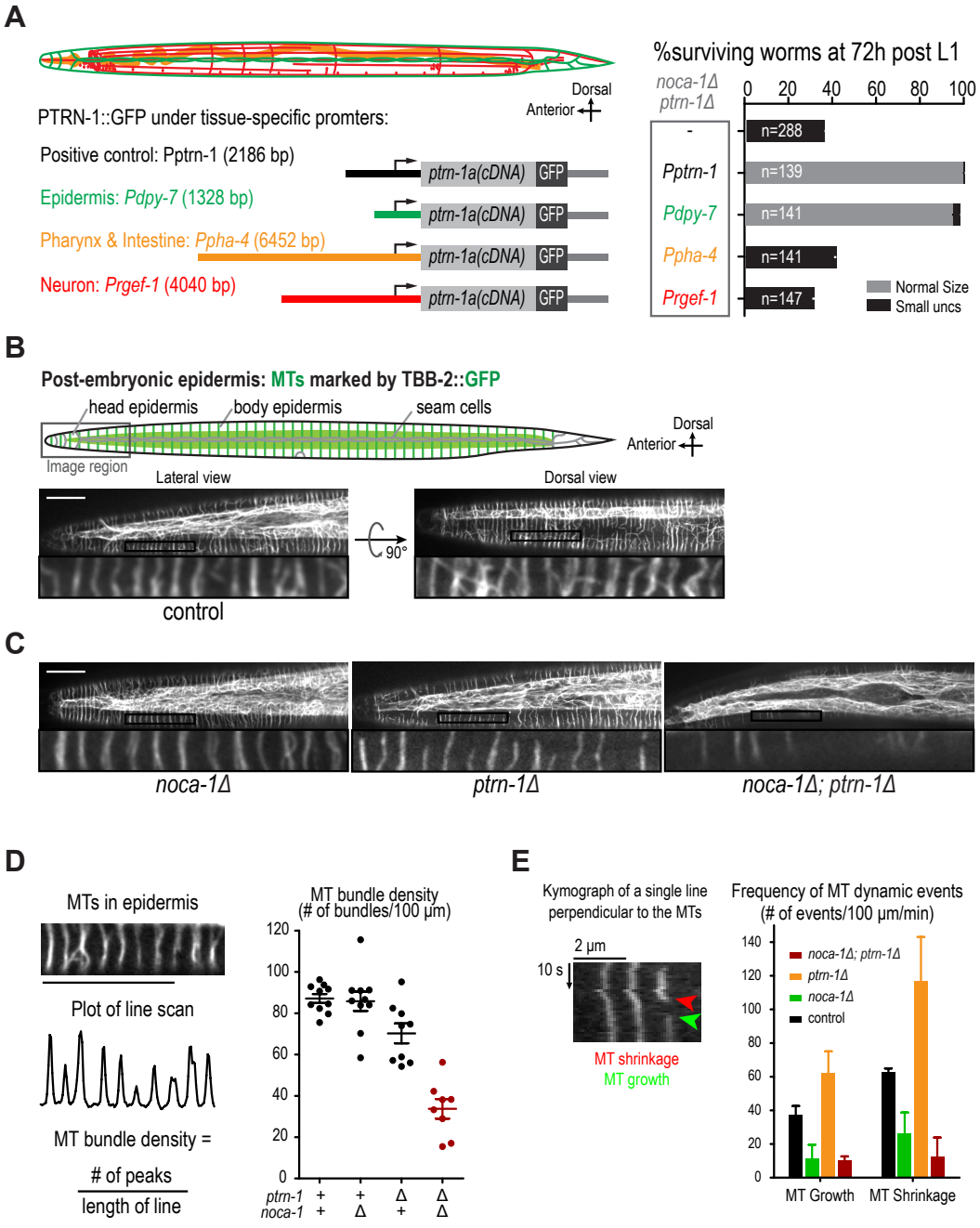
A
Dorsal
Anterior
PTRN-1::GFP under tissue-specific promters:
Positive control: Pptrn-1 (2186 bp)
Epidermis: Pdpy-7 (1328 bp)
Pharynx & Intestine: Ppha-4 (6452 bp)
Neuron: Prgef-1 (4040 bp)
ptrn-1a(cDNA)
GFP
%surviving worms at 72h post L1
noca-1Δ
ptrn-1Δ
0 20 40 60 80 100
-
Pptrn-1
Pdpy-7
Ppha-4
Prgef-1
n=288
n=139
n=141
n=141
n=147
Normal Size
Small uncs
B
Post-embryonic epidermis: MTs marked by TBB-2::GFP
head epidermis
body epidermis
seam cells
Image region
Dorsal
Anterior
Lateral view
Dorsal view
90°
control
C
noca-1Δ
ptrn-1Δ
noca-1Δ; ptrn-1Δ
D
MTs in epidermis
Plot of line scan
MT bundle density =
# of peaks
length of line
MT bundle density
(# of bundles/100 µm)
120
100
80
60
40
20
0
ptrn-1 + + Δ Δ
noca-1 + Δ + Δ
E
Kymograph of a single line
perpendicular to the MTs
2 µm
10 s
MT shrinkage
MT growth
Frequency of MT dynamic events
(# of events/100 µm/min)
140
120
100
80
60
40
20
0
noca-1Δ; ptrn-1Δ
ptrn-1Δ
noca-1Δ
control
MT Growth
MT Shrinkage

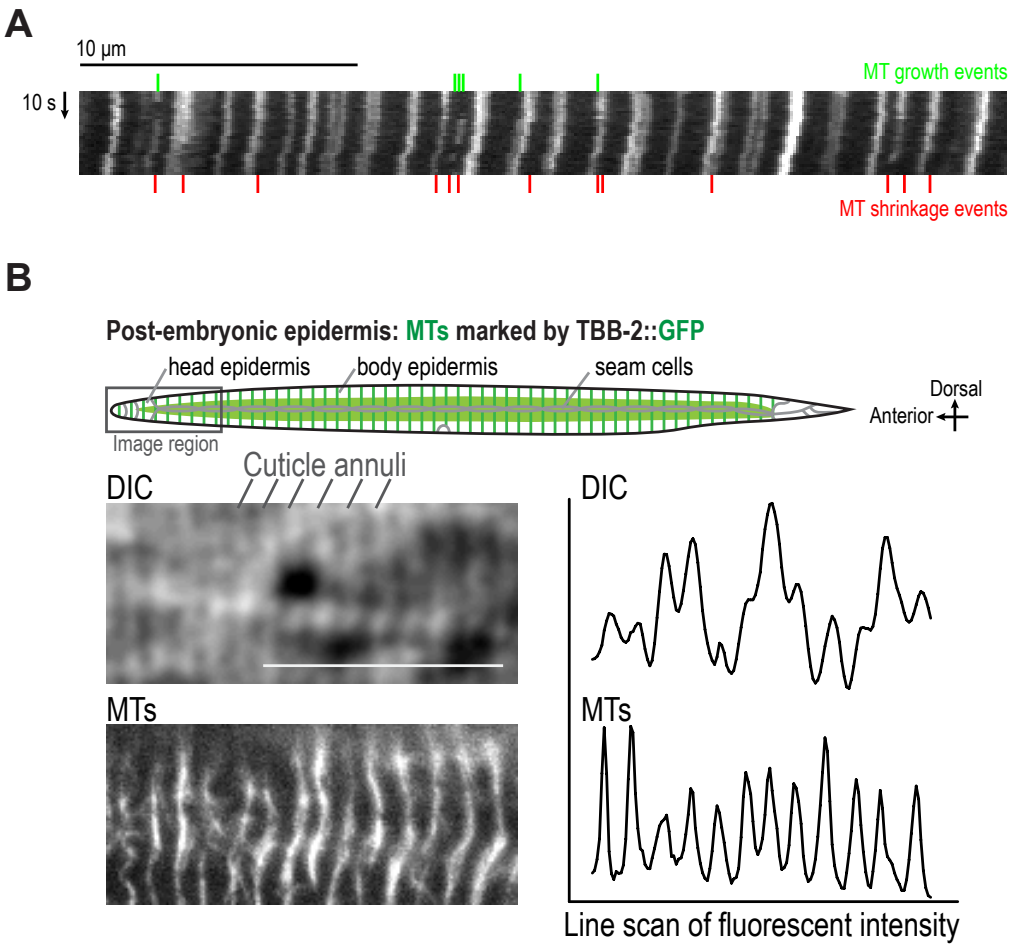

Figure 2.5: Post-embryonic MTs are dynamic and delineate the cuticle annuli. (A) Kymograph showing MT growth and shrinkage events in post-embryonic epidermal arrays.
(B) Top: schematic describing the organiation of post-embryonic epidermal MT arrays. Bottom left: DIC image showing the cuticle annuli and fluorescent image shoing the MT bundles. Bottom right: line scan plots of the images to their left. Scale bars, 10 μm unless specified.

2.3.3 NOCA-1 controls non-centrosomal MT assembly in the germline and embryonic epidermis

Besides the redundant role with PTRN-1 in the post-embryonic epidermis, NOCA-1 alone was shown to be important for non-centrosomal MT array formation in both the germline and embryonic epidermis (Green *et al.*, 2011). Consistent with that, we found that *noca-1*Δ worms had disorganized germlines and were completely sterile (Figure 2.6A). In addition, *noca-1*Δ worms all had nuclear migration defects due to its function in MT formation in the embryonic epidermis (Figure 2.6D). By contrast, *ptrn-1*Δ worms had normal germline morphology, normal brood size and no nuclear migration defects (Figure 2.6A and D).

Next, we wanted to determine whether MTs were directly affected when NOCA-1 was inhibited. In the germline syncytium, nuclei are positioned inside their own membrane comparments and each compartment has a small opening to the middle shared cytoplasm termed rachis (Figure 2.6B). Live imaging of a GFP labeled β-tubulin transgene (TBB-2::GFP) revealed that dense MT arrays almost filled up the cytoplasmic space both in the membrane compartments and the rachis (Figure 2.6B, right). The high MT density impaired phenotypic analysis by direct MT visualization. Instead, we capitalized on a GFP labeled EB1 transgene (EB1::GFP), which tracks the growing MT ends (Figure 2.6C). The number of growing MTs were reduced by more than 30% after depletion of NOCA-1 or γ-tubulin (Figure 2.6C, right). Therefore, we conclude that NOCA-1 is required for

MT array formation in the germline.

During nuclear migration, MTs in the dorsal epidermis of *C. elegans* embryos were oriented along the long axis of each cell (Figure 2.6E). It was reported that depleting NOCA-1 reduced the number of growing MT ends marked by EB1::GFP. We adopted a similar strategy to determine whether MTs are affected in *noca-1*Δ embryos. Our results showed the number of growing MTs was reduced by more than 50% in *noca-1*Δ embryos than in wild type embryos (Figure 2.6F). Thus, we conclude that NOCA-1 is required for MT array formation in the embryonic epidermis.

In sum, NOCA-1 alone controls assembly of non-centrosomal MT arrays in the germline to maintain the germline architecture and organismal fertility and linear MT arrays in the embryonic epidermis for nuclear migration.

Figure 2.6: NOCA-1 alone controls MT assembly in the germline and embryonic epidermis.
(A) Left: schematic of germline structure. Middle: images of the germline pachytene region of worms expressing membrane and DNA markers with indicated genotypes. Right: plot of the brood size of worms bwteen 24 and 48 hours post L4 stage. Error bars are SEM. Note that the Y axis is offset a bit to show the all 0 data of *noca-1*Δ.
(B) Left: schematic of MT arrays in the germline. Right: images and amplified region of the germline pachytene region of worms expressing GFP MT markers.
(C) Images of post-embryonic epidermis in worms with indicated genotypes.
(D) Left: schematic showing method to measure of the MT bundle density. Right: plot of the MT bundle density in worms with indicated genotypes. Error bars are SEM.
(E) Left: kymograph showing examples of MT shrinkage and MT growth. Right: plot of the frequency of indicated MT dynamic events, growth or shrinkage in worms with indicated genotypes.
Scale bars, 10 μm unless specified.

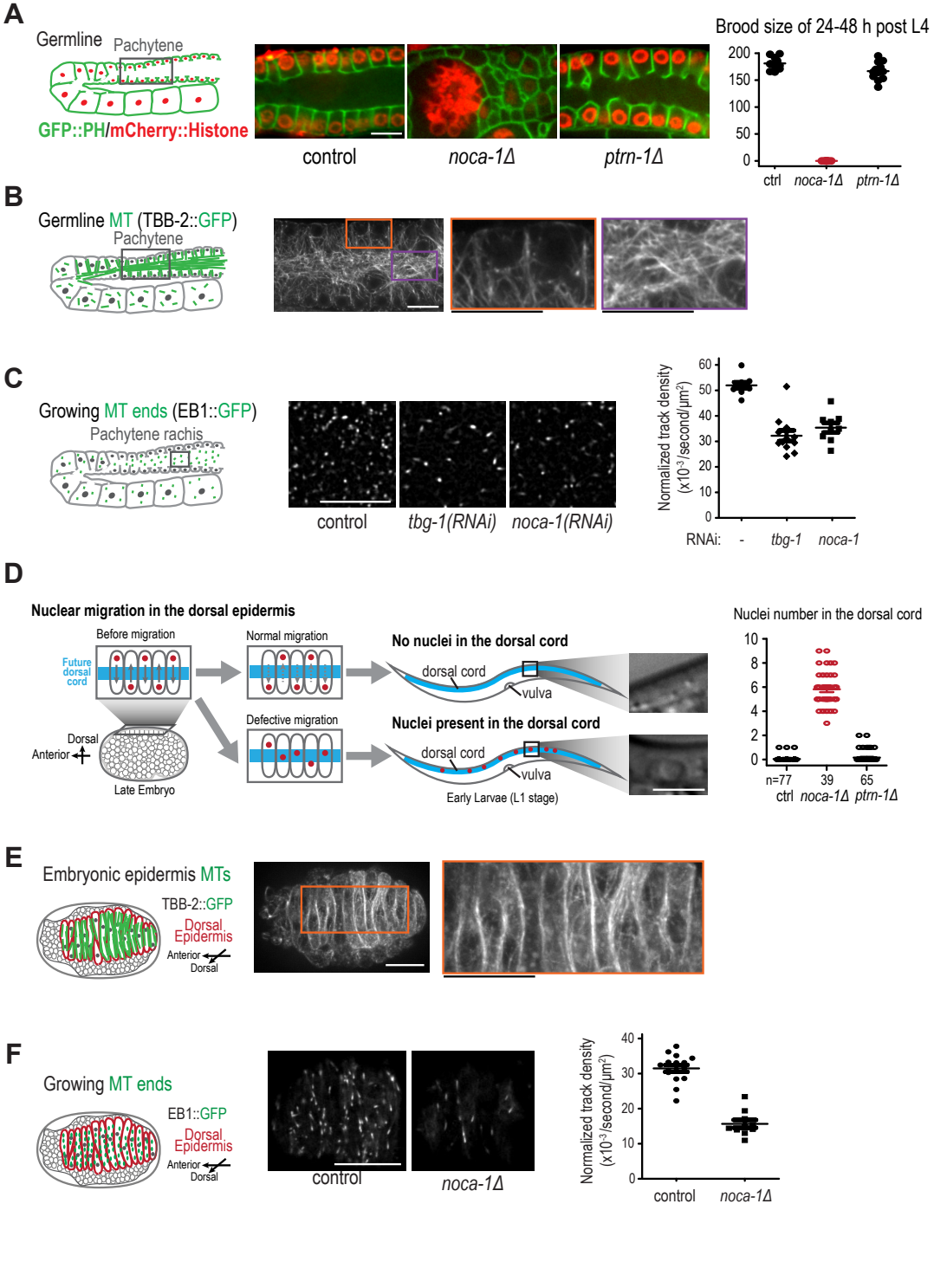
A
Germline
Pachytene
GFP::PH/mCherry::Histone
control
noca-1Δ
ptrn-1Δ
Brood size of 24-48 h post L4
200
150
100
50
0
ctrl
noca-1Δ
ptrn-1Δ
B
Germline MT (TBB-2::GFP)
Pachytene
C
Growing MT ends (EB1::GFP)
Pachytene rachis
control
tbg-1(RNAi)
noca-1(RNAi)
Normalized track density
(x10-3/second/μm2)
60
50
40
30
20
10
0
RNAi:
-
tbg-1
noca-1
D
Nuclear migration in the dorsal epidermis
Before migration
Future dorsal cord
Dorsal
Anterior
Late Embryo
Normal migration
Defective migration
No nuclei in the dorsal cord
Nuclei present in the dorsal cord
dorsal cord
vulva
Early Larvae (L1 stage)
Nuclei number in the dorsal cord
10
8
6
4
2
0
n=77
39
65
ctrl
noca-1Δ
ptrn-1Δ
E
Embryonic epidermis MTs
TBB-2::GFP
Dorsal Epidermis
Anterior
Dorsal
F
Growing MT ends
EB1::GFP
Dorsal Epidermis
Anterior
Dorsal
control
noca-1Δ
Normalized track density
(x10-3/second/μm2)
40
30
20
10
0
control
noca-1Δ

2.3.4 Distinct NOCA-1 isoforms function in different tissues

NOCA-1 had seven annotated splicing isoforms (Wormbase). We identified an eighth isoform (NOCA-1h) that was later shown to be both necessary and sufficient for the germline function. All NOCA-1 isoforms have a unique N-terminal domain fused to a common 466 amino-acid C-terminal domain that contains a coiled-coil region as its only identifiable feature (Figure 2.7A). Its five longest isoforms (a, b, c, f and h) have an additional 205 amino-acid common region (cyan box in Figure 2.7A). A 657 bp deletion of *noca-1* caused a frame shift and removed the majority of the protein including the coiled-coil domain from all NOCA-1 isoforms (ok3692; red line in Figure 2.7A). A polyclonal antibody raised against the coiled-coil region recognized four major species on a western blot. These bands represented NOCA-1 isoforms, because they were not present in *noca-1*Δ mutants (Figure 2.7B, black arrows). NOCA-1 is well conserved in other nematodes including the parasites *Brugia malayi* and *Loa loa* (Figure 2.8), but we have not yet identified homologs outside of nematodes.

We used isoform-secific RNAi to determine which NOCA-1 isoform functions in the germline. The 750 bp isoform-specific N-terminus of NOCA-1h allowed for specific and efficient depletion of NOCA-1 isoform h (Figure 2.7B, right). Depletion of NOCA-1h alone disrupted the germline architecture and resulted in sterility, similar to depleting all NOCA-1 isoforms (Figure 2.7C). Moreover, expressing a

RNAi resistant form of NOCA-1h in the germline rescued both the morphology defect and the sterility of NOCA-1 depletion (Figure 2.7D and E). Therefore, we conclude that NOCA-1 isoform h is both necessary and sufficient for the germline function.

To determine which isoform functions in the embryonic epidermis, we made single-copy transgenes expressing subsets of NOCA-1 isoforms and tested whether they could rescue the nuclear migration defect of *noca-1*Δ mutants. The *noca-1long* transgene expressing isoforms a, b, c, f, g and h rescued the nuclear migration defect of *noca-1*Δ, but the *noca-1gh* transgene expressing only isoforms g and h could not rescue (Figure 2.7F). Therefore, one or several isoforms of a, b, c and f function in the embryonic epidermis. To distinguish among the four isoforms, premature stop codens were introduced in the *noca-1long* transgene to delete these isoforms one by one (named *noca-1long*Δ*a, b, c or f*). Among the four isoform-deleted transgenes, only *noca-1long*Δ*b* failed to rescue the nuclear migration defect, indicating that NOCA-1 isoform b functions in the epidermis (Figure 2.7F). We then tested the sufficiency by expressing only NOCA-1 isoform b using an epidermis promoter (Plbp-1; Fridolfsson and Starr, 2010) and found expressing NOCA-1b alone rescued the nuclear migration defect of *noca-1*Δ mutants (Figure 2.7F). Thus, we conclude that NOCA-1 isoform b functions in the embryonic epidermis.

Using a similar strategy, we found a short NOCA-1 isoform (NOCA-1d) functions together with PTRN-1 in the post-embryonic epidermis. First, the *noca-1long* transgene that rescued both the sterility and the nuclear migration defects

in embryonic epidermis failed to rescue the synthetic lethality of *noca-1*Δ*;ptrn-1*Δ double mutants (Figure 2.7G), suggesting that the short isoforms were important in this case. Indeed, the *noca-1short::mCherry* transgene was able to rescue the synthetic lethality (Figure 2.7G). We then tested which of the two short NOCA-1 isoforms are responsible for this rescue by driving expression of either NOCA-1d::mCherry or NOCA-1e::mCherry and found that NOCA-1 isoform d, but not e, could rescue the synthetic lethality (Figure 2.7G). Therefore, we conclude that NOCA-1 isoform d functions together with PTRN-1 in the post-embryonic epidermis.

In sum, we found that NOCA-1 uses specific isoforms to function in specifc tissues in all three tested tissues. Two long isoforms of NOCA-1, h and b, functions in the gemline and embryonic epidermis, respectively. On the other hand, a short NOCA-1 isoform, NOCA-1d, functions in parallel with PTRN-1 in the post-embryonic epidermis.

Figure 2.7: NOCA-1 uses specific isoforms for functions in different tissues.
(A) Schematic of NOCA-1 isoforms.
(B) Immunoblot of NOCA-1 in worms with indicated genotypes or RNAi. Black arrows, NOCA-1 isoforms. Red arrow, NOCA-1 isoform h.
(C) Images showing the germline morphology marked by GFP::PH and mCherry::Histone of worms with indicated RNAi.
(D) Top: schematic showing a NOCA-1h::GFP transgene that is resistant to RNAi. Bottom: image showing the membrane localization of NOCA-1h::GFP transgene in the germline pachytene region.
(E) Plots of the brood size for worms with indicated perturbations.
(F) and (G) Left: schematic showing NOCA-1 transgenes expressing different sets of its isoforms. Right: plots of nuclei in the dorsal cord, or living worms after 3 days post-embryonic development, for worms with indicated genotypes.
Error bars are SEM of the plotted data points in (E) and (F), or of 3-5 independent experiments in (G). Scale bars, 10 μm unless specified.

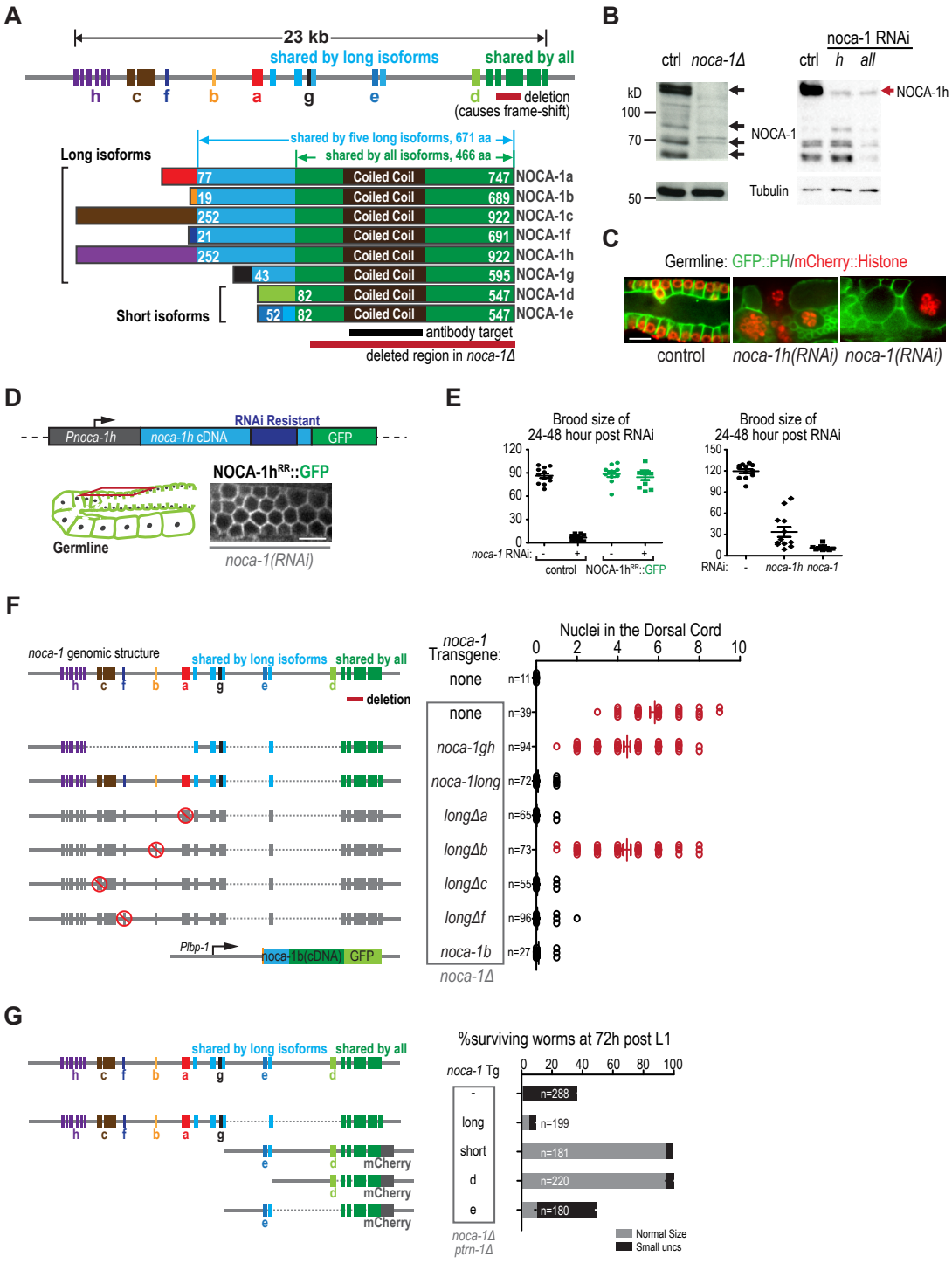
A
23 kb
shared by long isoforms
shared by all
h c f b a g e d
deletion
(causes frame-shift)
shared by five long isoforms, 671 aa
shared by all isoforms, 466 aa
Long isoforms
77 Coiled Coil 747 NOCA-1a
19 Coiled Coil 689 NOCA-1b
252 Coiled Coil 922 NOCA-1c
21 Coiled Coil 691 NOCA-1f
252 Coiled Coil 922 NOCA-1h
43 Coiled Coil 595 NOCA-1g
Short isoforms
82 Coiled Coil 547 NOCA-1d
52 82 Coiled Coil 547 NOCA-1e
antibody target
deleted region in noca-1Δ
B
noca-1 RNAi
ctrl noca-1Δ
ctrl h all
kD
100
70
50
NOCA-1
NOCA-1h
Tubulin
C
Germline: GFP::PH/mCherry::Histone
control
noca-1h(RNAi)
noca-1(RNAi)
D
RNAi Resistant
Pnoca-1h
noca-1h cDNA
GFP
NOCA-1hRR::GFP
Germline
noca-1(RNAi)
E
Brood size of
24-48 hour post RNAi
120
90
60
30
0
noca-1 RNAi:
control
NOCA-1hRR::GFP
Brood size of
24-48 hour post RNAi
150
120
90
60
30
0
RNAi:
noca-1h
noca-1
F
noca-1 genomic structure
shared by long isoforms
shared by all
h c f b a g e d
deletion
Plbp-1
noca-1b(cDNA)
GFP
noca-1
Transgene:
Nuclei in the Dorsal Cord
0 2 4 6 8 10
none n=11
none n=39
noca-1gh n=94
noca-1long n=72
longΔa n=65
longΔb n=73
longΔc n=55
longΔf n=96
noca-1b n=27
noca-1Δ
G
shared by long isoforms
shared by all
h c f b a g e d
mCherry
%surviving worms at 72h post L1
noca-1 Tg
0 20 40 60 80 100
-
long
short
d
e
n=288
n=199
n=181
n=220
n=180
noca-1Δ
ptrn-1Δ
Normal Size
Small uncs

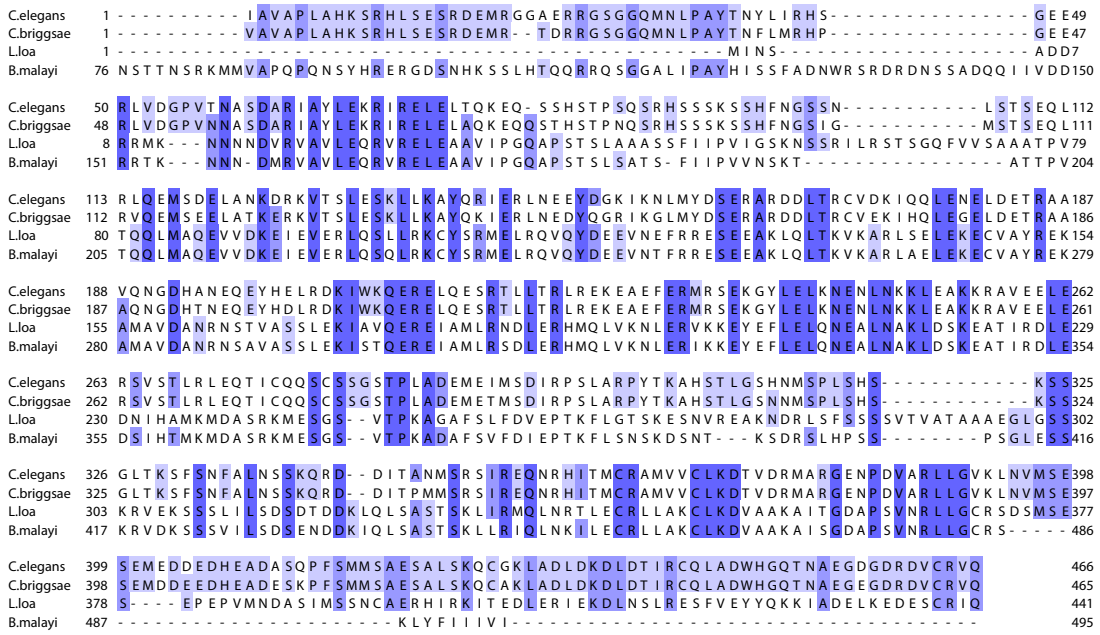

Figure 2.8: NOCA-1 is conserved across nematodes.
Alignment of NOCA-1 in *C. elegans, C. briggsae, Loa loa* and *Brugia malayi*. The region of NOCA-1 is the shared region of all isoforms (green colored region in Figure 2.7A). Blue color shows the percentage of identical amino acids.

2.3.5 A long isoform specifc domain is required for NOCA-1's function in the germline and embryonic epidermis

Two reasons could account for the fact that specific NOCA-1 isoforms function in specific tissues. First, it could be the isoform specific domain has special functions in corresponding tissues. Second, it could be only certain isoforms are expressed in certain tissues at the right time, while other isoforms is equally capable to function when properly expressed. Our results suggested it is a combination of both.

To start with, we did truncational analysis to test whether the N-terminal isoform-specific domain (differently colored in Figure 2.7A) or the long-isoform domain (cyan box in Figure 2.7A) was requried for NOCA-1's function in the three tissues of interest. In the germline, a transgene expressing NOCA-1h(252-922)::GFP which lacks the h-specific domain was fully capable to rescue the sterility caused by NOCA-1h depletion (Figure 2.9B). In contrast, a further truncation NOCA-1h(457-922)::GFP which also lacks the long-isoform domain failed to rescue, suggesting this long-isoform domain is functionally important in the germline (Figure 2.9B). The lack of rescue ability of (457-922)::GFP is not due to low expression levels, as western blot by a GFP antibody revealed similar expression levels of the two truncations (Figure 2.9A). Consistent with that, ectopic germline expression of another long isoform, NOCA-1c, but not a short isoform, NOCA-1d, was able to rescue the sterility caused by NOCA-1h depletion (Figure 2.10B).

Similarly, we found that the isoform b-specific domain was dispensable while the long-isoform domain was required for NOCA-1's function in the embryonic epidermis (Figure 2.9C and D). However, in the case of post-embryonic epidermis, both truncations with and without the long-isoform domain can rescue the lethality of *noca-1*Δ*;ptrn-1*Δ double mutants (Figure 2.9E). Thus, the (457-922)::GFP truncation is able to fold properly at least in some tissue, ruling out another trivial explanation for its inability to function in the germline and embryonic epidermis. To summarize, in all tested cases, the N-terminal isoform-specific domain is dispensable for NOCA-1's function, but the long-isoform domain is important for NOCA-1's function in the germline and embryonic epidermis, where NOCA-1 function by itself.

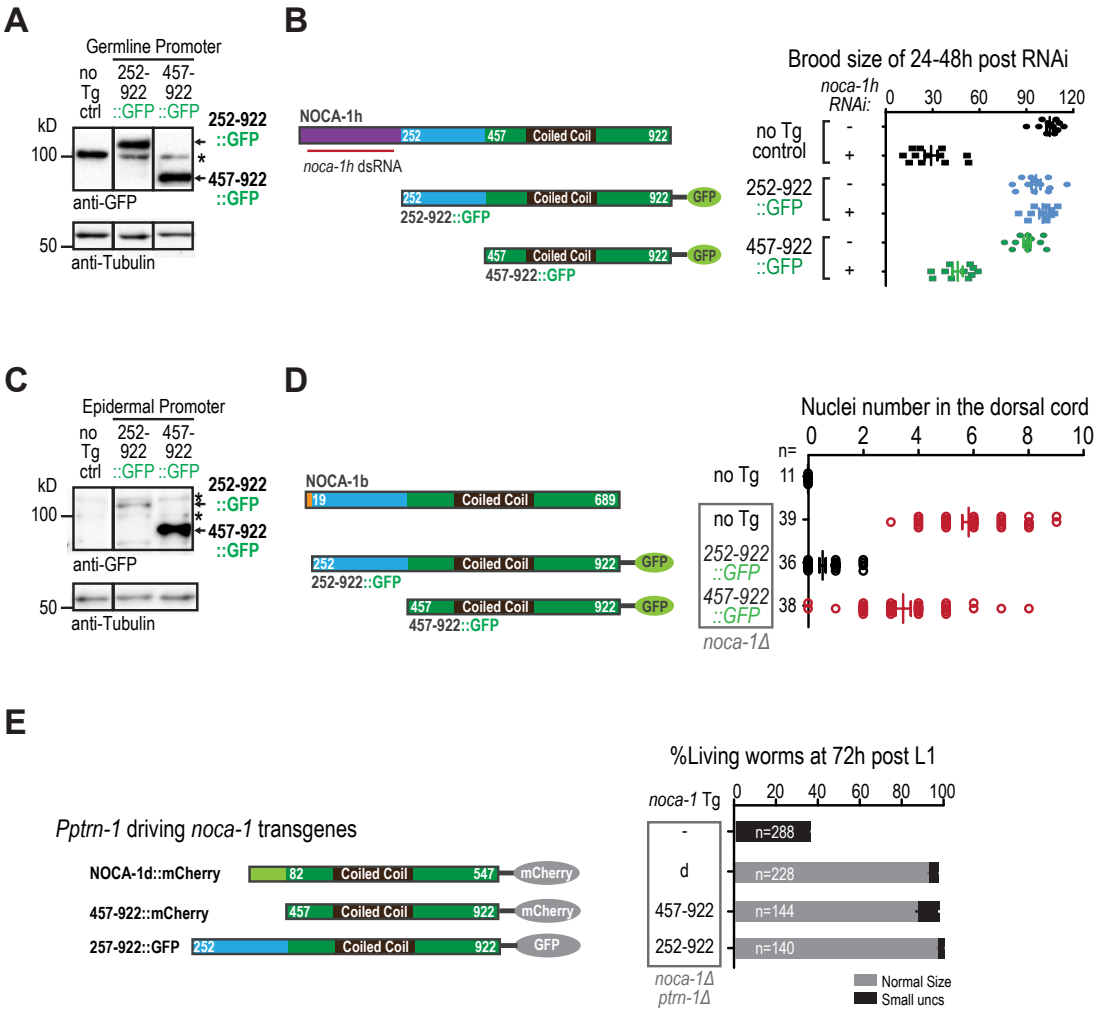

Figure 2.9: A long isoform specifc domain is required for NOCA-1's function in the germline and embryonic epidermis.
(A and C) Immunoblot of worms expressing indicated transgenes.
(B, D and E) Left: schematic of transgenes expressing indicated NOCA-1 truncations. Right: plots of the brood size, nuclei in the dorsal cord or living worms after 3 days of post-embryonic development.
Error bars are SEM for the plotted data points in (B) and (D), or of 3-5 independent experiments in (E). Scale bars, 10 μm unless specified.

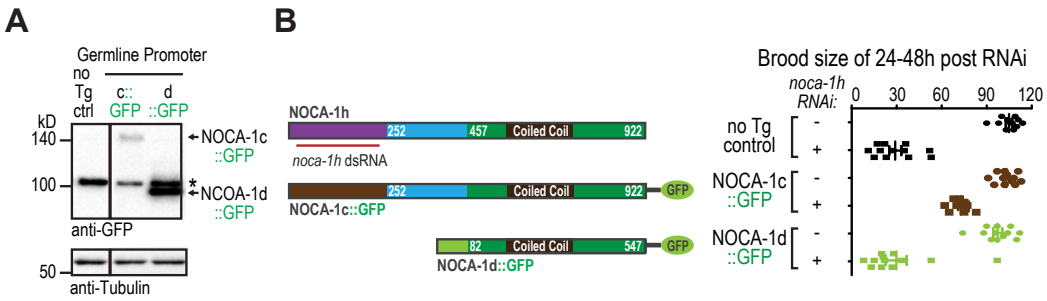

Figure 2.10: Another long isoform, NOCA-1c, can replace the germline function of NOCA-1h.
(A) Immunoblot of worms expressing indicated transgenes.
(B) Left: schematic of NOCA-1 transgenes expressing isoforms c and d. Right: plot of the brood size of worms expressing indicated transgenes after depleting endogenous NOCA-1h. Error bars are SEM.

2.3.6 NOCA-1 co-localizes with γ-tubulin

The membrane localization of NOCA-1 in the germline is reminiscent of the reported γ-tubulin localization (Zhou *et al.*, 2009). We crossed a NOCA-1::GFP transgene and a γ-tubulin::mCherry transgene together and found they indeed co-localized to the plasma membrane in the germline (Figure 2.11A). Interestingly, γ-tubulin::mCherry was also found at the centrosomes, while NOCA-1::GFP was not (red arrow in Figure 2.11A). Similarly, NOCA-1::GFP colocalized with γ-tubulin::mCherry at the apical surface and junctions in embryonic epidermis (Figure 2.11C). We conclude that NOCA-1 and γ-tubulin co-localize to the non-centrosomal sites in the germline and embryonic epidermis.

Because NOCA-1 and PTRN-1 function in parallel in the post-embryonic epidermis, it is thus interesting to compare the localization of NOCA-1, PTRN-1 and γ-tubulin in this tissue. NOCA-1::GFP, but not PTRN-1::GFP, co-localized with γ-tubulin::mCherry at the epithelial junctions between the seam cells and the major body epidermal syncytium (hyp7; Figure 2.11D). In addition, NOCA-1::GFP were also found at small punctates at the surface of the epidermal syncytium, where the circumferential MT arrays were found, but PTRN-1::GFP had a distinct localization pattern featured by both small punctates and short stretches (Figure 2.12). γ-Tubulin::mCherry did not have the punctate localization, presumably due to the dim signal of mCherry; indeed, γ-Tubulin::GFP had small punctates closely resembled that of NOCA-1::GFP (Figure 2.12). Interestingly,

γ-tubulin::mCherry, but not NOCA-1::GFP, was present at the centrosomes in the lateral epidermal cells termed seam cells (red arrow in Figure 2.11D). Thus, we conclude that NOCA-1, but not PTRN-1, co-localize with γ-tubulin to the non-centrosomal sites in post-embryonic epidermis.

The co-localization of NOCA-1 and γ-tubulin led to an attractive proposal that NOCA-1 might recruit γ-tubulin to non-centrosomal sites for MT nucleation. However, in the *noca-1*Δ mutants, γ-tubulin::mCherry still loclaized to the plasma membrane of the disorganized germline and to the epithelial junctions of post-embryonic epidermis, indicating that NOCA-1 is dispensable for the observed non-centrosomal localization of γ-tubulin (Figure 2.11B).

Conversely, γ-tubulin or the γ-tubulin nucleated MTs may recruit NOCA-1 to the non-centrosomal sites. We can approach this question in the germline due to its accessability for γ-tubulin depletion, but analysis in development is prevented by the requirement of γ-tubulin in early cell divisions. In the germline, full length NOCA-1h::GFP still localized to the membrane when the MT nucleator γ-tubulin or the MT subunit β-tubulin was depleted (Figure 2.11E, left). This result suggested that eigher γ-tubulin or the MTs that are nucleated by γ-tubulin were important for the membrane localization. We are currently doing experiments with nocodazole treatment to distinguish between these two possibilities.

Interestingly, the N-terminal isoform h-specific domain (purple colored box in the diagram) contains a predicted palmitoylation site (cysteine 10) which may account for a redundant membrane localization mechanism for full length NOCA-

1h (Ren *et al.*, 2008). Consistent with this idea, the h-specific domain (1-252)::GFP was able to localize to the plasma membrane and this membrane localization was abolished when the predicted palmitoylation site was mutated from cysteine to alanine (C10A, Figure 2.11F). To conclude, the core functional domain of NOCA-1h requires γ-tubulin and MTs for its membrane localization, while full length NOCA-1h has an additional membrane targeting mechanism conferred by the N-terminal domain, possibly through a lipid modification.

Figure 2.11: NOCA-1 co-localizes with γ-tubulin to non-centrosomal sites.
(A) Left: schematic of the imaged region in (A), (B), (E) and (F). Right: images of the pachytene surface of worms expressing both NOCA-1::GFP and γ::mCherry.
(B) Images showing the localization of γ-tubulin::mCherry in the germline of worms with indicated genotypes.
(C) Left: schematic of the imaged region. Right: images of a late stage embryo expressing both NOCA-1::GFP and γ-tubulin::mCherry.
(D) Top: schematic showing the imaged region. Middle and bottom, images of the post-embryonic epidermis of worms expressing indicated transgenes.
(E) Top: schematic of the transgenes. Bottom, images of the germline pachytene surface (as indicated in A) of worms depleted of γ-tubulin or β-tubulin.
(F) Left: schematic of the transgenes and corresponding images of the germline pachytene surface (as indicated in A). Right: immunoblot of worms expressed indicated transgenes using anti-GFP antibody.
Scale bars, 10 μm.

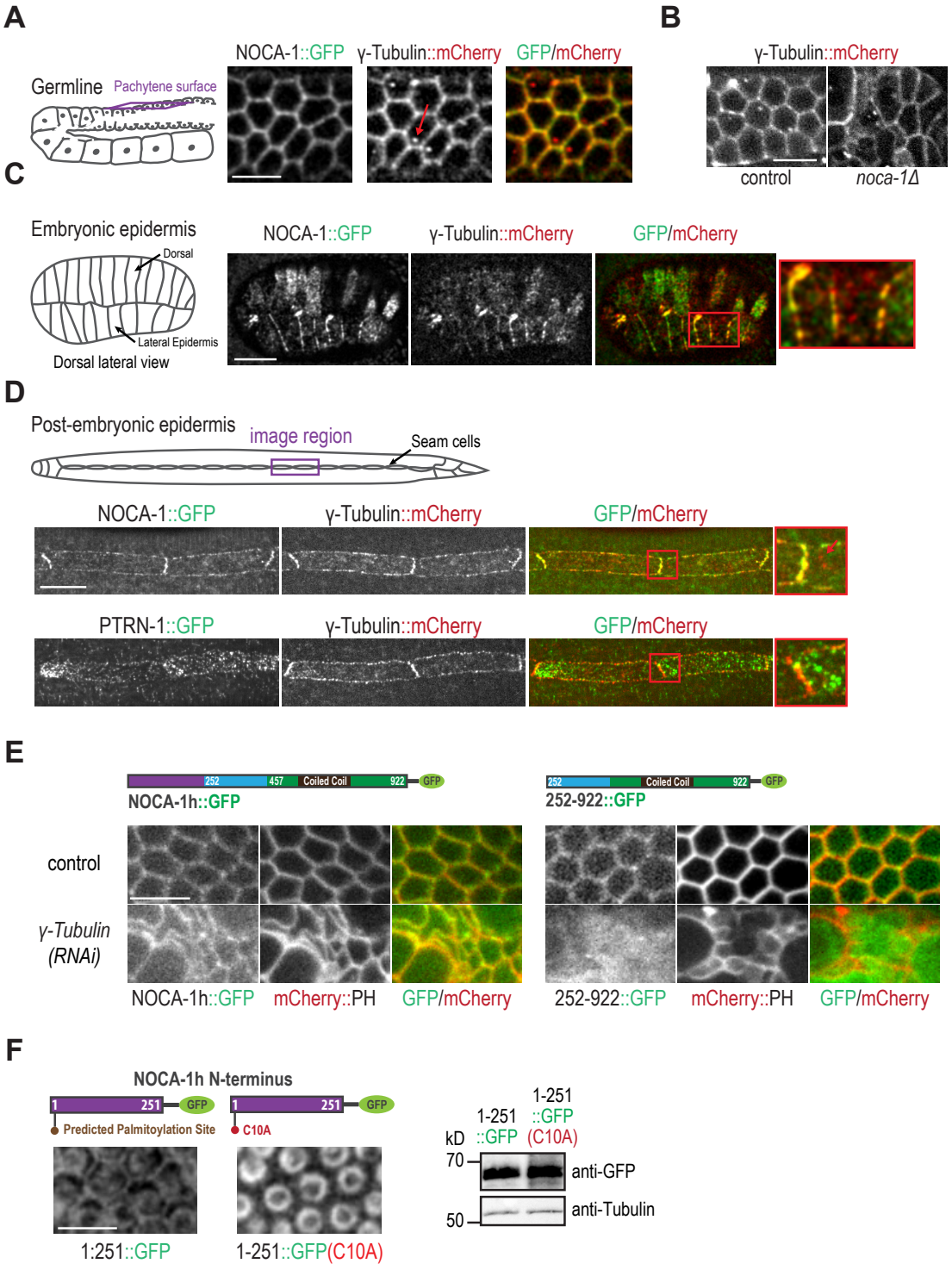
A
NOCA-1::GFP
γ-Tubulin::mCherry
GFP/mCherry
Germline
Pachytene surface
B
γ-Tubulin::mCherry
control
noca-1Δ
C
Embryonic epidermis
Dorsal
Lateral Epidermis
Dorsal lateral view
NOCA-1::GFP
γ-Tubulin::mCherry
GFP/mCherry
D
Post-embryonic epidermis
image region
Seam cells
NOCA-1::GFP
γ-Tubulin::mCherry
GFP/mCherry
PTRN-1::GFP
γ-Tubulin::mCherry
GFP/mCherry
E
NOCA-1h::GFP
252
457
Coiled Coil
922
GFP
252-922::GFP
control
γ-Tubulin (RNAi)
NOCA-1h::GFP
mCherry::PH
GFP/mCherry
252-922::GFP
mCherry::PH
GFP/mCherry
F
NOCA-1h N-terminus
1
251
GFP
Predicted Palmitoylation Site
C10A
1:251::GFP
1-251::GFP(C10A)
kD
1-251 ::GFP
1-251 ::GFP (C10A)
70
50
anti-GFP
anti-Tubulin

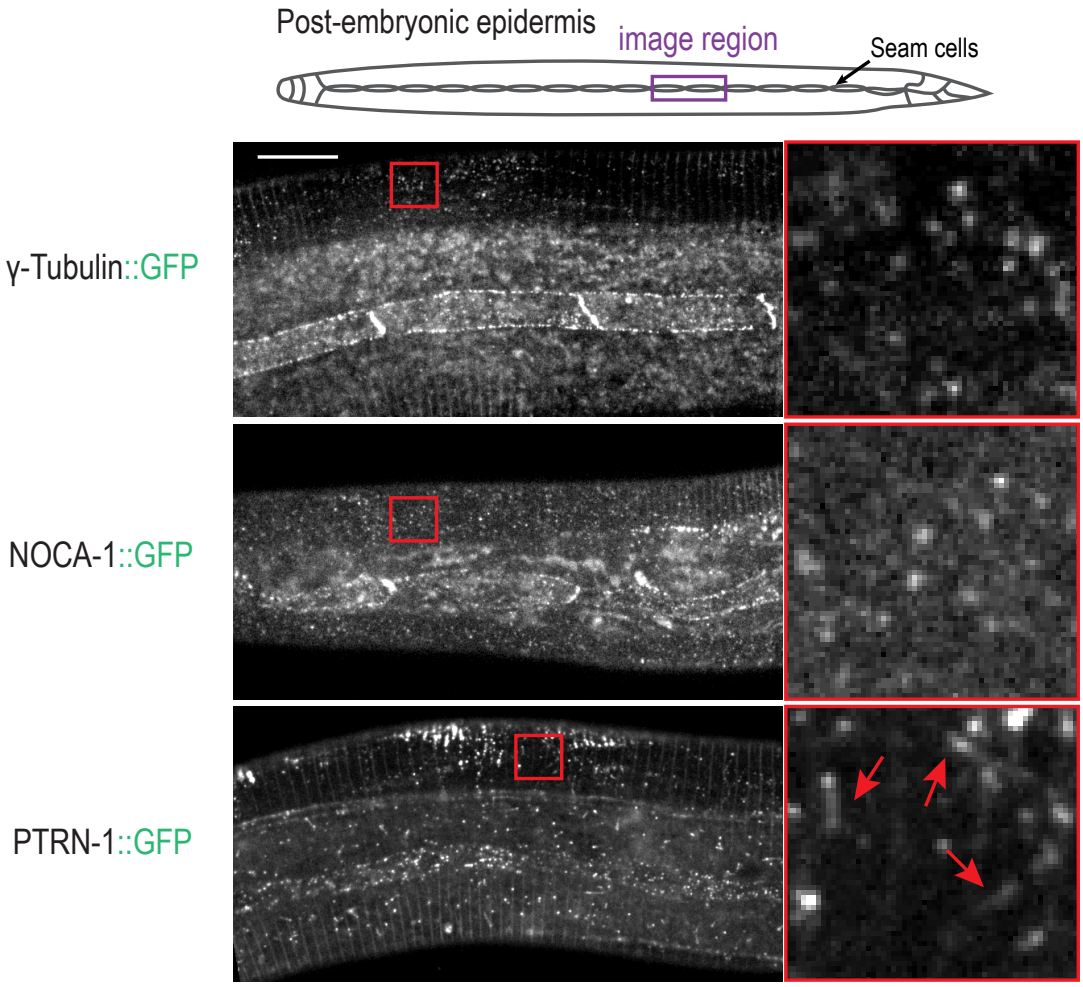

Figure 2.12: PTRN-1, but not NOCA-1 and γ-tubulin, has short stretch localization patterns.
Top: schematic of the imaged region in the post-embronic epidermis. Bottom: images of worms expressing indicated transgenes.
Scale bar, 10 μm. Note that the vertical lines in all images are green autofluorescence of the cuticle.

2.3.7 Purified NOCA-1 and PTRN-1 bind to the MT ends

The relatively sparse MTs in post-embryonic epidermis allowed us to analyze the localization of NOCA-1 and PTRN-1 in relation to the MTs. We found that both NOCA-1::GFP and PTRN-1::GFP could localize onto tagRFP labeled MTs (Figure 2.13A). In the case of both NOCA-1 and PTRN-1, some GFP punctates or stretches were clearly at the MT ends, while others appeared to be on the MT lattice of MT bundles (Figure 2.13A). Thus, NOCA-1 and PTRN-1 may bind to MTs to fulfill their functions. To determine whether NOCA-1 and PTRN-1 bind to MTs, we started with a MT co-sedimentation assay from the worm lysate. We found that both NOCA-1 and PTRN-1 co-sedimented with taxol-stabilized MTs from the worm lysate, suggesting they could both bind to MTs, either directly or indirectly (Figure 2.13B).

To characterize the biochemical activity of NOCA-1 and PTRN-1, we purified recombinant NOCA-1 fragment, PTRN-1 and *Drosophila* Patronin (DmPatronin) from baculovirus infected insect cells (Figure 2.13C). The DmPatronin was previously shown to bind to the MT minus ends, thus serving as a positive control for minus end binding (Goodwin and Vale, 2010). We determined the native molecular weight of the purified proteins using a method combining gel filtration and sucrose gradient analysis (Siegel and Monty, 1966), and found that NOCA-1 was dimers, while PTRN-1 and DmPatronin were monomers in solution (Table 2.1). The ratio of Smax and S for both NOCA-1 fragments are close to 2.0, indicating

that the protein dimer has a slightly elongated shape (Table 2.1; Siegel and Monty, 1966).

Table 2.1: Hydrodynamic analysis for NOCA-1 and PTRN-1

GFP&His tagged	S value	Rs (nm)	Mr S-M (Kd)	Mr aa(Kd)	Smax/S
DmPatronin	9.23	6.1	236.8	219.6	2.15
PTRN-1	7.7	5.5	178.1	153.3	1.88
NOCA-1h (252-922)	8.73	6.4	234.9	104.3	1.98
NOCA-1h (457-922)	8.18	5.1	175.4	81.7	2.12

We then tested whether NOCA-1 and PTRN-1 directly bind to the MTs and whether they bind to the MT ends using a MT anchoring assay (Goodwin and Vale, 2010). In this assay, GFP labeled test proteins were immobilized onto the coverslip through GFP antibodies and rhodamine labeled MTs were subsequently added for visualization analysis. There are three possible outcomes: no binding, end binding or lattice binding. In a GFP-His negative control, no MTs were stably attached to the coverslip, indicative of no binding. In the end binding conrol of DmPatronin, most MTs were attached to the coverslip through one end, while the other end cound wiggle around. In the lattice binding control of a kinesin motor domain (K560-GFP), MTs were stably attached from the side, thus no obvious movement could be observed. The differences between MT end binding and side

bindng can be easily visualized in the maximum intensity projection of time lapse images, where a fan-out MT appearance indicates end binding and a linear MT appearance indicates side binding. Using this assay, we found that purified NOCA-1 and PTRN-1 can both bind to the MT ends (Figure 2.13D).

To determine which ends NOCA-1 and PTRN-1 may bind to, we used a kinesin gliding assay. In this assay, a conventional kinesin motor K560 was immobilized on the coverslip and red MTs were added in the presence of Mg^{2+} and ATP to allow kinesin-driven MT movement. Since conventional kinesin moves to the MT plus ends, the leading MT ends in this assay are the minus ends (Figure 2.13E). As the positive control DmPatronin, PTRN-1 also bound specifically to the MT minus ends (Figure 2.13E). However, the gliding assay requires the test protein to function in low salt buffer ($\leq$ 100 mM), but purified NOCA-1 protein do not. For the time being, we could not yet determine which MT ends that NOCA-1 binds to, although we have tried a number of buffer conditions for NOCA-1 fragments (252-922), (457-922) with or without GFP tag, as well as the NOCA-1 homolog from the closely related nematode *C. briggsae*. This lack of functionality in solutions may indicate a missing binding partner of NOCA-1 has to be present for its proper function. To conclude, we found that NOCA-1 and PTRN-1 can both bind to the MT ends, and PTRN-1 specifically binds to the minus ends.

Figure 2.13: NOCA-1 uses specific isoforms for functions in different tissues.
(A) Top and middle: images of worms expressing indicated transgenes. Bottom: schematic showing the imaged region.
(B) Immunoblots and coomassie staining of protein pellets from worm lysates with indicated treatments. DMSO is solvent control, nocodazole depolymerizes MTs and taxol stabilizes MTs.
(C) Left: schematic showing recombinant proteins purified from baculovirus infected insect cells or bacteria (only K560-GFP-His is from bacteria). Right: coomassie staining of indicated recombinant proteins.
(D) Left: schematic showing the experiment set up and image processing. Middle: representative images showing end binding or lattice binding of MTs. Right: plot of percentage of end-binding or lattice binding of indicated recombinant proteins.
(E) Left: schematic showing the experiment set up. Middle: kymographs showing gliding MTs with the leading end ends decorated by green dots. Right: plot of percentage of plus end binding, minus end binding or lattice binding for indicated recombinant proteins.
Scale bars, 10 μm.

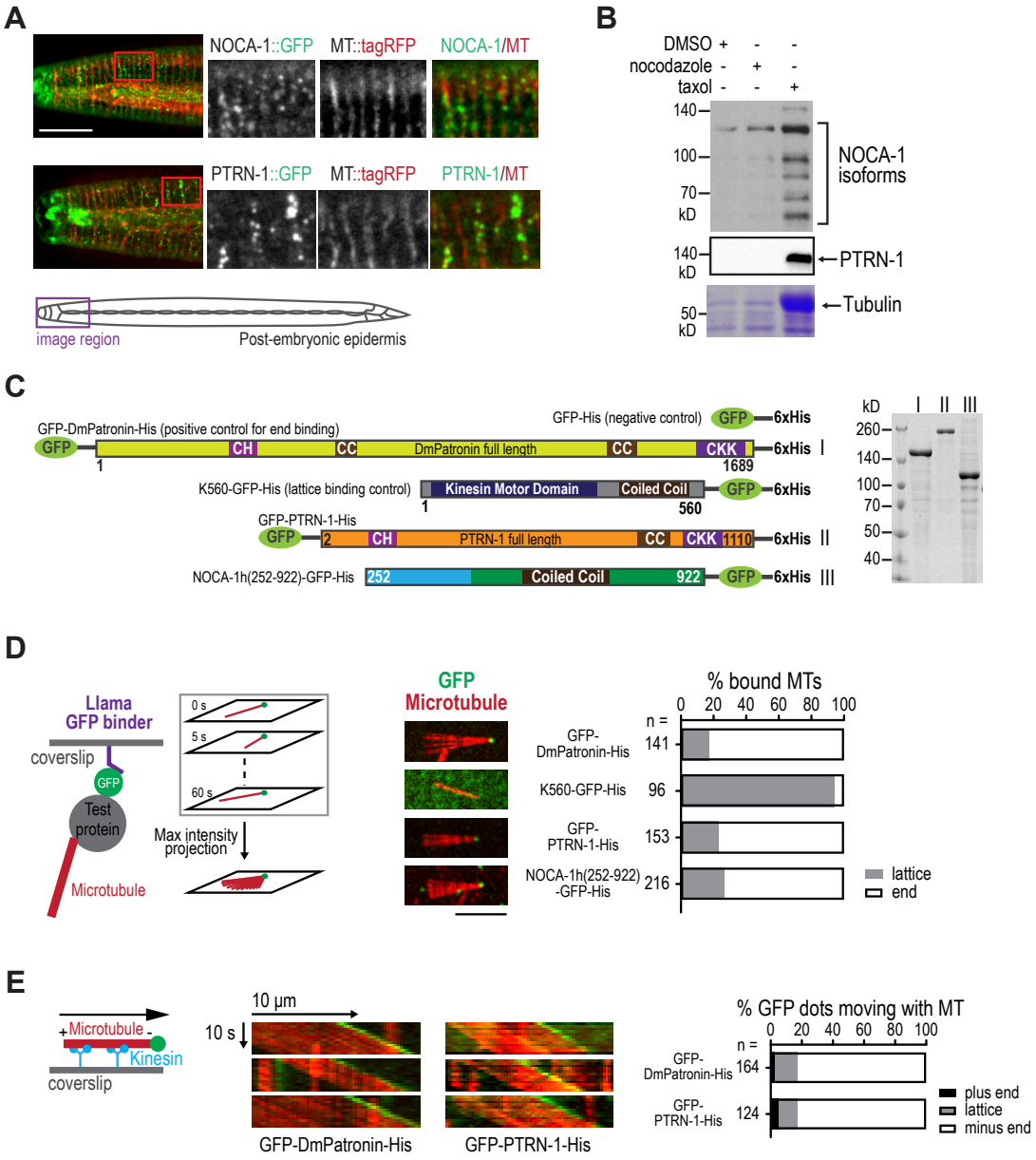
A
NOCA-1::GFP
MT::tagRFP
NOCA-1/MT
PTRN-1::GFP
MT::tagRFP
PTRN-1/MT
image region
Post-embryonic epidermis
B
DMSO + - -
nocodazole - + -
taxol - - +
140
100
70
kD
NOCA-1 isoforms
140 kD
PTRN-1
50 kD
Tubulin
C
GFP-DmPatronin-His (positive control for end binding)
GFP
CH
CC
DmPatronin full length
CC
CKK
6xHis
1
1689
I
GFP-His (negative control)
K560-GFP-His (lattice binding control)
Kinesin Motor Domain
Coiled Coil
1
560
GFP-PTRN-1-His
2
PTRN-1 full length
1110
II
NOCA-1h(252-922)-GFP-His
252
Coiled Coil
922
III
kD
260
140
100
70
50
40
D
Llama GFP binder
coverslip
GFP
Test protein
Microtubule
0 s
5 s
60 s
Max intensity projection
GFP Microtubule
% bound MTs
0 20 40 60 80 100
n =
GFP-DmPatronin-His 141
K560-GFP-His 96
GFP-PTRN-1-His 153
NOCA-1h(252-922) -GFP-His 216
lattice
end
E
+Microtubule-
Kinesin
coverslip
10 µm
10 s
GFP-DmPatronin-His
GFP-PTRN-1-His
% GFP dots moving with MT
0 20 40 60 80 100
n =
GFP-DmPatronin-His 164
GFP-PTRN-1-His 124
plus end
lattice
minus end

2.4 Discussion

In this study, we have found that NOCA-1 is a novel MT end binding protein that controls non-centrosomal MT array formation in multiple *C. elegans* tissues, either on its own or in parallel with a minus end binding protein PTRN-1. Genetic analysis and transgene rescue experiments show that two distinct long NOCA-1 isoforms are required to assemble non-centrosomal arrays in the germline and embryonic epidermis, while a short NOCA-1 isoform and PTRN-1 function together to promote non-centrosomal array assembly in the post-embryonic epidermis. Mechanistically, both NOCA-1 and PTRN-1 can localize to MT ends in cells, co-sediment with taxol-stabilized MTs from worm lysates and bind to the MT ends in vitro. This study identified a new class of MT end binding protein represented by NOCA-1 and established the functional importance of MT end binding proteins in non-centrosomal MT array formation in the context of a developing organism for the first time.

2.4.1 NOCA-1 is a novel MT end binding protein

Several lines of evidence support that NOCA-1 binds to MTs and to the MT ends. First, NOCA-1::GFP can localize to the MT ends in post-embryonic epidermis (Figure 2.13A). Second, NOCA-1 co-sediments with taxol-stabilized MTs from the worm lysate (Figure 2.13B), where many MT associating proteins are competing for the binding sites on MTs. Third, purified NOCA-1 binds to the MT

ends as demonstrated in the MT anchoring assay (Figure 2.13D). Nonetheless, we want to point out that the MT anchoring assay may not represent the physiological condition, since it assays the coverslip immobilized protein aggregates. It would be ideal to examine the MT binding in solution based assays, such as the kinesin gliding assay used for DmPatronin and PTRN-1, but purified NOCA-1 behaves poorly in low salt buffer, preventing the analysis using solution based assays. On the other hand, NOCA-1 does localize at some MT ends in post-embryonic epidermis (Figure 2.13A) and MT end binding is not commonly seen, arguing that the MT end binding of NOCA-1 is real. Thus, we propose that NOCA-1 represents a new class of MT end binding protein.

Alternatively, NOCA-1 could stimute the MT nucleation activity of γ-tubulin. In the germline, embryonic and post-embryonic epidermis, NOCA-1 co-localizes with γ-tubulin at non-centrosomal sites, although it is not reqruied to recruit γ-tubulin (Figure 2.11A-D). However, a functional NOCA-1 truncation in the germline requires γ-tubulin for its plasma membrane localization (Figure 2.9B, Figure 2.11E). Thus, it is plausible that the γ-tubulin complex needs to recruit NOCA-1 for its nucleation activity. However, NOCA-1 is not found at the centrosomes in the germline, where γ-tubulin is also localized to (Figure 2.11A), suggesting that either γ-tubulin need to be activated on the plasma membrane, or the nucleated MTs rather than γ-tubulin itself are recruiting NOCA-1.

2.4.2 PTRN-1 selectively binds to the MT minus ends

PTRN-1 belongs to the CAMSAP protein family, whose members have been shown to bind to the MT minus ends. The only *Drophophila* homolog of CAMSAP, Patronin, and the three human CAMSAPs, CAMSAP1/2/3, are all shown to bind specifically to the MT minus ends (Meng *et al.*, 2008; Goodwin and Vale, 2010; Jiang *et al.*, 2014; Hendershott and Vale, 2014). Here we presented direct evidence to show that PTRN-1 also binds specifically to the MT minus ends. Most importantly, purified PTRN-1 binds to the leading ends of gliding MTs in the kinesin gliding assay (Figure 2.13E). Thus, it seems that minus end binding is a conserved activity of the CAMSAP family members.

However, there are some interesting differences among the characterized CAMSAP proteins, although all of them can bind to the minus ends. First, human CAMSAPs and DmPatronin affect the minus end dynamics differently. Binding of CAMSAP2, CAMSAP3 and DmPatronin dramatically slows down the minus end polymerization rate and stabilize the ends from being depolymerization by either kinesin-13 or breakage (Goodwin and Vale, 2010; Jiang *et al.*, 2014; Hendershott and Vale, 2014), but CAMSAP1 does not affect the minus end polymerization and does not confer stability (Jiang *et al.*, 2014). Second, CAMSAP2 and CAMSAP3 decorate a short MT stretch as they track the growing minus ends, while CAMSAP1 and DmPatronin only track the ends without forming stretches (Jiang *et al.*, 2014; Hendershott and Vale, 2014). The short MT stretches decorated by CAM-

SAP2 and CAMSAP3 can serve as "MT seeds" for MT outgrowth in mammalian cells (Jiang *et al.*, 2014). Third, human CAMSAPs and DmPatronin use different domains to achieve minus end binding and stabilization. CAMSAPs use their CKK domain for minus end binding, while an additional MBD domain in CAMSAP2 and CAMSAP3 is reqruied for MT stabilization. In contrast, DmPatronin uses a different domain containing the coiled coil region for minus end binding and its CKK domain for MT stabilization (Jiang *et al.*, 2014; Hendershott and Vale, 2014).

Interestingly, PTRN-1 can form short stretches in the post-embryonic epidermis (Figure 2.12), suggesting that PTRN-1 may function similarly to CAMSAP2 and CAMSAP3 in mammalian cells. Our in vitro study only looked at binding of PTRN-1 to GMPCPP stabilized MTs. It will be interesting to test with dynamic MTs to see whether PTRN-1 binding affects the minus end dynamics and whether it decorates short MT stretches. It is also interesting to determine whether PTRN-1 uses its C-terminal CKK domain or other domains for the minus end binding.

2.4.3 NOCA-1 and PTRN-1 are different

Although NOCA-1 and PTRN-1 are genetically redundant in post-embryoni epidermis, they share no sequence similarity and have different functions. First, NOCA-1 is required in the germline for MT array formation and thus for organismal fertility. Although PTRN-1 is not endogenously expressed in the germline,

ectopic expression of PTRN-1 in the germline fails to complement the NOCA-1 function, indicating they are not interchangeable. Second, both NOCA-1 and PTRN-1 are endogenously expressed in the embryonic epidermis, but only NOCA-1 is reqruied for the MT-dependent nuclear migration (Figure 2.6D). In both cases, a long NOCA-1 isoform is functioning and the long-isoform domain is reqreuid for their functions (Figure 2.9B and D). The presence of this long-isoform domain may account for NOCA-1 specific functions that cannot be replaced by PTRN-1.

Additionally, the MT arrays in post-embryonic epidermis are differently affected by *noca-1*Δ and *ptrn-1*Δ. We found fewer dynamic MTs in *noca-1*Δ mutants and more dynamic MTs in *ptrn-1*Δ worms. In addition, MTs in *ptrn-1*Δ mutants are slightly more fragmented (Figure 2.4E). The nature of this phenotypic difference is currently not understood. One clue is the different localization of NOCA-1 and PTRN-1: NOCA-1 co-localizes with γ-tubulin, while PTRN-1 does not (Figure 2.11A, C and D). We speculate that NOCA-1 may stabilize the minus ends generated by γ-tubulin dependent nucleation, while PTRN-1 prefers binding to the minus ends generated by MT severing, or recruits MT severing enzymes (discussed later). Under this speculation, the plus ends generated by these two means can be different in terms of nucleotide state or tubulin modifications, thus explaining the different MT dynamics in *noca-1*Δ and *ptrn-1*Δ worms. It will be interesting to test whether MT severing contributes to MT generation and whether PTRN-1 would follow the MT severing enzymes in this tissue.

2.4.4 MTs: two ways to generate, two ways to stabilize?

Assembly of non-centrosomal MT arrays often involves localized MT generation and minus end stabilization/anchoring. MTs can be generated by γ-TuRC mediated nucleation or MT severing mediated amplification. In the case of γ-TuRC mediated nucleation, it is conceptually possible that γ-TuRC remains at and protects/anchors the MT minus ends. However, MT nucleation and anchoring are separable events even at mitotic centrosomes, where γ-TuRC mediated nulceation dominates the MT generation (Dammermann *et al.*, 2003). Ninein is a good candidate for minus end anchoring in this case, although in vitro work is required to clarify its biochemical activity (Mogensen *et al.*, 2000). We showed here that NOCA-1 is a novel MT end binding protein required for MT array formation and it closely follows the localization of γ-tubulin. We speculate that NOCA-1 might protect the ends of MTs released from γ-TuRC, although direct evidence for this idea is difficult to obtain.

MT severing is another way to generate more MTs. The MT severing enzymes katanin and spastin have been shown to generate MTs in meiotic spindle assembly, neurite outgrowth, axon branching and plant cortical arrays re-orientation (McNally *et al.*, 2006; Yu *et al.*, 2008; Lindeboom *et al.*, 2013b). For effective generation of "MT seeds", the MT severing activities need to be closely regulated to prevent complete MT disassembly, and the exposed MT ends need be stabilized. Interestingly, CAMSAP2 and CAMSAP3 are recently reported to recruit

the MT severing enzyme katanin to regulate the lengths of CAMSAP2/3 stabilized MT stretches (Jiang *et al.*, 2014). We showed in this study that PTRN-1 also forms short stretches in the post-embryonic epidermis (Figure 2.12), suggesting that PTRN-1 might use a similar mechanism to control the lengths of stabilized MT stretches. It will be interesting to test whether MT severing enzymes are recruited by PTRN-1 in the post-embryonic epidermis and whether they are required to regulate the lengths of PTRN-1 stretches.

2.4.5 Functions of the circumferential MT arrays in post-embryonic epidermis

The circumferential MT arrays in post-embryonic epidermis of *C.elegans* may be important for secreting the cuticle, a multi-layer collagenous extracellular matrix serving as a protective barrier (Page and Johnstone, 2007). Due to the limited stretchability of the cuticle, worms periodically secrete a larger new cuticle to replace the smaller old one to allow body growth (a phenomenon called molting; Page and Johnstone, 2007). The cuticle is not smooth, but is patterned with circumferential ridges termed annuli except at two seams. During each molting, circumferential actin filament bundles precisely delineating the annular furrows are assembled and these actin filaments are proposed to establish the annular patterns (Costa *et al.*, 1997). However, these actin filaments bundles disassemble after the outer layer cuticle is synthesized, so the inner layers of cuticle have to be synthe-

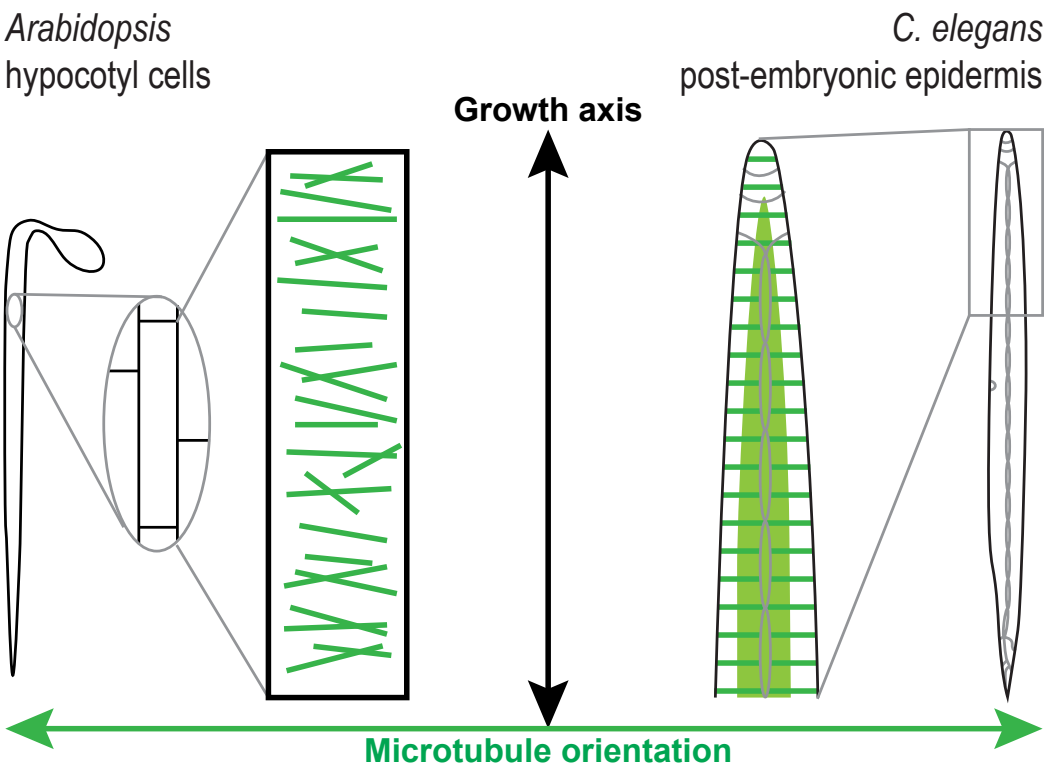

Figure 2.14: MT orientation is perpendicular to the growth axis in both plant and animal cells.

sized in the absence of circumferential actin filaments (Page and Johnstone, 2007). In contrast, the circumferential MT array is present throughout animal growth and they also match the annular patterns, suggesting they may be important to transport cuticle components or processing enzymes. In support of this idea, when this circumferential array is disrupted in *noca-1*Δ*;ptrn-1*Δ double mutants, the worms grow much slower and their cuticles become permeable to a DNA dye (Figure 2.2B and C), both are indicative of cuticle defects. Therefore, we propose that the circumferential MT arrays in post-embryonic epidermis are important for normal cuticle secretion and thus for normal organismal growth.

Interestingly, this proposed body growth mechanism closely resembles the growth mechanism of *Arabidopsis* hypocotyl cells. Plant cells have cell walls which are made of cellulose microfibrils. During the elongation of plant hypocotyl cells, the cortical MT arrays are transversely oriented to guide cellulose deposition. In fact, a fluorescence labeled cellulose synthase was observed to move along cortical MTs (Paredez *et al.*, 2006). In both *C. elegans* epidermis and *Arabidopsis* hypocotyl cells, MT arrays are transversely oriented so that they are perpendicular to the major growth axis (Figure 2.14). Moreover, both the cuticle of *C. elegans* epidermis and the cell wall of *Arabidopsis* hypocotyl cells are patterned similarly to the MT arrays. This intriguing similarity may suggest a common strategy of using MT cytoskeleton to direct organismal or cellular growth that are comfined by non-stretchable extracellular matrix or cell walls. It will be particularly interesting to examine whether cuticle syntheis is affected when circumferential MT arrays are

disrupted and whether cuticle components move long the MTs.

In summary, this study shows that MT end binding proteins are important to organize non-centrosomal MT arrays in multiple *C. elegans* tissues. In particular, NOCA-1 is a novel MT end binding protein, which functions in parallel with PTRN-1 to promote assembly of circumferential MT arrays in the post-embryonic epidermis. We propose that these circumferential arrays serve as transportation tracks for cuticle components during cuticle secretion, and MT end binding proteins promote their assembly by stabilizing MTs. The stabilization conferred by MT end binding — probably minus end binding — is likely broadly required to promote non-centrosomal MT array assembly.

2.5 Material and methods

2.5.1 Worm Strains

Table 2.2: Strains used in Chapter 2

Strain#	**Genotype**
OD522	unc-119(ed3)III; ltSi62[pOD1110/pSW008; CEOP3608 TBG-1::mCherry; cb-unc-119(+)]II
OD523	unc-119(ed3)III; ltSi63[pOD1111/pSW009; CEOP3608 TBG-1::GFP; cb-unc-119(+)]II

Table 2.2: Strains used in Chapter 2 (continued)

Strain#	Genotype
OD528	unc-119(ed3)III; ttTi22935 V (Mos1 insertion)
OD690	unc-119(ed3)III; ltSi159[pOD1113/pSW031; P-CEOP3608::noca-1g(cDNA)::GFP; cb-unc-119(+)]II
OD721	unc-119(ed3)III; ltSi173[pOD1114/pSW046; Pnoca-1::noca-1gh; cb-unc-119(+)]II
OD722	unc-119(ed3)III; ltSi174[pOD1115/pSW053; Pnoca-1::noca-1gh; cb-unc-119(+)]I
OD723	noca-1(ok3692)V/nT1[qIs51](IV;V)
OD726	ltSi77[pOD1112/pSW032; Plbp-1::mCherry; cb-unc-119(+)]V
OD729	unc-119(ed3)III; ltSi180[pOD1115/pSW053; Pnoca-1::noca-1gh; cb-unc-119(+)]I
OD739	unc-119(ed3)III?; ltSi173[pOD1114/pSW046; Pnoca-1::noca-1gh; cb-unc-119(+)]II; noca-1(ok3692)V
OD747	unc-119(ed3) III; ttTi21011 X
OD752	unc-119(ed3)III; ltSi182[pOD1237/pSW055; Pnoca-1::noca-1abcfgh; cb-unc-119(+)]II
OD753	unc-119(ed3)III; ltSi183[pOD1238/pSW047; Pptrn-1::ptrn-1::mCherry; cb-unc-119(+)]II

Table 2.2: Strains used in Chapter 2 (continued)

Strain#	Genotype
OD758	unc-119(ed3)III?; ltSi182[pOD1237/pSW055; Pnoca-1::noca-1abcfgh; cb-unc-119(+)]II; noca-1(ok3692)V
OD843	unc-119(ed3) III?; ltIs38 [pAA1; pie-1/GFP::PH(PLC1delta1); unc-119 (+)]; ltIs37 [pAA64; pie-1/mCHERRY::his-58; unc-119 (+)] IV; noca-1(ok3692)V/nT1[qIs51](IV;V)
OD851	unc-119(ed3) III?; ltSi62[pOD1110/pSW008; CEOP3608 TBG-1::mCherry; cb-unc-119(+)]II; noca-1(ok3692)V/nT1[qIs51](IV;V)
OD852	unc-119(ed3)III; ltSi211[pOD1245/pSW065; Pnoca-1::noca-1abcfgh-mCherry; cb-unc-119(+)]II
OD854	ptrn-1(lt1::cb-unc-119+)X
OD862	unc-119(ed3)III; ltSi215[pOD1247/pSW074; Pnoca-1h::GFP-PH(PLC1delta1); cb-unc-119(+)]II
OD866	ltSi219[pOD1248/pSW076; Pmex-5::GFP-PH(PLC1delta1)-operon-linker-mCherry-his-11; cb-unc-119(+)]I
OD868	ltSi220[pOD1249/pSW077; Pmex-5::GFP-tbb-2-operon-linker-mCherry-his-11; cb-unc-119(+)]I

Table 2.2: Strains used in Chapter 2 (continued)

Strain#	Genotype
OD870	unc-119(ed3)III; ltSi222[pOD1250/pSW078; Plbp-1::GFP-tbb-2-operon-linker-mCherry-his-11; cb-unc-119(+)]I
OD872	unc-119(ed3)III?; ltSi211[pOD1245/pSW065; Pnoca-1::noca-1abcfgh-mCherry; cb-unc-119(+)]II; noca-1(ok3692)V
OD891	noca-1(ok3692)V/nT1[qIs51](IV;V); ptrn-1(lt1::cb-unc-119+)X
OD893	unc-119(ed3)III?; ltSi183[pOD1238/pSW047; Pptrn-1::ptrn-1::mCherry; cb-unc-119(+)]II; ptrn-1(lt1::cb-unc-119+)X
OD952	unc-119(ed3)III; ltSi246[pOD1270/pSW082; Pnoca-1::noca-1abcfgh-sGFP; cb-unc-119(+)]II
OD953	ltSi183[pOD1238/pSW047; Pptrn-1::ptrn-1::mCherry; cb-unc-119(+)]II; unc-119(ed3)III?; noca-1(ok3692)V/nT1[qIs51](IV;V); ptrn-1(lt1::cb-unc-119+)X
OD961	ltSi249[pOD1274/pSW098; Pdlg-1delta7::dlg-1-GFP::unc-54-3'UTR; cb-unc-119(+)]I
OD998	ltSi246[pOD1270/pSW082; Pnoca-1::noca-1abcfgh-sGFP; cb-unc-119(+)]II; noca-1(ok3692)V

Table 2.2: Strains used in Chapter 2 (continued)

Strain#	Genotype
OD1108	unc-119(ed3)III; ltSi323[pOD1297/pSW129; Pnoca-1h::noca-1g(cDNA)::sGFP; cb-unc-119(+)]II
OD1110	unc-119(ed3)III; ltSi325[pOD1298/pSW130; Pnoca-1h::noca-1c(cDNA)::sGFP; cb-unc-119(+)]II
OD1112	unc-119(ed3)III; ltSi327[pOD1299/pSW131; Pnoca-1h::noca-1a(cDNA)::sGFP; cb-unc-119(+)]II
OD1113	unc-119(ed3)III; ltSi328[pOD1300/pSW132; Pnoca-1h::noca-1d(cDNA)::sGFP; cb-unc-119(+)]II
OD1219	ItSi174[pOD1115/pSW053; Pnoca-1::noca-1gh; cb-unc-119(+)]I; unc-119(ed3)III?; noca-1(ok3692)V/nT1[qIs51](IV;V); ptrn-1(lt1::cb-unc-119+)X
OD1221	ItSi182[pOD1237/pSW055; Pnoca-1::noca-1abcfgh; cb-unc-119(+)]II; unc-119(ed3)III?; noca-1(ok3692)V/nT1[qIs51](IV;V); ptrn-1(lt1::cb-unc-119+)X
OD1223	unc-119(ed3)III; ltSi364[pOD1330/pSW147; Pnoca-1h::noca-1g(1-251)::sGFP; cb-unc-119(+)]II
OD1225	unc-119(ed3)III; ltSi366[pOD1332/pSW149; Pnoca-1h::noca-1g(457-922)::sGFP; cb-unc-119(+)]II

Table 2.2: Strains used in Chapter 2 (continued)

Strain#	Genotype
OD1227	unc-119(ed3)III; ltSi368[pOD1334/pSW151; Pnoca-1h::noca-1g(252-922)::sGFP; cb-unc-119(+)]II
OD1233	ltSi369[pOD1335/pSW152; Pnoca-1h::noca-1gRR::sGFP; cb-unc-119(+)]II
OD1339	unc-119(ed3)III; ltSi417[pOD1342/pSW159; Pnoca-1de::noca-1de::mCherry; cb-unc-119(+)]II
OD1345	ltSi417[pOD1342/pSW159; Pnoca-1de::noca-1de::mCherry; cb-unc-119(+)]II; unc-119(ed3)III?; noca-1(ok3692)V/nT1[qIs51](IV;V); ptrn-1(lt1::cb-unc-119+)X
OD1359	ltSi716[pOD1935/pDC208; Pmex-5::EBP-2::GFP::tbb-2_3'UTR; cb-unc-119(+)]I; unc-119(ed3)III
OD1394	ltSi443[pOD1471/pSW182; Pnoca-1h::noca-1g(1-251)::sGFP (C10A); cb-unc-119(+)]II; unc-119(ed3)III
OD1398	ltSi447[pOD1469/pSW181; Ppha-4in1::ptrn-1a::opLinker::mCherry-histone; cb-unc-119(+)]II
OD1426	ltSi449[pOD1461/pSW173; Plbp-1::EBP-2-GFP::opLinker::mCherry-PH; cb-unc-119(+)]I; unc-119(ed3)III

Table 2.2: Strains used in Chapter 2 (continued)

Strain#	Genotype
OD1431	ltSi454[pOD1479/pSW190; Pptrn-1::noca-1d(cDNA)::mCherry; cb-unc-119(+)]II; unc-119(ed3)III
OD1432	ltSi455[pOD1480/pSW191; Pptrn-1::noca-1h(457-922)::mCherry; cb-unc-119(+)]II; unc-119(ed3)III
OD1442	ltSi458[pOD1477/pSW188; Pnoca-1d::noca-1d(cDNA)::mCherry; cb-unc-119(+)]II; unc-119(ed3)III
OD1443	ltSi459[pOD1478/pSW189; Pnoca-1e::noca-1e(cDNA)::mCherry; cb-unc-119(+)]II; unc-119(ed3)III
OD1446	ltSi461[pOD1340/pSW157; Pnoca-1::noca-1abcgh (STOP in the first exon of isoform f); cb-unc-119(+)]II; unc-119(ed3)III
OD1504	ltSi449[pOD1461/pSW173; Plbp-1::EBP-2-GFP::opLinker::mCherry-PH; cb-unc-119(+)]I; unc-119(ed3)?III; noca-1(ok3692)V/nT1[qIs51](IV;V)
OD1505	ltSi449[pOD1461/pSW173; Plbp-1::EBP-2-GFP::opLinker::mCherry-PH; cb-unc-119(+)]I; unc-119(ed3)?III; ltSi77[pOD1112/pSW032; Plbp-1::mCherry; cb-unc-119(+)]V

Table 2.2: Strains used in Chapter 2 (continued)

Strain#	Genotype
OD1508	ltSi454[pOD1479/pSW190; Pptrn-1::noca-1d(cDNA)::mCherry; cb-unc-119(+)]II; unc-119(ed3)?III; noca-1(ok3692)V/nT1[qIs51](IV;V); ptrn-1(lt1::cb-unc-119+)X
OD1509	ltSi455[pOD1480/pSW191; Pptrn-1::noca-1h(457-922)::mCherry; cb-unc-119(+)]II; unc-119(ed3)?III; noca-1(ok3692)V/nT1[qIs51](IV;V); ptrn-1(lt1::cb-unc-119+)X
OD1510	ltSi249[pOD1274/pSW098; Pdlg-1delta7::dlg-1-GFP::unc-54-3'UTR; cb-unc-119(+)]I; noca-1(ok3692)V/nT1[qIs51](IV;V)
OD1511	ltSi249[pOD1274/pSW098; Pdlg-1delta7::dlg-1-GFP::unc-54-3'UTR; cb-unc-119(+)]I; ptrn-1(lt1::cb-unc-119+)X
OD1512	ltSi249[pOD1274/pSW098; Pdlg-1delta7::dlg-1-GFP::unc-54-3'UTR; cb-unc-119(+)]I; noca-1(ok3692)V/nT1[qIs51](IV;V); ptrn-1(lt1::cb-unc-119+)X
OD1516	ltSi458[pOD1477/pSW188; Pnoca-1d::noca-1d(cDNA)::mCherry; cb-unc-119(+)]II; unc-119(ed3)?III; noca-1(ok3692)V/nT1[qIs51](IV;V); ptrn-1(lt1::cb-unc-119+)X

Table 2.2: Strains used in Chapter 2 (continued)

Strain#	Genotype
OD1517	ltSi459[pOD1478/pSW189; Pnoca-1e::noca-1e(cDNA)::mCherry; cb-unc-119(+)]II; unc-119(ed3)?III; noca-1(ok3692)V/nT1[qIs51](IV;V); ptrn-1(lt1::cb-unc-119+)X
OD1521	ltSi461[pOD1340/pSW157; Pnoca-1::noca-1abcgh (STOP in the first exon of isoform f); cb-unc-119(+)]II; unc-119(ed3)?III; noca-1(ok3692)V
OD1558	ltSi518[pOD1338/pSW155; Pnoca-1::noca-1acfgh(STOP coden in the first exon of isoform b); cb-unc-119(+)]II; unc-119(ed3)III
OD1578	ltSi523[pOD1339/pSW156; Pnoca-1::noca-1abfgh(STOP coden in the first exon of isoform c); cb-unc-119(+)]II; unc-119(ed3)III
OD1580	ltSi518[pOD1338/pSW155; Pnoca-1::noca-1acfgh(STOP coden in the first exon of isoform b); cb-unc-119(+)]II; unc-119(ed3)III?; noca-1(ok3692)V
OD1600	ltSi523[pOD1339/pSW156; Pnoca-1::noca-1abfgh(STOP coden in the first exon of isoform c); cb-unc-119(+)]II; unc-119(ed3)III?; noca-1(ok3692)V
OD1605	ltSi531[pOD1337/pSW154; Pnoca-1::noca-1bcfgh(STOP coden in the first exon of isoform a); cb-unc-119(+)]II; unc-119(ed3)III

Table 2.2: Strains used in Chapter 2 (continued)

Strain#	Genotype
OD1606	ltSi531[pOD1337/pSW154; Pnoca-1::noca-1bcfgh(STOP coden in the first exon of isoform a); cb-unc-119(+)]II; unc-119(ed3)III?; noca-1(ok3692)V
OD1652	ltSi540[pOD1343/pSW160; Pnoca-1de::noca-1de::sGFP; cb-unc-119(+)]II; unc-119(ed3)III
OD1653	ltSi541[pOD1505/pSW210; Pdpy-7::PTRN-1(cDNA)::sGFP; cb-unc-119(+)]II; unc-119(ed3)III
OD1654	ltSi542[pOD1506/pSW211; Pptrn-1::PTRN-1(cDNA)::sGFP; cb-unc-119(+)]II; unc-119(ed3)III
OD1690	ltSi561[pOD1508/pSW213; Pptrn-1::NOCA-1g(457-922)::sGFP; cb-unc-119(+)]II; unc-119(ed3)III
OD1691	ltSi562[pOD1509/pSW214; Pptrn-1::NOCA-1g(252-922)::sGFP; cb-unc-119(+)]II; unc-119(ed3)III
OD1708	ltSi568[pOD1518/pSW223; Pmex-5::mCherry::PH::tbb-2_3'UTR; cb-unc-119(+)]I; unc-119(ed3)III
OD1709	ltSi569[oxTi185; pOD1110/pSW008; CEOP3608 TBG-1::mCherry; cb-unc-119(+)]I; unc-119(ed3)III

Table 2.2: Strains used in Chapter 2 (continued)

Strain#	Genotype
OD1727	ltSi569[oxTi185; pOD1110/pSW008; CEOP3608 TBG-1::mCherry; cb-unc-119(+)]I; ltSi246[pOD1270/pSW082; Pnoca-1::noca-1abcfgh-sGFP; cb-unc-119(+)]II; unc-119(ed3)III?
OD1731	ltSi568[pOD1518/pSW223; Pmex-5::mCherry::PH::tbb-2_3'UTR; cb-unc-119(+)]I; ltSi369[pOD1335/pSW152; Pnoca-1h::noca-1gRR::sGFP; cb-unc-119(+)]II; unc-119(ed3)III?
OD1735	ltSi540[pOD1343/pSW160; Pnoca-1de::noca-1de::sGFP; cb-unc-119(+)]II; unc-119(ed3)III?; noca-1(ok3692)V/nT1[qIs51](IV;V); ptrn-1(lt1::cb-unc-119+)X
OD1737	ltSi542[pOD1506/pSW211; Pptrn-1::PTRN-1(cDNA)::sGFP; cb-unc-119(+)]II; unc-119(ed3)III?; noca-1(ok3692)V/nT1[qIs51](IV;V); ptrn-1(lt1::cb-unc-119+)X
OD1739	ltSi561[pOD1508/pSW213; Pptrn-1::NOCA-1g(457-922)::sGFP; cb-unc-119(+)]II; unc-119(ed3)III?; noca-1(ok3692)V/nT1[qIs51](IV;V); ptrn-1(lt1::cb-unc-119+)X
OD1740	ltSi562[pOD1509/pSW214; Pptrn-1::NOCA-1g(252-922)::sGFP; cb-unc-119(+)]II; unc-119(ed3)III?; noca-1(ok3692)V/nT1[qIs51](IV;V); ptrn-1(lt1::cb-unc-119+)X

Table 2.2: Strains used in Chapter 2 (continued)

Strain#	Genotype
OD1741	ltSi570[pOD1527/pSW232; Pdpy-7::GFP-tbb-2::mCherry-his-11; cb-unc-119(+)]I; unc-119(ed3)III
OD1780	ltSi570[pOD1527/pSW232; Pdpy-7::GFP-tbb-2::mCherry-his-11; cb-unc-119(+)]I; unc-119(ed3)III?; noca-1(ok3692)V/nT1[qIs51](IV;V)
OD1781	ltSi570[pOD1527/pSW232; Pdpy-7::GFP-tbb-2::mCherry-his-11; cb-unc-119(+)]I; unc-119(ed3)III?; ptrn-1(lt1::cb-unc-119+)X
OD1782	ltSi570[pOD1527/pSW232; Pdpy-7::GFP-tbb-2::mCherry-his-11; cb-unc-119(+)]I; unc-119(ed3)III?; noca-1(ok3692)V/nT1[qIs51](IV;V); ptrn-1(lt1::cb-unc-119+)X
OD1864	ltSi598[pOD1553/pSW252; Plbp-1::noca-1b::sGFP::opLinker::mCherry-PH; cb-unc-119(+)]II; unc-119(ed3)III
OD1865	ltSi599[pOD1554/pSW253; Plbp-1::noca-1h(252-922)::sGFP::opLinker::mCherry-PH; cb-unc-119(+)]II; unc-119(ed3)III

Table 2.2: Strains used in Chapter 2 (continued)

Strain#	**Genotype**
OD1866	ltSi600[pOD1555/pSW254; Plbp-1::noca-1h(457-922)::sGFP::opLinker::mCherry-PH; cb-unc-119(+)]II; unc-119(ed3)III
OD1867	ltSi601[pOD1542/pSW244; Ppha-4int1::PTRN-1(cDNA)::sGFP; cb-unc-119(+)]II; unc-119(ed3)III
OD1869	ltSi603[pOD1544/pSW246; Prgef-1::PTRN-1(cDNA)::sGFP; cb-unc-119(+)]II; unc-119(ed3)III
OD1908	ltSi598[pOD1553/pSW252; Plbp-1::noca-1b::sGFP::opLinker::mCherry-histone; cb-unc-119(+)]II; unc-119(ed3)III?; noca-1(ok3692)V/nT1[qIs51](IV;V)
OD1909	ltSi599[pOD1554/pSW253; Plbp-1::noca-1h(252-922)::sGFP::opLinker::mCherry-histone; cb-unc-119(+)]II; unc-119(ed3)III?; noca-1(ok3692)V/nT1[qIs51](IV;V)

Table 2.2: Strains used in Chapter 2 (continued)

Strain#	Genotype
OD1910	ltSi600[pOD1555/pSW254; Plbp-1::noca-1h(457-922)::sGFP::opLinker::mCherry-histone; cb-unc-119(+)]II; unc-119(ed3)III?; noca-1(ok3692)V/nT1[qIs51](IV;V)
OD1911	ltSi601[pOD1542/pSW244; Ppha-4int1::PTRN-1(cDNA)::sGFP; cb-unc-119(+)]II; unc-119(ed3)III?; noca-1(ok3692)V/nT1[qIs51](IV;V); ptrn-1(lt1::cb-unc-119+)X
OD1913	ltSi603[pOD1544/pSW246; Prgef-1::PTRN-1(cDNA)::sGFP; cb-unc-119(+)]II; unc-119(ed3)III?; noca-1(ok3692)V/nT1[qIs51](IV;V); ptrn-1(lt1::cb-unc-119+)X
OD1914	ltSi219[pOD1248/pSW076; Pmex-5::GFP-PH(PLC1delta1)-operon-linker-mCherry-his-11; cb-unc-119(+)]I; ptrn-1(lt1::cb-unc-119+)X
OD2006	ltSi541[pOD1505/pSW210; Pdpy-7::PTRN-1(cDNA)::sGFP; cb-unc-119(+)]II; unc-119(ed3)III?; noca-1(ok3692)V/nT1[qIs51](IV;V); ptrn-1(lt1::cb-unc-119+)X

Table 2.2: Strains used in Chapter 2 (continued)

Strain#	Genotype
OD2073	ltSi669[pSW267/pOD1785; Pmex-5::NOCA-1g(457-922)-sGFP::opLinker::mCherry-PH; cb-unc-119(+)]I; unc-119(ed3)III
OD2074	ltSi670[pSW268/pOD1786; Pmex-5::NOCA-1g(252-922)-sGFP::opLinker::mCherry-PH; cb-unc-119(+)]I; unc-119(ed3)III
OD2111	ltSi673[pSW279/pOD1787; Pdpy-7::tagRFP::tbb-2; cb-unc-119(+)]I; unc-119(ed3)III
OD2112	unc-119(ed3)III; ltSi674[oxTi177; pSW283/pOD1788; Pptrn-1::PTRN-1(cDNA)::tagRFP; cb-unc-119(+)]IV
OD2113	ltSi673[pSW279/pOD1787; Pdpy-7::tagRFP::tbb-2; cb-unc-119(+)]I; ltSi540[pOD1343/pSW160; Pnoca-1de::noca-1de::sGFP; cb-unc-119(+)]II; unc-119(ed3)III?
OD2114	ltSi673[pSW279/pOD1787; Pdpy-7::tagRFP::tbb-2; cb-unc-119(+)]I; ltSi542[pOD1506/pSW211; Pptrn-1::PTRN-1(cDNA)::sGFP; cb-unc-119(+)]II; unc-119(ed3)III

Table 2.2: Strains used in Chapter 2 (continued)

Strain#	Genotype
OD2115	ltSi569[oxTi185; pOD1110/pSW008; CEOP3608 TBG-1::mCherry; cb-unc-119(+)]I; ltSi540[pOD1343/pSW160; Pnoca-1de::noca-1de::sGFP; cb-unc-119(+)]II; unc-119(ed3)III?
OD2116	ltSi569[oxTi185; pOD1110/pSW008; CEOP3608 TBG-1::mCherry; cb-unc-119(+)]I; ltSi542[pOD1506/pSW211; Pptrn-1::PTRN-1(cDNA)::sGFP; cb-unc-119(+)]II; unc-119(ed3)III?
OD2117	ltSi540[pOD1343/pSW160; Pnoca-1de::noca-1de::sGFP; cb-unc-119(+)]II; unc-119(ed3)III?; ltSi674[oxTi177; pSW283/pOD1788; Pptrn-1::PTRN-1(cDNA)::tagRFP; cb-unc-119(+)]IV

The *C. elegans* strains used in this study were listed in Table 2.2. All worm strains were maintained at 20°C on standard NGM plates with OP-50 bacteria as food.

The *noca-1(ok3692)* allele is balanced with a translocation balancer (nT1), but the exact noca-1 locus is slightly outside of the balanced region (2 cM away from the translocation joint). Therefore, all worms containing nT1 balanced *noca-*

1(ok3692) were carefully maintained by singling out individual worms at each generation from worms giving correct phenotype segregations: $\frac{4}{5}$ of fertile worms with pharyngeal GFP marker and $\frac{1}{5}$ of sterile worms without pharyngeal GFP marker.

A transposon-based deletion strategy was used to make the null ptrn-1 allele (ptrn-1(lt1::cb-unc-119+)) (Figure 2.3; Frøkjær-Jensen *et al.*, 2010). Briefly, a repairing plasmid containing a Cb-unc-119 selection marker and homology arms (pOD1877/pSW62, 50 ng/μL) was injected together with a plasmid encoding the Mos1 transposase (pJL43.1, Pglh-2::Mos1 transposase, 50 ng/μL), and three plasmids encoding different fluorescent markers for negative selection: pCFJ90 (Pmyo-2::mCherry, 2.5 ng/μL), pCFJ104 (Pmyo-3::mCherry, 5 ng/μL), and pGH8 (Prab-3::mCherry, 10 ng/μL), into the strain OD747 (IE21011 x DP38). After one week, the moving progeny worms without fluorescent markers were identified as candidates under a fluorescent dissection scope. The deletion of candidate worms was then confirmed by PCR spanning both homology regions.

A similar transposon-based strategy was used to generate all transgenes used in this study (MosSCI; Frøkjær-Jensen *et al.*, 2008). To make the noca-1::sGFP transgene RNAi resistant, a 999 bp region close to the 3end of NOCA-1 coding sequence was re-encoded by codon shuffling (Figure 2.15). Depending on the insertion sites, transgenes were cloned into pCFJ151 (ChrII insertion, ttTi5605; UniI insertion, oxTi185; UniIV insertion, oxTi177), pCFJ352 (ChrI insertion, ttTi4348) or *de novo* (ChrV insertion, ttTi22935) by Gibson Assembly (Gibson

et al., 2009) to generate the repairing plasmids. In most cases, an improved transposase plasmid using a stronger promoter (pCFJ601, Peft-3::Mos1 transposase, 50 ng/μL) and an additional negative selection marker pMA122 (Phsp-16.41::peel-1, 10 ng/μL) were used in the injection mix. Single copy transgenes were generated by injecting a mixture of repairing plasmid, transposase plasmid and selection markers into strains EG6429 (outcrossed from EG4322; ttTi5605, Chr II), EG6701 (ttTi4348, Chr I), EG8078 (oxTi185, Chr I) or EG8081 (oxTi177, Chr IV). After one week, progeny of injected worms were heat-shocked at 34°C for 2 hours to induce the expression of PEEL-1, in order to kill the exo-chromosome array containing worms. Moving progeny worms without fluorescent markers were identified as candidates and transgene integration was confirmed by PCR on both sides.

2.5.2 RNA Interference

The DNA templates for synthesizing double-stranded RNA (dsRNA) were PCR-amplified from the N2 cDNA using the oligos listed in Table 2.3. Single-stranded RNAs (ssRNAs) were first synthesized in 50 μL T3 and T7 reactions using cleaned PCR reactions as templates (MEGAscript, Invitrogen), and then cleaned using the MEGAclear kit (Invitrogen). The ssRNAs from 50 μL T3 and 50 μL T7 reactions were then mixed with 50 μL of 3× soaking buffer (32.7 mM Na_2HPO_4, 16.5 mM KH_2PO_4, 6.3 mM NaCl, 14.1 mM NH_4Cl). To make dsRNA, the mixed ssRNAs were first incubated at 68°C for 10 min to denature, and then incubated at 37°C for 30 min to anneal.

Figure 2.15: NOCA-1 sequence re-encoding.
Schematic of the *NOCA-1hRR::GFP* transgene showing the sequence of the RNAi-resistant region. The DNA sequence in this region was altered by codon shuffling to prevent the transgene from being targeted by RNAi, while maintaining the codon bias and amino acid sequence. The capital letters indicate the altered codons.

Table 2.3: Oligos used for dsRNA production

Gene	**Oligonucleotide 1**	**Oligonucleotide 2**	**mg/mL**
T09E8.1 (ncoa-1)	AATTAACCCTCAC-TAAAGGggcgaacaag-gatcgtaaag	TAATACGACTCAC-TATAGGctg-catttgtttgaccatgc	1.8
T09E8.1h (noca-1h)	AATTAACCCTCAC-TAAAGGgcttg-caataactgctggaa	TAATACGACTCAC-TATAGGaagcgactcg-gttccttttt	15.7
F58A4.8 (tbg-1)	AATTAACCCTCAC-TAAAGGctcaagc-cttctggaaatcg	TAATACGACTCAC-TATAGGccat-gctcttcagcaacg	1.1
F26E4.8 (tba-1)	AATTAACCCTCAC-TAAAGGccgatactg-gaaacggaaga	TAATACGACTCAC-TATAGGtggtg-taacttggacggtca	1.4

For localization analysis in Figure 2.11, dsRNAs were delivered by injecting the L4 hermaphrodites. For all other experiments, dsRNAs were delivered by soaking the L4 hermaphrodites for 24 hours at 20°C. After recovery from injection or soaking, worms were incubated at 20°C for 24-54 hours before different experiments. For brood size counting and embryonic lethality assays, worms were singled out at 24 hours post recovery and removed from the plates at 48 hours post recovery. The number of hatched larvae and unhatched embryos were counted one day later. For germline imaging, injected worms were incubated at 20°C for 48-54 hours before imaging.

2.5.3 Worm Assays

For larval lethality assays, embyos were obtained by bleaching the adult worms with freshly mixed 20% household bleach and 0.5 N NaOH for 10 min. After that, embryos were rinsed twice in M9 and rotated in M9 at room temperature (∼23°C) for overnight to allow hatching. On the following day, synchronized and starved L1 worms were recovered on food. The phenotype was quantified at 72 hours after recovery.

For the permeability assay, synchronized worms at different stages and of different genotypes were first rinsed with M9 in a depression slide well and transferred into 1 μg/mL HOECHST 33258 in M9 (Sigma). After 15 min incubation, worms were rinsed twice in M9 and anesthetized in a mixture of 1 mg/ml Tricaine (ethyl 3-aminobenzoate methanesulfonate salt, Fluka analytical, A5040-25G) and

0.1 mg/ml of TMHC (tetramisole hydrochloride, Sigma, T1512-10G) dissolved in M9 for 30 min. Then worms were mounted onto a 2% agarose pad and imaged using the Metamorph (see Light Microscopy section).

For brood size counting assays, L4 hermaphrodites of different genotypes were incubated at 20°C and singled out 24 hours later. After another 24 hours, the adult worms were removed from the plates. The brood size was counted on the following day.

For nuclear migration assays, worms of different genotypes were maintained at 20°C. Healthy L1 worms were partially anesthetized in 20 mM NaN_3 and mounted on 2% agarose pad. Number of nuclei in the dorsal cord was counted while the worms were imaged using DIC on the Zeiss microscope (see Light Microscopy section).

2.5.4 Light Microscopy

Images in Figure 2.2D, Figure 2.4, Figure 2.5, Figure 2.6B-F, Figure 2.11D, Figure 2.12 and Figure 2.13A were acquired using an inverted Zeiss Axio Observer Z1 system with a Yokogawa spinning-disk confocal head (CSU-X1), a 63× 1.40 NA Plan Apochromat lens (Zeiss), and a Hamamatsu ORCA-ER camera (Model C4742-95-12ERG, Hamamatsu photonics). Images in Figure 2.1, Figure 2.6A, Figure 2.7C-D, Figure 2.11B, Figure 2.11F and Figure 2.13D-E were acquired using the same system with an EMCCD camera (QuantEM:512SC, Photometrics) to boost the signal to noise ratio. Imaging parameters were controlled using the

AxioVision software (Zeiss).

Images in Figure 2.11A, C and E were acquired using a Nikon TE2000-E inverted microscope with a Yokogawa spinning-disk confocal head (CSU-10), a 60× 1.40 NA Plan Apochromat lens (Nikon) and an EMCCD camera (iXon DV887ECS-BV, Andor Technology). Imaging parameters were controlled using the Andor iQ2 software.

Images in Figure 2.2C were acquired using a Nikon eclipse E800 microscope with a 60× 1.40 NA Plan Apo lens (Nikon) and a Hamamatsu ORCA-ER camera (Model C4742-95-12ERG, Hamamatsu photonics). Imaging parameters were controlled using the Metamorph software (Molecular Devices).

Images in Figure 2.2A were acquired using the DinoEye eyepiece camera (AM7023B, Dino-Lite) mounted on a Nikon SMZ800 dissection scope. Imaging parameters were controlled using the DinoXcope software (Dino-Lite).

2.5.5 Image Analysis

EB1 comet tracking was performed using Image J. The tiff images were first subject to Gaussian blur (sigma = 1 pixel), subtract background (rolling ball based, r = 20 pixels) and threshold (manually adjusted parameters to retain most comets). Then the MTrack2 plugin was called (parameters: minimum and maximum object size = 1 and 100 pixels, maximum velocity = 12 pixels/frame, minimum track length = 3 frames) to obtain the total number of tracks within the analyzed region of interest. To obtain the effective area of analyzed regions (excluding the nuclei

area), images were first sub threshold so that only the cytoplasmic region was highlighted and then measured. Normalized track densities were ratios of the total track number and the effective area for all analyzed images.

2.5.6 Antibody Production

Table 2.4: Oligos used in antibody production

Target	Oligonucleotide 1	Oligonucleotide 2
NOCA-1	ttgaattcCTCcgattgcaa-gaaatga	ttgaattcTTAgagttcttcaact-gctcg
PTRN-1	aagttctgttccaggggcccAAG-GAGCTCGGTGCTGAG	agtcgacccgggaattcttaGT-TATTCTTATGAGCCG-GAGTTC

To generate the NOCA-1 and PTRN-1 antibodies, oligos listed in Table 2.4 were used to PCR-amplify the regions encoding the amino acids 569-717 of NOCA-1h and the amino acids 910-1110 of PTRN-1a from the N2 cDNA library. The PCR products were cloned into the pGEX6P-1 vector. The GST fused antigens were purified from bacteria and outsourced for injection into rabbits (Covance). NOCA-1 antibodies were affinity purified using the same antigen after cleavage of the GST tag as previously described (Desai *et al.*, 2003). PTRN-1 antibodies were affinity purified using a GFP-PTRN-1-His fusion purified from insect cells (see Protein Purification section).

2.5.7 Western Blots

For the Western blot in Figure 2.7B (right panel), 20∼50 control, *noca-1(RNAi)* or *noca-1h(RNAi)* worms were transferred into a pre-weighted tube containing 1 mL of M9 + 0.1% Triton X-100 and washed for three times. After the last wash, excess buffer was removed until the net weight of worms and buffer was proportional to the number of worms (1 mg per worm). Worms were then sonicated in a sonicating water bath at ∼70°C for 10 min and boiled for 3 min.

For all other Western blots, a mixed population of worms growing at 20°C were collected and washed three times using M9 + 0.1% Triton X-100 in an Eppendorf tube. After the last wash, ∼100 μL buffer was left, and then 50 μL of 4x sample buffer and 100 μL of glass beads were added. Worms were vortexed for 5 min, boiled for 3 min, and then vortexed and boiled again. Samples were run on an SDS-PAGE gel, transferred to a nitrocellulose membrane, probed with 1 μg/ml anti-NOCA-1, anti-PTRN-1 or anti-α-tubulin (mouse monoclonal DM1-α; Sigma-Aldrich T9026), and detected with an HRP-conjugated secondary antibody (rabbit or mouse; GE Healthcare).

2.5.8 MT Co-Sedimentation from Worm Extract

The *C.elegans* extract was made as previously described (Zanin *et al.*, 2011). Briefly, ∼1 g of frozen worms from a large-scale liquid culture were weighed and resuspended in 1.5× volume of the worm lysis buffer (50 mM Hepes-KOH pH 7.6,

1 mM $MgCl_2$, 1 mM EGTA, 75 mM KCl, 0.5 mM DTT, 1 μg/mL Pepstatin A, 1 tablet of Roche cOmplete EDTA-free protease inhibitor per 50 mL). The resuspension was sonicated to get the crude extract. The crude extract was first centrifuged at 20,000 g for 10 min at 2°C, after which the supernatant was again centrifuged at 50,000 g for 20 min at 2°C. The supernatant after the second centrifugation was used for the experiment.

To determine whether NOCA-1 and PTRN-1 co-pellet with taxol-stabilized microtubules (MTs), a modified procedure from Kellogg et al. (Kellogg *et al.*, 1989) was used to compare the amounts of NOCA-1 or PTRN-1 pelleting down with no microtubule control and taxol-stabilized microtubules. For each experimental condition, 200 μL of worm extract prepared as above was supplemented with 0.5 mM DTT, 1 mM GTP and 0.4 μL of DMSO (solvent control), 0.5 mg/mL nocodazole (no MT control) or 10 mM taxol (stabilized MT). The samples were warmed to 23°C for 10 min to allow MT polymerization, incubated on ice for 15 min and then pelleted through a glycerol cushion (worm lysis buffer with 40% glycerol) by centrifugation at 48,000 g for 30 min at 2°C. The sample/cushion interface was washed three times with worm lysis buffer. The pellet was resuspended in 200 μL 1× sample buffer. 12 μL of each sample were run on an SDS-PAGE gel for either Coomassie staining or Western blots.

2.5.9 Protein Purifications

For MT anchoring and MT gliding assays, DmPatronin, PTRN-1, NOCA-1h(252-922) and NOCA-1(457-922) were PCR-amplified from a plasmid or the N2 cDNA, and then cloned into the pFL vector (Berger *et al.*, 2004) downstream of the p10 viral promoter with GFP and His tags. These plasmids were transformed into DH10EMBacY to generate bacmids, which were then transfected into Sf9 cells to produce baculoviruses. High Five cells were infected at 1-2 $\times$ 10^6 cells/mL using the baculoviruses and cultured for 48 hours at 27°C before being collected. Expressions of GFP tagged proteins were monitored using a fluorescence dissection scope.

To purify the proteins, baculovirus infected High Five cells from 150 mL culture were lysed in 50 mL lysis buffer (50 mM Hepes pH 7.6, 500 mM NaCl, 10 mM imidazole, 10% sucrose, 1 mM DTT, 0.1% Tween-20, 1 μg/mL pepstatin A, 1 tablet of Roche cOmplete EDTA-free protease inhibitor), pelleted and the soluble fraction was incubated with nickel beads for 1 hour at 4°C. The beads were then washed three times with wash buffer (50 mM Hepes pH 7.6, 500 mM NaCl, 25 mM imidazole, 10% sucrose, 1 mM DTT, 0.1% Tween-20) and eluted with 1 mL fractions of elution buffer (50 mM Hepes pH 7.6, 500 mM NaCl, 250 mM imidazole, 10% sucrose, 1 mM DTT, 0.1% Tween-20). Elutions were used for flow-cell assays either directly or stored at -80°C after snap-frozen in 50-100 μL aliquots in liquid nitrogen.

The kinesin motor domain with or without GFP tag was expressed in E.coli cells (Rosetta) induced at OD 0.6-0.8 and cultured at 13°C for overnight. Bacteria cells were lysed in lysis buffer (50 mM Hepes-K pH 7.6, 500 mM KCl, 10 mM imidazole, 10% Glycerol, 1 mM DTT, 1 mM ATP, 1 mM $MgCl_2$, 1 μg/mL pepstatin A, 1 tablet of Roche cOmplete EDTA-free protease inhibitor), pelleted and the soluble fraction was incubated with nickel beads for 1 hour at 4°C. The beads were then washed three times with wash buffer (50 mM Hepes-K pH 7.6, 500 mM KCl, 25 mM imidazole, 10% Glycerol, 1 mM DTT, 1 mM ATP, 1 mM $MgCl_2$) and eluted with 1 mL fractions of elution buffer (50 mM Hepes-K pH 7.6, 500 mM KCl, 250 mM imidazole, 10% Glycerol, 1 mM DTT, 1 mM ATP, 1 mM $MgCl_2$). Elutions were used for flow-cell assays either directly or stored at -80°C after snap-frozen in 50-100 μL aliquots in liquid nitrogen.

2.5.10 MT Flow-Cell Assays

Coverslips were cleaned by 10 min sonication in 5 M KOH dissolved in pure ethanol followed by 10 min sonication in clean water, 2× rinse with water and 1× rinse with ethanol. After being dried in 37°C incubator for overnight, the coverslips were used to make flow cells using microscope slides (Gold Seal, Thermo Scientific) and double-sided tape (Scotch).

To make rhodamine-labeled GMPCPP MTs, labeled and unlabeled bovine tubulin were clarified by centrifugation at 90,000 rpm for 5 min at 2°C. Then the concentrations of labeled and unlabeled tubulins were measured. An elongation

mix was prepared by mixing labeled and un-labeled bovine tubulin at 1:20 ratio and 10 μM total concentration in 1× BRB80 (80 mM Pipes-KOH pH 6.8, 1 mM $MgCl_2$, 1 mM EGTA) supplemented with 1 mM DTT and 1 mM GTP. The mix was snap-frozen in liquid nitrogen at 5 μL and stored at -80°C. The stock of labeled MTs were made by thawing an elongation mix aliquot, dilute with 5 μL of 1× BRB80 with 1 mM DTT and incubated in a 37°C water-bath for 30-60 min.

For MT anchoring assays, 10 μg/mL of the llama GFP binder diluted in Tris-KAc buffer (50 mM Tris-HCl 8.0, 150 mM KAc, 10% Glycerol, 1 mM DTT) was squirted in the flow cell and incubated for 5 min. Then the coverslip was blocked with 1 mg/mL casein diluted in the Tris-KAc buffer for 5 min. 5 nM of tested GFP tagged proteins diluted in the Tris-KAc buffer were then delivered and incubated for another 5 min. Finally, 0.1 μM of rhodamine-labeled GMPCPP MTs diluted in the MT solution with an oxygen scavenger mix (1× BRB80, 1 mM DTT, 1 mg/mL casein, 0.8 mg/mL glucose, 0.04 mg/mL glucose oxidase, 0.016 mg/mL catalase) was flowed in before imaging.

For kinesin gliding assays, the kinesin motor domain K560 (most concentrated fraction after His purification) was squirted in the flow cell and incubated for 5 min. The coverslip was then blocked with the Gliding Buffer (1× BRB80, 1 mg/mL Casein, 100 mM KCl, 0.1% Tween-20, 10% Sucrose, 1 mM DTT, 1 mM ATP). After that, 0.1 μM of rhodamine-labeled GMPCPP MTs diluted in the Gliding Buffer was flowed in and incubated for 5 min. ∼200 pM of GFP-DmPatronin or ∼300 pM of GFP-PTRN-1 diluted in the Gliding Buffer were then flowed in

before imaging.

2.6 Acknowledgements

We thank: Marian Chuang and Suhong Xu (Chisholm lab) and Mellisa Hendershott (Vale lab) for plasmids; Renat Khaliullin for help with python scripts and image analysis; Kim Laband and Rebecca Green for making the NOCA-1 antibody; Dhanya Cheerambathur for making the germline EB1::GFP strain; Dhanya Cheerambathur, Yao Wong and Molly Lettman for biochemistry help; Other OD lab members for helpful discussions; Joo Seok Han (Cleveland lab) for baculovirus and insect cells; Sasha Dehenau for palmitoylation prediction help; CGC and the nemagenetag for strains; and Wormbase for unlimited support of the *C. elegans* genome.

Chapter 2, in part, is currently being prepared for submission for publication. Wang, Shaohe; Desai, Arshad; Oegema, Karen. The dissertation author was the primary investigator and author of this material.

Chapter 3

Non-centrosomal MT arrays contribute to embryonic morphogenesis

3.1 Summary

The *C. elegans* embryonic morphogenesis requires the contribution of all three cytoskeletal filaments: actin, intermediate filaments and MTs. Actin and myosin contribute to the main contraction force that deforms the embryos and intermediate filaments link the hemidesmosomes together to connect the inside muscle with the outside cuticle. On the other hand, the contribution of MTs remains elusive. Early pharmocological experiments established the requirement of MTs for elongation, but we don't know anything beyond that. Here, we estab-

lished two independent methods of inhibiting or degrading MTs specifically in the embryonic epidermis and found that inhibiting MTs by itself did not cause any elongation defects. However, inhibiting MTs synergizes with reducing actomyosin contractility by a partial loss-of-function mutant of *let-502*. We found that two MT regulators, NOCA-1 and γ-tubulin both localized to the adherens junctions and hemidesmosomes and maturation of these junction structures required intact MTs. We conclude that microtubules in the embryonic epidermis contribute to elongation, but only is required when actomyosin contractility is reduced.

3.2 Introduction

During morphogenesis, oval-shaped *C.elegans* embryos elongate four times to be a long thin worm. This striking elongation event occurs with almost no cell divisions or migrations; instead, it is driven by coordinated change of cell shapes (Sulston *et al.*, 1983). Laser killing experiments have established that epidermal cells are the major contributors to elongation, as laser killing of epidermal cells, but not neurons, pharynx and intestinal cells, cause elongation defects (Sulston *et al.*, 1983; Priess and Hirsh, 1986). Early elongation between the comma stage and the 2-fold stage does not seem to need any other cells. However, elongation beyond the 2-fold stage requires the body wall muscle, as embryos with mutations affecting muscle funtions are arrested at 2-fold stage (pat phenotype, for Paralyzed and Arrested at Two-fold; Williams and Waterston, 1994). So far, however, it is

unclear how the muscle contraction promotes elongation. Thus, *C.elegans* embryonic elongation appears to have an early elongation phase that is mainly driven by the epidermis, and a late elongation phase which requires muscle, although how muscle drives epidermal shape change is elusive.

All three cytoskeleton filaments are important for elongation. Early pharmocological studies found that treatment with actin filament inhibitor cytochalasin D completely abolishes elongation and this effect is reversible (Priess and Hirsh, 1986). Treatment with MT inhibitors results in abnormal and partial elongation (Priess and Hirsh, 1986). Later, genetic analysis implicated the cytoplasmic intermediate filaments in elongation, since mutations in both IFB-1 and IFA-3 causes elongation defects (Woo *et al.*, 2004). Thus, the MTs, actin and intermediate filaments, are all required for elongation.

Actomyosin contraction activity in the epidermal cells are essential for normal elongation. The non-muscle myosins NMY-1 and NMY-2 (myosin heavy chains) have partially redundant functions in the eipdermal cells to promote contractility (Piekny *et al.*, 2003). The actomyosin contractility is positively regulated by the Rho kinase (ROCK) LET-502 and negatively regulated by the MEL-11 myosin phosphatase (Wissmann *et al.*, 1997, 1999; Piekny *et al.*, 2000). Based on the localizations of these regulators, it is thought that actomyosin contractility mainly acts in the lateral epidermal cells (the seam cells). Consistent with that, the Rho1 GAP RGA-2, a negative regulator of the acomyosin activity, is required to counteract the LET-502/ROCK activity in the dorsal and ventral epi-

dermis for normal elongation (Diogon *et al.*, 2007). Interestingly, only the early elongation (from comma to 2-fold) requires LET-502/ROCK and RGA-2 (Diogon *et al.*, 2007). Overall, a high acomyosin contractility in the lateral epidermis and a relatively low contractility in the dorsoventral epidermis are balanced to promote epidermal morphogenesis in the early elongation phase.

Intermediate filaments are found at the attachment structure hemidesmosomes in the epidermis. Hemidesmosomes attach the epidermis to the extracellular matrix. At the apical surface, they attach the epidermis to the cuticle exoskeleton; at the basal surface, they attach the epidermis to the basal membrane, which is then attached to the body wall muscle (Labouesse, 2006). Intermediate filaments link the apical and basal hemidesmosome attachment structures together so that the muscle is connected with the cuticle exoskeleton. IFB-1 and IFA-3 are the major cytoplasmic intermediate filament components expressing in the epidermis and mutations in both of them cause elongation defects (Woo *et al.*, 2004). Recently, the hemidesmosomes are found to be mechanosensors that transduce the muscle caused tension to a kinase activity in the epidermis at the hemidesmosomes (Zhang *et al.*, 2011). One important output of this mechanosensation pathway is the phosphorylation of intermediate filaments and the maturation of hemidesmosomes (Zhang *et al.*, 2011). Thus, intermediate filaments are important for both attachment and mechanosensation purposes.

The role of MTs are elusive. The MT drug treatment causes elongation defects including abnormal surface constrictions and depressions (Priess and Hirsh,

1986). Based on that, Priess and Hirsh (1986) proposed that MTs are important to distribute the force generated by actomyosin contraction evenly in the epidermis. Recently, a computational model is proposed where MTs are important to provide the anisotropic property in the dorsoventral epidermis, distribute the force evenly, as well as buffer the changes in distribution of the actomyosin activities (Ciarletta *et al.*, 2009). However, the lack of a molecular handle precludes the examination of proposed models. Although genetic analysis of embryonic elongation has identified many regulators controlling the actomyosin contractility and intermediate filament attachment, no MT regulators in the elongation process have been found. This is partly due to the essential role of MTs in early cell divisions, so that mutations in generic MT regulators causes early arrest of embryos.

NOCA-1 is a novel MT regulator that only affect non-centrosomal MT array formation (Figure 2.1; Green *et al.*, 2011). RNAi or genetic deletion of NOCA-1 do not cause cell division defects, but greatly reduce the MT density in several differentiated cells, including the embryonic epidermis. Therefore, NOCA-1 provides an excellent molecular handle to study the function of MTs in the elongation process without destroying the overall embryonic structure as the drug treatment does. In addition, MT severing enzymes can be used to degrade MTs when it is overexpressed. Overexpressing the MT severing enzyme Spastin in tissue culture cells or in vivo disassembles MTs (Errico *et al.*, 2002; Sherwood *et al.*, 2004; Trotta *et al.*, 2004).

In this study, we established two methods to degrade MTs in the embryonic

epidermis during elongation and found that inhibiting MTs alone does not abolish elongation. However, MTs become essential for elongation when the actomyosin contractility is compromised by a partial loss of function allele of LET-502/ROCK. We found two MT regulators — NOCA-1 and γ-tubulin — both localize to the adherens junctions and hemidesmosomes in the epidermis and intact MTs are required for maturation of both attachment structures. Thus, we conclude that MTs contribute to embryonic elongation, but only is essential when actomyosin contractility is limited.

3.3 Results

3.3.1 Establishing two methods to disrupt MTs in developing embryos

In order to perturb MTs specifically in the embryonic epidermis, we established two methods. First, we overexpressed the MT severing enzyme Spastin using a strong epidermal promoter, Pdpy-7 (Matsushita-Ishiodori *et al.*, 2007). We used un-tagged Spastin to preserve its enzymatic activity. To follow the expression of untagged Spastin, we linked its expression with a NLS-mCherry using an operon linker from CEOP1032 (Figure 3.1A). An operon linker works as an internal ribosome entry site (IRES). Thus, the Spastin expression was effectively reported by the nuclear mCherry expression. As expected, the MTs in the epidermis were

efficiently degraded by the expression of Spastin, but not by a deletion mutant of Spastin which removed the ATPase domain (Figure 3.1B). The MTs were affected from the 1.8-fold stage of the embryo, although the nuclear mCherry was expressed before that. Thus, we have established a Spastin overexpression (*Spastin(O/E)*) system to effectively degrade MTs from the epidermis from 1.8-fold stage.

In the second method, we used a genetic mutation of *noca-1*, which was shown to affect the epidermal MTs (Green *et al.*, 2011). Because *noca-1*Δ mutants were completely sterile, homozygous *noca-1*Δ embryos had to be obtained from the heterozygous mother (Figure 2.6A). To distinguish the homozygous *noca-1*Δ embryos from its siblings, we inserted a reporter transgene (cytoplasmic mCherry driven by an epidermis promoter) precisely at a site only 0.06 cM from the *noca-1* locus using MosSCI (Frøkjær-Jensen *et al.*, 2008). After mating this transgenic worms with balanced *noca-1*Δ mutants, we now had a heterozygous mother whose wild type *noca-1* is linked with cytoplasmic mCherry in the epidermis. Therefore, embryos without mCherry marker were homozygous for *noca-1*Δ (Figure 3.2A). To maximize the depletion of NOCA-1 from the epidermis, we used RNAi against the heterozygous mothers to obtain embryos depleted with both maternal and zygotic NOCA-1 (*noca-1(m/z)*; Figure 3.2A). The epidermis MTs in *noca-1(m/z)* embryos were severely affected from as early as dorsal epidermal intercalation (one hour before elongation start) and continued to have defective epidermal MTs through the elongation process (Figure 3.2B). Therefore, we have established a genetic system to inhibit MT formation in the epidermis throughout the elongation process.

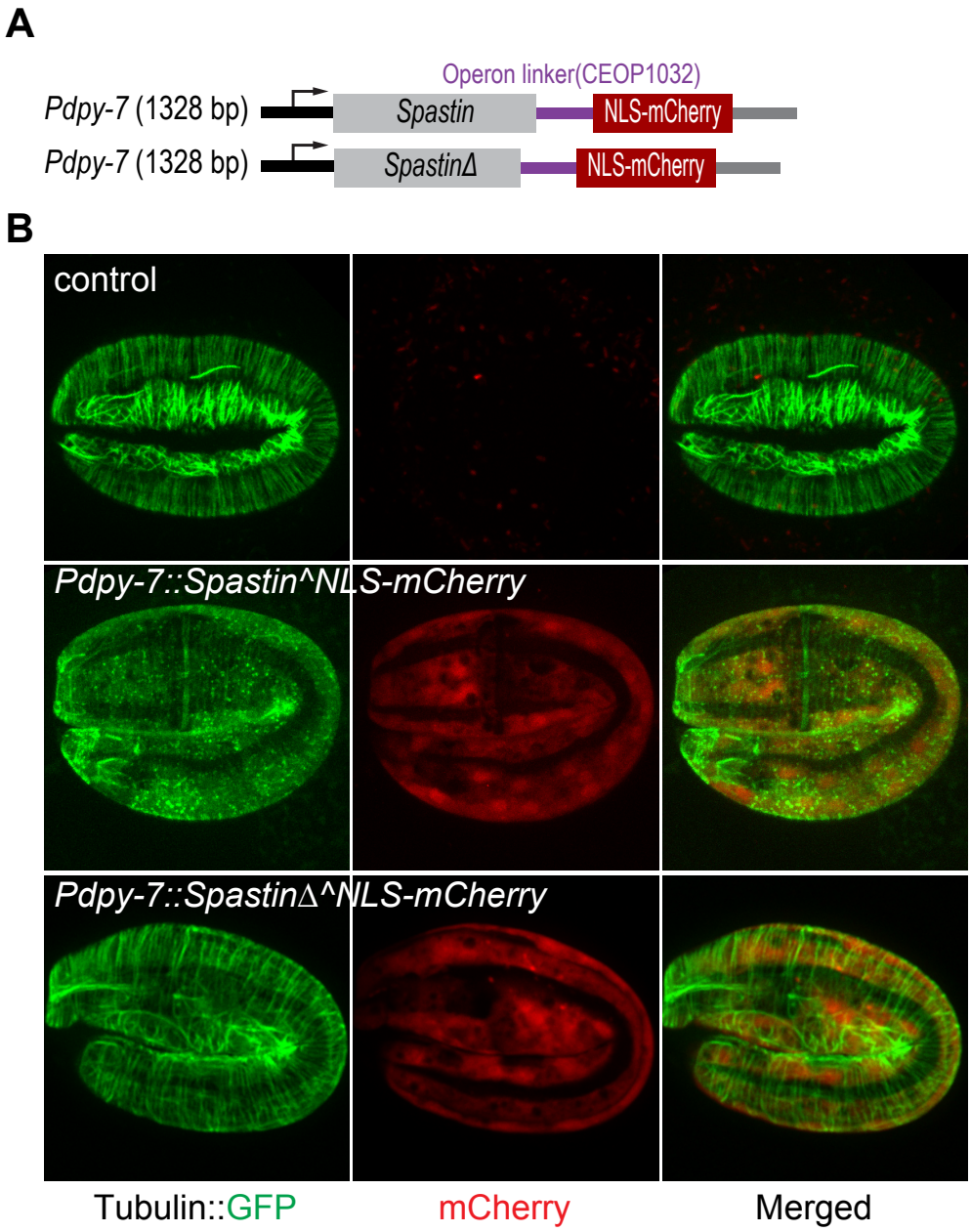

Figure 3.1: Spastin expression degrades MTs in the epidermis.
(A) Schematic showing the constructs expressing Spastin or a Spastin deletion mutant and the expression reporter NLS-mCherry.
(B) Images of *C. elegans* embryos expressing a epidermal Tubulin::GFP transgene with or without Spastin expression.
This figure is courtesy of Sophie Quintin from the Labouesse lab.

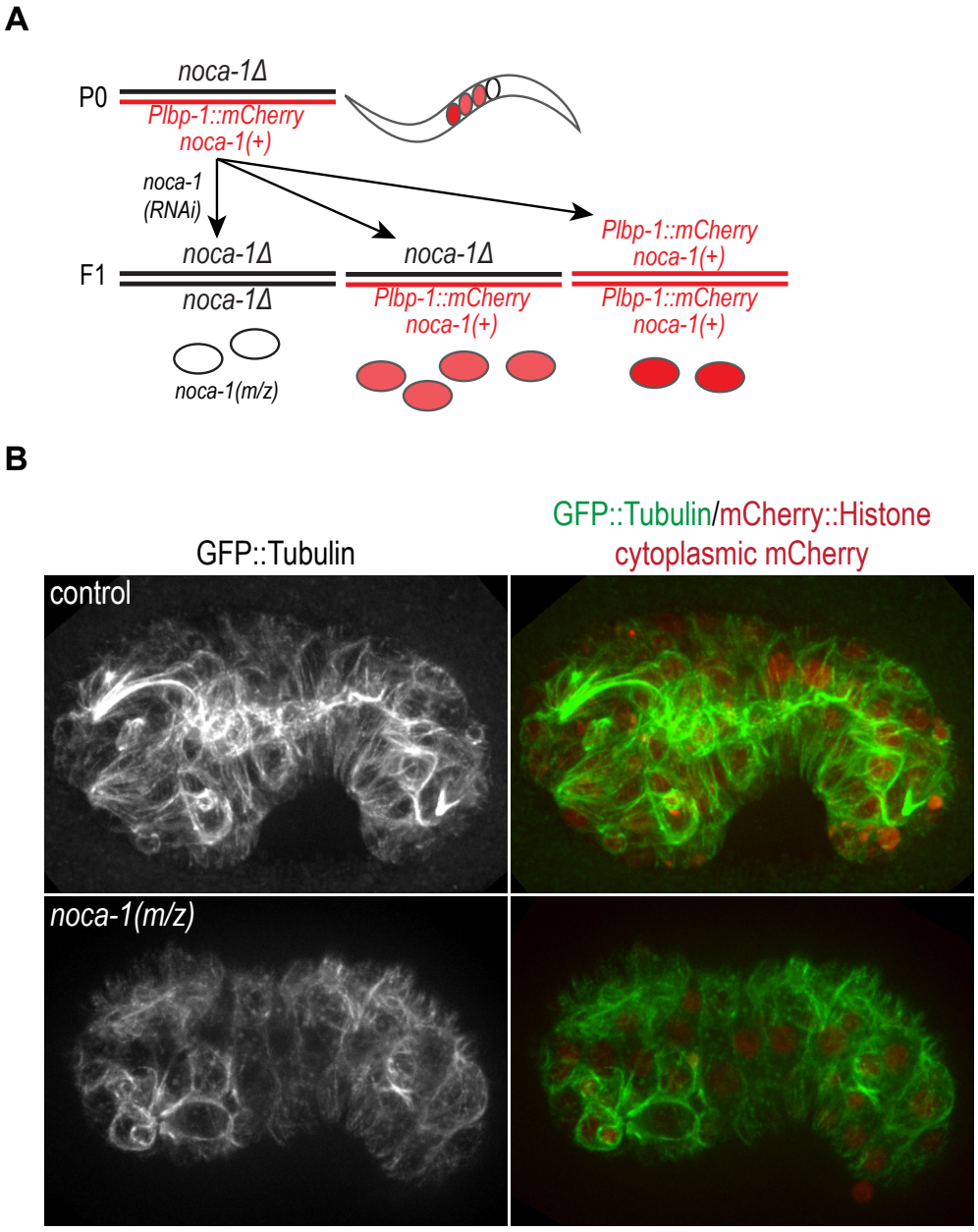

Figure 3.2: *noca-1(m/z)* embryos have less dense MTs in the epidermis. (A) Schematic showing the transgenic strategy to obtain *noca-1(m/z)* embryos. (B) Images of *C. elegans* embryos expressing a epidermal Tubulin::GFP transgene with indicated genotypes.

3.3.2 A ROCK partial loss of function allele synergizes with MT inhibition to cause elongation defects

Treatment with MT depolymerizing drugs disrupted embryonic elongation and epidermis was the major tissue responsible for driving elongation based on laser killing experiments (Priess and Hirsh, 1986). Thus, we may think that inhibiting MTs specifically in the epidermis would cause elongation defects. However, in both *Spastin(O/E)* and *noca-1(m/z)* embryos, we observed no elongation defects (data not shown). Therefore, either epidermal MTs are not important for elongation, or they have some redundant role with other players.

We then considered the possibility of a redundant role of MTs and the actomyosin filaments. Previously, a computational model predicted that MTs could buffer the embryos against changes of actomyosin contractility (Ciarletta *et al.*, 2009). To test this idea, we used a partial loss of function allele of the Rho Kinase LET-502 (*let-502(sb118)*; Diogon *et al.*, 2007). The Rho kinase positively regulates the actomyosin contractility in two ways. First, it could directly phosphorylate and activity the regulatory myosin light chain; second, it could phosphorylate and inhibit a inhibitory phosphatase that removes the phosphate from the light chain (Wissmann *et al.*, 1997, 1999). The *let-502(sb118)* allele is especially useful because it is temperature sensitive so that its activity can be adjusted by shifting the temperature. In this study, we used three different temperatures: 20°C as the permissive temperature, 23.5°C as the semi-permissive temperature and 25°C as

the restrictive temperature. At both 20°C and 23.5°C, the *let-502(sb118)* mutants were morphologically normal, while at 25°C, the *let-502(sb118)* mutants were almost 100% dead at embryonic or larval stage (Figure 3.3B; Diogon *et al.*, 2007). Thus, *let-502(sb118)* provides a nice tool for modulating the acomyosin contractility.

Interestingly, we found that MTs became essential for elongation when the actomyosin contractility was reduced. While both *Spastin(O/E)* and *noca-1(m/z)* embryos elongate normally, these MT inhibited embryos failed the elongation in the background of *let-502(sb118)* at 23.5C (Figure 3.3A and B). The *noca-1(m/z);let-520* embryos were arrested slightly earlier than the *Spastin(O/E);let-502* embryos, presumably due to the MT inhibition was effective earlier than in the *Spastin(O/E)* embryos. Therefore, we conclude that MTs in the epidermis contribute to the embryonic elongation, and they become essential when the actomyosin contractility was reduced.

3.3.3 MTs contribute to maturation of both the adherens junctions and hemidesmosome

In order to understand what MTs may do to contribute to elongation, we started by examining the localization of NOCA-1 and the MT nucleator γ-tubulin in elongating embryos. We found that both NOCA-1 and γ-tubulin localized to the adherens junctions and hemidesmosomes (Figure 3.4). Based on the localiza-

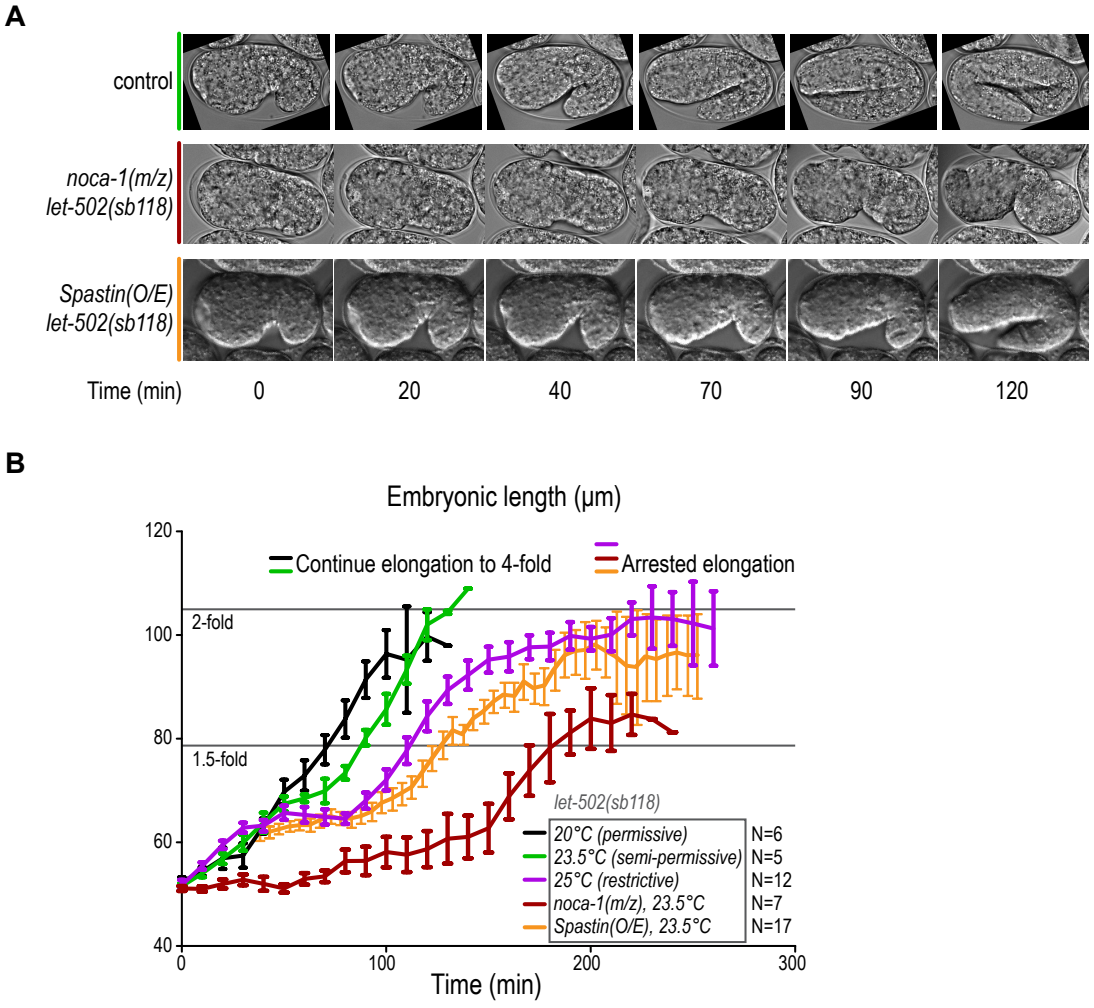

Figure 3.3: MT inhibition synergizes with reduced actomyosin contractility to cause elongation defects.
(A) DIC images from time lapse series showing the embryonic elongation process in embryos with indicated genotypes.
(B) Plot of embryonic length measured along the long axis of embryos. 5-17 worms were measured for each condition. Error bars are SEM.
The images in the bottom panel of (A) and the corresponding quantification data are courtesy of Sophie Quintin from the Labouesse lab.

tion of these two MT regulators, we speculated that MTs may contribute to the maturation of these junction structures.

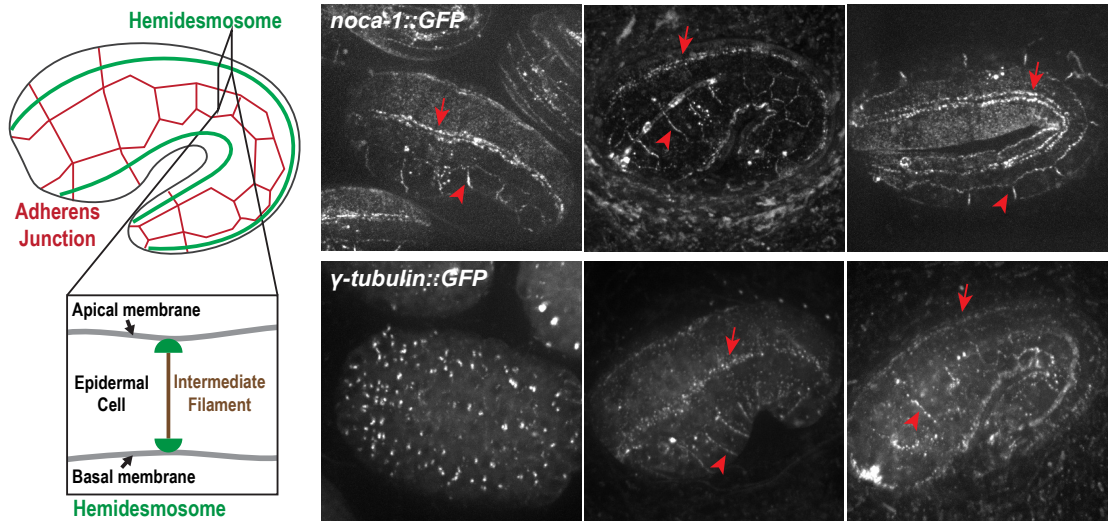

Figure 3.4: Both NOCA-1 and γ-tubulin localizes to adherens junctions and hemidesmosomes.
Left, schematic showing the adherens junctions and hemidesmosomes in an elongating embryo. Right, images of embryos expressing NOCA-1::GFP or γ-tubulin::GFP. Arrows point to the hemidesmosomes and arrowheads point to the adherens junctions.
The transgenic strains were generated by the dissertation author; the images are courtesy of Sophie Quintin from the Labouesse lab.

The adherens junctions are essential to hold the epidermis together and the epidermal integrity is critical for elongation to happen (Costa *et al.*, 1998; Priess and Hirsh, 1986). We started by examining the adherens junction marked by E-cadherin::GFP. We found the E-cadherin::GFP clustering at the adherens junction appeared to be fragmented in both the *Spastin(O/E)* embryos and the *noca-1(RNAi)* embryos (Figure 3.5A). In the presence of *let-502(sb118)*, the ratio of affected embryos were increased by 20% and 50% for *Spastin(O/E)* and *noca-1(RNAi)* embryos, respectively (Figure 3.5B). Thus, we conclude that E-cadherin

clustering at adherens junctions requires MTs and LET-502.

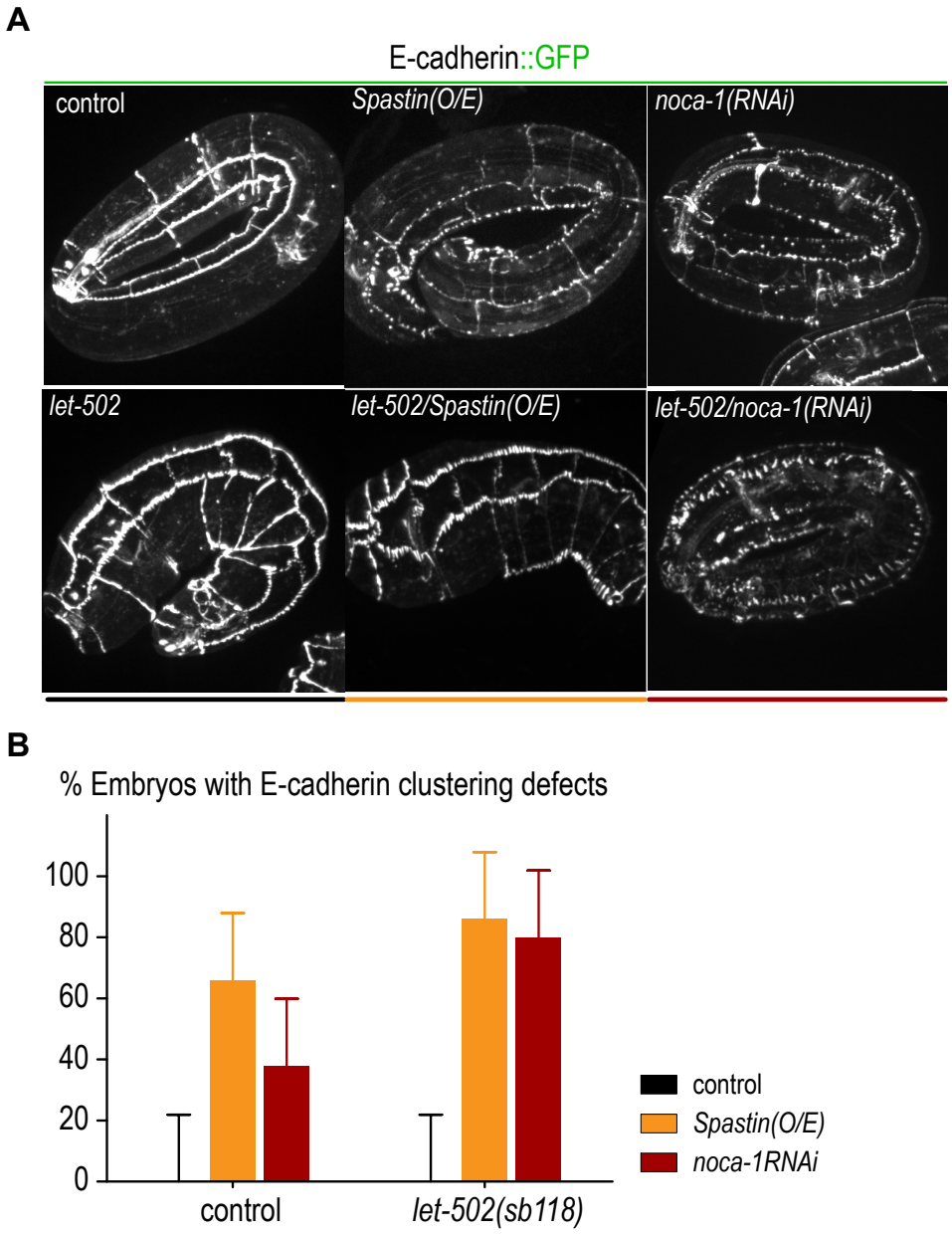

Figure 3.5: E-cadherin clustering at adherens junctions requires MTs and LET-502.
(A) Images of embryos expressing E-cadherin::GFP with indicated perturbations. (B) Plot of percentage of embryons with fragmented E-cadherin clustering. At least 20 worms were tested for each condition. Error bars are margin of error at 95% confidence.
This figure is courtesy of Sophie Quintin from the Labouesse lab.

The hemidesmosomes of *C. elegans* are both attachment structures and mechanosensors. They are zipper like structures attaching the epidermis to the extracellular matrix at both apical and basal surfaces. Matured hemidesmosomes are linked with intermediate filaments, so that the inside body wall muscle is connected with the outer cuticle (Schematic in Figure 3.4). As a mechanosensor, the HD transduces muscle-induced tension to activate the PAK-1 kinase to promote intermediate filament phosphorylation (Zhang *et al.*, 2011). The localization of MT regulators on the hemidesmosomes suggested a potential link between MTs and hemidesmosomes. Therefore, we examined whether hemidesmosome maturation was affected by immunostaining with an intermediate filament antibody. We found that the intermediate filaments in *let-502/Spastin(O/E)* embryos were initially normal (10 out of 10), but disrupted when muscle started to contract (14 out of 17, Figure 3.6). We also have preliminary data that the intermediate filaments were disrupted in *noca-1(m/z* embryos (data not shown). Therefore, we conclude that intact MTs and LET-502 are required for hemidesmosome maturation.

3.4 Discussion

In this study, we found that MTs contribute to embryonic elongation, but only is essential when actomyosin contractility is limited. Early pharmocological studies have established that MTs are required for normal elongation (Priess and Hirsh, 1986). However, whether the MT drug caused defects are due to specific

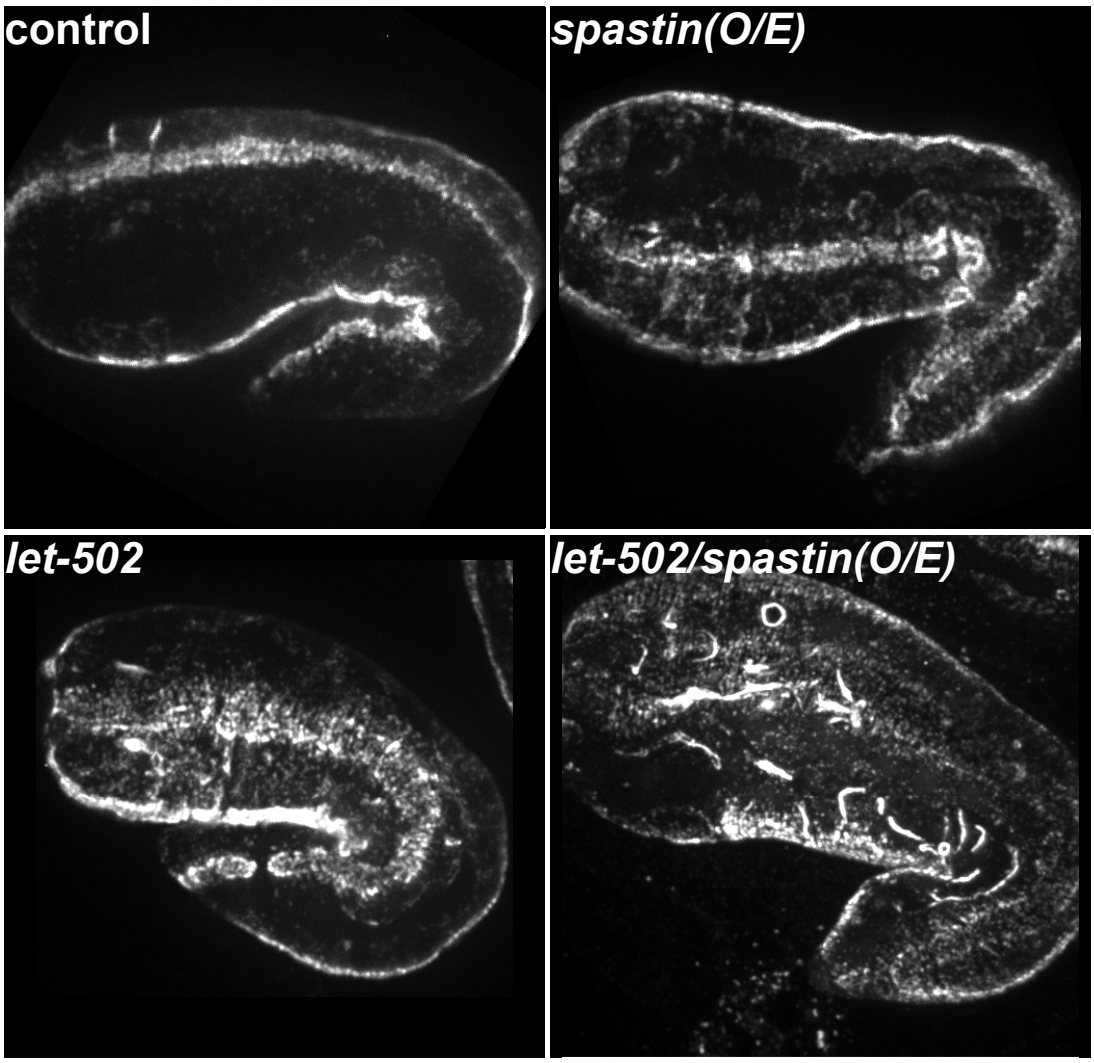

Figure 3.6: Hemidesmosome maturation requires intact MTs.
Immunostaining images using MH4 antibody which recognizes the intermediate filaments in hemidesmosomes.
This figure is courtesy of Sophie Quintin from the Labouesse lab.

requirement of MTs in the epidermis or due to overall disruption of the embryonic structures are not known. We have shown here that disrupting MTs by either a *noca-1*Δ mutant or by overexpressing the MT severing enzyme spastin do not cause elongation defects on their own. However, when the actomyosin contractility is compromised by a partial loss of function allele of LET-502/ROCK, MT inhibition causes dramatic elongation defects. Two MT regulators — the MT end binding protein NOCA-1 and the MT nucleator γ-tubulin — localize to the adherens junctions and hemidesmosomes in the epidermis and intact MTs are required for maturation of both attachment structures. This study identified a synergistic effect of MTs and actomyosin contractility in controlling embryonic elongation and demonstrated a role of MTs in maturation of adherens junctions and hemidesmosomes.

3.4.1 MTs contribute to epidermal morphogenesis during embryonic elongation

There are two ways to explain the synergistic defects caused by disrupted MTs and reduced contractility. First, MT inhibition could reduce the actomyosin contractility in a LET-502/ROCK independent manner, and its combination with the *let-502* mutation mediated reduction made the contractility lower than the threshold required for normal elongation. It is known that LET-502/ROCK is not the only pathway regulating the actomyosin contractility, since null mutations in

the positive regulator LET-502/ROCK and the negative regulator MEL-11 can suppress each other (Wissmann *et al.*, 1997; Piekny *et al.*, 2000). One example of parallel pathways involves FEM-2, a PP2c phosphatase better known for its role in sex determination, since *fem-2* mutations stop the nearly normal elongation in *let-502;mel-11* double mutants (Piekny *et al.*, 2000). In addition, two other kinases, MRCK-1 and PAK-1, function redundantly with ROCK during *C. elegans* elongation (Gally *et al.*, 2009). Thus, it is possible that MTs control actomyosin activities in parallel to the LET-502/MEL-11 pathway.

Second, the effects of MTs could be solely explained by their mechanical properties. During embryonic elongation, MTs are organized into circumferential arrays in the dorsoventral epidermis (Figure 3.2). MTs are stiff polymers, as a consequence, their circumferential organization probably renders the dorsoventral cells more resistant to pushing and pulling forces. The anisotropic organization of MTs is conceptually important for morphogenesis, especially taking into account that the actomyosin activities are not uniformly distributed in all epidermis. Normally, the actomyosin activity is high in the lateral epidermis and low in the dorsoventral epidermis (Wissmann *et al.*, 1997, 1999; Diogon *et al.*, 2007). A mathematical model for elongation is proposed based on simple assumptions that embryos are noncompressible continuum, the driving force is actomyosin contractility and the passive response is coming from the MTs (Ciarletta *et al.*, 2009). In this model, the anisotropy in dorsoventral epidermis provided by MTs are required for maximum stretch of the embryos. Conceptually, the circumferential MTs make the

dorsoventral epidermis harder to stretch along the circumferential axis. When the dorsoventral epidermis passively responds to the contraction of lateral epidermis, the circumferential MT bundles make it preferentially stretch along the longitudinal axis of embryos. Moreover, this anisotropic response conferred by circumferential MTs are more important when the relative difference of actomyosin activities between lateral and dorsoventral epidermis is reduced (Ciarletta *et al.*, 2009). Therefore, the synergistic elongation defects of MT inhibition and contractility reduction can be explained by the disrupted anisotropy in dorsoventral epidermis and the reduced actomyosin activity in the lateral epidermis.

3.4.2 MTs are important for maturation of epidermal junction structures

Two pieces of evidence support that MTs are important for maturation of epidermal junction structures. Two MT regulators, the MT nucleator γ-tubulin and the MT end binding protein NOCA-1, localize to the adherens junctions and hemidesmosomes during embryonic elongation (Figure 3.4). Moreover, E-cadherin clustering onto the adherens junctions and hemidesmosomes are disrupted when MTs are degraded by *Spastin(O/E)* or NOCA-1 inhibition (Figure 3.6, Figure 3.5). In cultured epithelial cells, non-centrosomal MTs have been shown to recruit the minus-end directed kinesin moter KIFC3 for proper organization of the zonula adherens (Meng *et al.*, 2008). Another study showed that non-centrosomal MTs

recruit type II myosins to engage the adherens junctions and then potentiate the tight junction integrity (Sumigray *et al.*, 2012). By similarity, non-centrosomal MTs in the embryonic epidermis of *C. elegans* embryos may also serve as transportation tracks to recruit factors for maturation of the adherens junctions and the hemidesmosomes.

3.5 Material and methods

3.5.1 Worm Strains

Table 3.1: Strains used in Chapter 3

Strain#	**Genotype**
OD523	unc-119(ed3)III; ltSi63[pOD1111/pSW009; CEOP3608 TBG-1::GFP; cb-unc-119(+)]II
OD723	noca-1(ok3692)V/nT1[qIs51](IV;V)
OD726	ltSi77[pOD1112/pSW032; Plbp-1::mCherry; cb-unc-119(+)]V
OD761	let-502(sb118ts)I (6× outcrossed)
OD844	let-502(sb118ts)I; ltSi77[pSW032; Plbp-1::mCherry; cb-unc-119(+)]V
OD845	let-502(sb118ts)I; nT1[qIs51](IV;V)
OD846	let-502(sb118ts)I; noca-1(ok3692)V/nT1[qIs51](IV;V)

Table 3.1: Strains used in Chapter 3 (continued)

Strain#	Genotype
OD907	ltSi222[pOD1250/pSW078; Plbp-1::GFP-tbb-2-operon-linker-mCherry-his-11; cb-unc-119(+)]I; noca-1(ok3692)V/nT1[qIs51](IV;V)
OD909	ltSi222[pOD1250/pSW078; Plbp-1::GFP-tbb-2-operon-linker-mCherry-his-11; cb-unc-119(+)]I; ltSi77[pOD1112/pSW032; Plbp-1::mCherry; cb-unc-119(+)]V
OD1252	let-502(sb118ts)I; ItSi173[pOD1114/pSW046; Pnoca-1::noca-1gh; cb-unc-119(+)]II; noca-1(ok3692)V
OD1253	let-502(sb118ts)I; ItSi182[pOD1237/pSW055; Pnoca-1::noca-1abcfgh; cb-unc-119(+)]II; noca-1(ok3692)V
ML748	let-502(sb118ts)I; mcls35[Plin-26::GFP::tba-2; pat-4::CFP; pRF4]V
ML752	mcls35[Plin-26::GFP::tba-2; pat-4::CFP; pRF4]V
ML1652	mcIs46[pCL08(dlg-1::RFP); cb-unc-119(+)] (4× outcrossed)
ML1654	mcIs46[pCL08(dlg-1::RFP); cb-unc-119(+)]; mcSi53[Pdpy-7::EB1::GFP; cb-unc-119(+)]II

Table 3.1: Strains used in Chapter 3 (continued)

Strain#	**Genotype**
ML2282	mcIs54[pML497; Pdpy-7::SPAS-1_IRES_NLSmCherry, cb-unc-119(+)]
ML1896	mcIs35; mcIs54
ML1824	mcIs35; mcEx606(pML494; Pdpy-7::SPAS-1Δ_IRES_NLSmCherry; myo-2::GFP)
ML1931	let-502(sb118ts)I; mcIs54
ML1617*	xnIs96[pJN455; Phmr-1::HMR-1::GFP; cb-unc-119(+)] (outcrossed)
ML1913	let-502(sb118ts)I; xnIs96
ML1915	let-502(sb118ts)I; mcIs54/+; xnIs96

* ML1617 is an outcrossed version of a gift from J. Nance lab (Achilleos *et al.*, 2010).

The *C. elegans* strains used in this study were listed in Table 3.1. All worm strains were maintained at 20°C on standard NGM plates with OP-50 bacteria as food.

The *noca-1(ok3692)* allele is balanced with a translocation balancer (nT1),

but the exact noca-1 locus is slightly outside of the balanced region (2 cM away from the translocation joint). Therefore, all worms containing nT1 balanced noca-1(ok3692) were carefully maintained by singling out individual worms at each generation from worms giving correct phenotype segregations: $\frac{4}{5}$ of fertile worms with pharyngeal GFP marker and $\frac{1}{5}$ of sterile worms without pharyngeal GFP marker.

A transposon-based strategy was used to generate single copy transgenes used in this study (MosSCI; Frøkjær-Jensen *et al.*, 2008). Depending on the insertion sites, transgenes were cloned into pCFJ151 (ChrII insertion, ttTi5605), pCFJ352 (ChrI insertion, ttTi4348) or *de novo* (ChrV insertion, ttTi22935) by Gibson Assembly (Gibson *et al.*, 2009) to generate the repairing plasmids. In most cases, an improved transposase plasmid using a stronger promoter (pCFJ601, Peft-3::Mos1 transposase, 50 ng/μL) and an additional negative selection marker pMA122 (Phsp-16.41::peel-1, 10 ng/μL) were used in the injection mix. Single copy transgenes were generated by injecting a mixture of repairing plasmid, transposase plasmid and selection markers into strains EG6429 (outcrossed from EG4322; ttTi5605, Chr II), EG6701 (ttTi4348, Chr I), EG8078 (oxTi185, Chr I) or EG8081 (oxTi177, Chr IV). After one week, progeny of injected worms were heat-shocked at 34°C for 2 hours to induce the expression of PEEL-1, in order to kill the exo-chromosome array containing worms. Moving progeny worms without fluorescent markers were identified as candidates and transgene integration was confirmed by PCR on both sides.

Exochromosome arrays were made by microinjecting a mixture of trangene plasmid and marker plasmid at various concentrations. In some cases, arrays were integrated into the genome by X-ray.

3.5.2 RNA Interference and Embryo Length Measurement

The DNA templates for synthesizing the *noca-1* dsRNA were amplified by PCR from the N2 cDNA using oligos AATTAACCCTCACTAAAGGgcgaacaag-gatcgtaaag and TAATACGACTCACTATAGGctgcatttgtttgaccatgc.

Single-stranded RNAs (ssRNAs) were first synthesized in 50 μL T3 and T7 reactions using cleaned PCR reactions as templates (MEGAscript, Invitrogen), and then cleaned using the MEGAclear kit (Invitrogen). The ssRNAs from 50 μL T3 and 50 μL T7 reactions were then mixed with 50 μL of 3x soaking buffer (32.7 mM Na_2HPO_4, 16.5 mM KH_2PO_4, 6.3 mM NaCl, 14.1 mM NH_4Cl). To make dsRNA, the mixed ssRNAs were first incubated at 68°C for 10 min to denature, and then incubated at 37°C for 30 min to anneal.

dsRNAs were delivered by soaking the L4 hermaphrodites for 24 hours at 20°C. After recovery from soaking, worms were incubated at 20°C for ∼18 hours before their embryos were dissected out for imaging at indicated temperatures in the figures.

Embryo length was measured using Image J. Briefly, a segmented line was mannually drawn along the midline of the embryo from the tip of nose to the tip of tail. The total length of this segmented line was taken as the embryo length. The

starting time point for elongation was determined by the first visual appearance of constriction, since *noca-1(m/z);let-502(sb118)* embryos had no distinctive comma stage for time alignment. This visual appearance of constriction was roughly correlated with the completion of ventral enclosure.

3.5.3 Immunofluorescence

Embryos were fixed and stained by indirect immunofluorescence, as described in (Bosher *et al.*, 2003). MH4 antibody (anti-intermediate filament), which was obtained from DSHB, was diluted 1:100.

3.5.4 Light Microscopy

Images in Figure 3.2 were acquired using an inverted Zeiss Axio Observer Z1 system with a Yokogawa spinning-disk confocal head (CSU-X1), a 63× 1.40 NA Plan Apochromat lens (Zeiss), and a Hamamatsu ORCA-ER camera (Model C4742-95-12ERG, Hamamatsu photonics). Imaging parameters were controlled using the AxioVision software (Zeiss).

Images in Figure 3.3A top and middle panels (control and *noca-1(m/z);let-502(sb118)* embryos) were acquired using an inverted Olympus IX70 microscope with a Delta-Vision system (Applied Precision), a 100× 1.35 NA U Plan Apochromat lens (Olympus), and a Roper Scientific CCD camera (CoolSNAP). Imaging parameters were controlled using the softWoRx software (Applied Precision).

Images in Figure 3.3A bottom panels (*Spastin(O/E);let-502(sb118)* em-

bryos) were captured using a Leica DMRXA2 (HCX 40× 1.25 NA Plan Apochromat lens) coupled to a Coolsnap HQ (Roper Scientific) camera, monitored by the MetaMorph software (Molecular Devices).

Images in Figure 3.1, Figure 3.4, Figure 3.5 and Figure 3.6 were captured using a Leica DMI6000 B spinning-disk confocal microscope (100× 1.43 NA Plan Apochromat lens), coupled with an Andor Revolution spinning-disk system (Ixon EMCCD 512X512 camera and Yokogawa spinning-disk head). Images were computationally projected using the MetaMorph software (Molecular Devices).

3.6 Acknowledgments

The research presented in this chapter was a collaboration effort with Sophie Quintin from the Labouesse lab. Figures contributed by Sophie Quintin were indicated at the end of the figure legends. We thank Tom Blumenthal for help designing the operon linker in the Spastin overexpression construct.

Chapter 3, in part, is currently being prepared for submission for publication. Quintin, Sophie; Wang, Shaohe; Pontabry, Julien; Bender, Ambre; Oegema, Karen; Labouesse, Michel. The dissertation author was one of the primary investigators and the second author of this material.

Chapter 4

Conclusions and discussions

4.1 Conclusions

The focus of this dissertation is the assembly mechanism and cellular function of non-centrosomal MT arrays. In Chapter 2, we focused on a specific non-centrosomal MT regulator NOCA-1 and found that NOCA-1 is a novel MT end binding protein. NOCA-1 uses eight splicing isoforms to function either on its own, or together with PTRN-1, to control non-centrosomal MT assembly in multiple *C. elegans* tissues. In Chapter 3, we established two methods to perturb the MT arrays in elongating *C. elegans* embryos to demonstrate the role of MTs during embryoni elongation. We found that MTs in the epidermis contribute to the elongation, but become essential only when the actomyosin contractility is reduced.

4.1.1 NOCA-1 is a novel MT end binding protein and PTRN-1 binds specifically to MT minus ends

Previous studies have shown that NOCA-1 specifically functions in non-centrosomal MT array formation, but does not contribute to centrosome-driven cell divisions (Figure 2.1; Green *et al.*, 2011). NOCA-1 has eight splicing isoforms, all of which share a 466 amino acid long C-teminus, while five of the longest isoforms also share an additional 205 amino acid long region termed the long-isoform domain (Figure 2.7). The shared C-terminus of NOCA-1 contains a coiled coil domain, which may explain the dimerization of NOCA-1 in solution (Table 2.1). NOCA-1 is well conserved among nematodes (Figure 2.8), but we have not yet identified homologs outside of nematodes.

We believe NOCA-1 binds to the MT ends for three reasons. First, NOCA-1::GFP localizes to the MTs and sometimes to the ends in post-embryonic epidermis (Figure 2.13A). Second, NOCA-1 co-sediments with taxol-stabilized MTs from the worm lysate (Figure 2.13B), where many MT associating proteins are competing for the binding sites on MTs. Third, purified NOCA-1 binds to the MT ends as demonstrated in the MT anchoring assay (Figure 2.13D). Although the MT anchoring assay may not represent the physiological condition, the end specific binding makes us think the activity is meaningful. On the other hand, NOCA-1 does localize at some MT ends in post-embryonic epidermis (Figure 2.13A). Therefore, we conclude that NOCA-1 binds to the MT ends.

We may expect PTRN-1 to bind to the MT minus ends based on studies on its homologs. Both the *Drophophila* and mammalian homologs of PTRN-1 bind to the MT minus ends (Meng *et al.*, 2008; Goodwin and Vale, 2010; Jiang *et al.*, 2014; Hendershott and Vale, 2014). Here we provided direct evidence that the *C. elegans* CAMSAP homolog also binds specifically to the minus ends of MTs. In vitro, purified GFP labeled PTRN-1 protein binds to the leading ends of moving MTs in a kinesin gliding assay (Figure 2.13E). In vivo, PTRN-1::GFP loclaizes to the MTs and sometimes to the ends in post-embryonic epidermis (Figure 2.13A). Interestingly, PTRN-1::GFP has both punctate and stretch loclaization patterns, indicating that it may function more similarly to CAMSAP2 and CAMSAP3, both of which have been reported to form short stabilized MT stretches in vivo and in vitro (Jiang *et al.*, 2014; Hendershott and Vale, 2014).

4.1.2 Two MT end binding proteins control MT array formation in *C.elegans* tissues

Based on phenotypic analysis, NOCA-1 by itself controls non-centrosomal MT array formation in the germline and embryonic epidermis. First, *noca-1*Δ mutants have completely disorganized germlines and they are completely sterile, indicating that NOCA-1 is reqruied for the germline function (Figure 2.6A). Depletion of NOCA-1 reduces the growing MT numbers similar to depletion of the MT nucleator γ-tubulin, demonstrating that NOCA-1 is involved in MT formation

in the germline (Figure 2.6C). Second, *noca-1*Δ mutants have nuclear migration defects in the embryonic epidermis (Figure 2.6D), while the nuclear migration is mediated by MT motor activity (Fridolfsson and Starr, 2010). Moreover, *noca-1*Δ mutant embryos have fewer growing MTs in the embryonic epidermis, indicating that NOCA-1 is required for MT formation here (Figure 2.6F). Taken together, we conclude that NOCA-1 is by itself required for MT formation in the germline and embryonic epidermis.

A genetic interaction has revealed that NOCA-1 and PTRN-1 have parallel functions in the post-embryonic epidermis. Single *noca-1*Δ and *ptrn-1*Δ mutants can both grow up to be morphologically normal adults. In contrast, *noca-1*Δ*; ptrn-1*Δ double mutants are synthetic larval lethal and the lethality originated from the post-embryonic epidermis (Figure 2.2, Figure 2.4). MT arrays in the post-embryonic epidermis are evenly spaced MT bundles running circumferentially around the animal. These MT arrays are only subtly affected in single *noca-1*Δ and *ptrn-1*Δ mutants, but nearly completely eliminated in *noca-1*Δ*;ptrn-1*Δ worms. Thus, we conclude that NOCA-1 and PTRN-1 function redundantly to control non-centrosomal array formation in the post-embryonic epidermis.

In sum, we have found that NOCA-1 by itself controls non-centrosomal MT array formation in the germline and embryonic epidermis, and function in parallel with PTRN-1 to control non-centrosomal array formation in the post-embryonic epidermis.

4.1.3 MTs contribute to embryonic elongation

We have shown that MTs in the epidermis of elongating *C. elegans* embryos can be inhibited by overexpressing the MT severing enzyme Spastin (Figure 3.1), or by inhibiting the MT end binding protein NOCA-1 (Figure 3.2). Although embryos elongate normally in both conditions, we found that elongation is abolished when MT inhibition is combined with reduced actomyosin contractility (Figure 3.3). Therefore, we conclude that MTs in the epidermis contribute to embryonic elongation, but only become essential if actomyosin contractility is limited.

4.2 Discussions

4.2.1 NOCA-1 and PTRN-1: similarity and difference

We showed that both NOCA-1 and PTRN-1 binds to the MT ends and both promote MT arrary formation in the post-embryoni epidermis. However, the two proteins share no sequence similarity and their functions are different. First, ectopic germline expression of PTRN-1 does not compensate the loss of NOCA-1, suggesting they are not interchangeable. Second, both NOCA-1 and PTRN-1 are present in the embryonic epidermis, but only NOCA-1 is reqruied for the MT-dependent nuclear migration (Figure 2.6D). Third, the MT arrays in post-embryonic epidermis are differently affected in single *noca-1*Δ and *ptrn-1*Δ mutants. We observed fewer dynamic MTs in *noca-1*Δ single mutants, but more

dynamic MTs in *ptrn-1*Δ mutants (Figure 2.4E).

The phenotypic differences between NOCA-1 and PTRN-1 deletion mutants can be partially explained by their different localizations. In every tissue of interst, NOCA-1 co-localizes with the MT nucleator γ-tubulin (Figure 2.11), but PTRN-1 does not. Based on that, we may speculate that NOCA-1 and PTRN-1 may selectively stabilize the minus ends generated by different means. For example, NOCA-1 may preferentially stabilize the γ-tubulin nucleated MTs, while PTRN-1 prefers the minus ends generated by MT severing. Under this speculation, the plus ends generated by these two means can be different in terms of nucleotide state or tubulin modifications, thus explaining the different MT dynamics in *noca-1*Δ and *ptrn-1*Δ worms. This idea predicts that PTRN-1 mediated MT formation requires MT severing activity. Thus, it will be interesting to test whether MT severing contributes to MT generation in the post-embryonic epidermis. If it is the case, then it will be interesting to see (1) whether the MT severing enzymes co-localizes with PTRN-1, and (2) whether *noca-1*Δ genetically interacts with mutations in the corresponding MT severing enzymes.

4.2.2 MTs: two ways to generate, two ways to stabilize?

Assembly of non-centrosomal MT arrays often involves localized MT generation and minus end stabilization/anchoring. MTs can be generated by γ-TuRC mediated nucleation or by MT severing mediated amplification. In the case of γ-TuRC mediated nucleation, it is conceptually possible that γ-TuRC remains at and

protects/anchors the MT minus ends. However, MT nucleation and anchoring are separable events even at mitotic centrosomes, where γ-TuRC mediated nulceation dominates the MT generation (Dammermann *et al.*, 2003). Ninein is a good candidate for minus end anchoring in this case, although in vitro work is required to clarify its biochemical activity (Mogensen *et al.*, 2000). We showed here that NOCA-1 is a novel MT end binding protein required for MT array formation and it closely follows the localization of γ-tubulin. We speculate that NOCA-1 might protect the ends of MTs released from γ-TuRC, although direct evidence for this idea is difficult to obtain.

MT severing is another way to generate more MTs. The MT severing enzymes katanin and spastin have been shown to generate MTs in meiotic spindle assembly, neurite outgrowth, axon branching and plant cortical arrays re-orientation (McNally *et al.*, 2006; Yu *et al.*, 2008; Lindeboom *et al.*, 2013b). For effective generation of "MT seeds", the MT severing activities need to be closely regulated to prevent complete MT disassembly, and the exposed MT ends need be stabilized. Interestingly, CAMSAP2 and CAMSAP3 are recently reported to recruit the MT severing enzyme katanin to regulate the lengths of CAMSAP2/3 stabilized MT stretches (Jiang *et al.*, 2014). We showed in this study that PTRN-1 also forms short stretches in the post-embryonic epidermis (Figure 2.12), suggesting that PTRN-1 might use a similar mechanism to control the lengths of stabilized MT stretches. It will be interesting to test whether MT severing enzymes are recruited by PTRN-1 in the post-embryonic epidermis and whether they are required

to regulate the lengths of PTRN-1 stretches.

We proposed here two ways of generating stabilized MTs for MT array formation: one is based on γ-TuRC mediated nucleation and NOCA-1 mediated stabilization, while the other is based on MT severing amplification and CAMSAP mediated protection. Different tissues could preferentially use one or both means to generate non-centrosomal MT arrays. In *C. elegans*, it appears that the MT severing and CAMSAP mediated MT generation predominates the neurites, while the γ-TuRC and NOCA-1 controlled MT formation predominates the germline and embryonic epidermis. In the post-embryonic epidermis, however, the two seem to function in parallel.

4.2.3 Non-centrosomal MT arrays in developing organisms

The functions of non-centrosomal MT arrays in the germline and embryonic epidermis of *C. elegans* are both related to nuclear positioning. While disruption of non-centrosomal arrays in the germline causes deleterious defects, disrupting MTs in the embryonic epidermis does not cause noticeable defects for the organism. This difference could be understood as the different susceptiblity to nuclear positioning between syncytium and individual cells. The *C. elegans* germline is a large syncytium, where thousands of nuclei are arranged in their membrane compartments; nulcear positioning defects would thus cause many nuclei falling out into the rachis to completely disrupt the germline architecture. In contrast, the nulear migration in embryonic epidermis happens when they are still individual cells, so

even the nuclei lose their migration tracks, they do not have much freedom to go around.

The circumferential MT arrays in the embryonic epidermis also contributes to the embryonic elongation. Although disrupting the MTs alone does not cause elongation defects, MT inhibition combined with reduced actomyosin contractility causes severe elongation defects (Figure 3.3). We proposed that these MT arrays are important for that they confer the mechanical anisotropy of the dorsoventral epidermis based on a mathematical model (Ciarletta *et al.*, 2009).

We have proposed the circumferential MT arrays in the post-embryonic epidermis are important for secreting the cuticle. Due to the limited stretchability of the cuticle, worms periodically secrete a larger new cuticle to replace the smaller old one to allow body growth (a phenomenon called molting; Page and Johnstone, 2007). Supporting evidence includes that the circumferential MT array match the annular patterns of cuticles (Figure 2.5B) and when the array is disrupted in *noca-1*Δ*;ptrn-1*Δ double mutants, the worms grow much slower and their cuticles become permeable to a DNA dye (Figure 2.2B and C).

Interestingly, this proposed body growth mechanism closely resembles the growth mechanism of plant cells. Plant cells have cell walls which are made of cellulose microfibrils. During the elongation of plant hypocotyl cells, the cortical MT arrays are transversely oriented to guide cellulose deposition. In both *C. elegans* epidermis and *Arabidopsis* hypocotyl cells, MT arrays are transversely oriented so that they are perpendicular to the major growth axis (Figure 2.14). Moreover,

both the cuticle of *C. elegans* epidermis and the cell wall of *Arabidopsis* hypocotyl cells are patterned similarly to the MT arrays. This intriguing similarity may suggest a common strategy of using MT cytoskeleton to direct organismal or cellular growth that are comfined by non-stretchable extracellular matrix or cell walls. It will be particularly interesting to examine whether cuticle syntheis is affected when circumferential MT arrays are disrupted and whether cuticle components move long the MTs.

In the end, we propose that non-centrosomal MT arrays in developing organisms function in nuclear positioning and intracellular transportations. Most interestingly, non-centrosomal MT directed cellular growth may represent a conserved mechanism across animals and plants.

References

Achilleos, A., Wehman, A. M., and Nance, J. (2010). PAR-3 mediates the initial clustering and apical localization of junction and polarity proteins during C. elegans intestinal epithelial cell polarization. *Development*, 137(11):1833–1842.

Akhmanova, A. and Steinmetz, M. O. (2008). Tracking the ends: a dynamic protein network controls the fate of microtubule tips. *Nature Reviews Molecular Cell Biology*, 9(4):309–322.

Akhmanova, A. and Steinmetz, M. O. (2010). Microtubule +TIPs at a glance. *Journal of cell science*, 123(20):3415–3419.

Askham, J. and Vaughan, K. (2002). Evidence that an interaction between EB1 and p150Glued is required for the formation and maintenance of a radial microtubule array anchored at the centrosome. *Molecular biology of the cell*, 13(10):3627–3645.

Baas, P. W. and Brown, A. (1997). Slow axonal transport: the polymer transport model. *Trends in cell biology*, 7(10):380–384.

Baas, P. W., Deitch, J. S., Black, M. M., and Banker, G. A. (1988). Polarity orientation of microtubules in hippocampal neurons: uniformity in the axon and nonuniformity in the dendrite. *Proceedings of the National Academy of Sciences of the United States of America*, 85(21):8335–8339.

Baas, P. W. and Joshi, H. C. (1992). Gamma-tubulin distribution in the neuron: implications for the origins of neuritic microtubules. *The Journal of Cell Biology*, 119(1):171–178.

Baas, P. W., White, L. a., and Heidemann, S. R. (1987). Microtubule polarity reversal accompanies regrowth of amputated neurites. *Proceedings of the National Academy of Sciences of the United States of America*, 84(15):5272–5276.

Bacallao, R., Antony, C., Dotti, C., Karsenti, E., Stelzer, E. H., and Simons, K. (1989). The subcellular organization of Madin-Darby canine kidney cells during the formation of a polarized epithelium. *The Journal of Cell Biology*, 109(6):2817–2832.

Baines, A. J., Bignone, P. a., King, M. D. a., Maggs, A. M., Bennett, P. M., Pinder, J. C., and Phillips, G. W. (2009). The CKK domain (DUF1781) binds microtubules and defines the CAMSAP/ssp4 family of animal proteins. *Molecular biology and evolution*, 26(9):2005–2014.

Bartolini, F. and Gundersen, G. G. (2006). Generation of noncentrosomal microtubule arrays. *Journal of cell science*, 119(20):4155–4163.

Basto, R., Lau, J., Vinogradova, T., Gardiol, A., Woods, C. G., Khodjakov, A., and Raff, J. W. (2006). Flies without centrioles. *Cell*, 125(7):1375–1386.

Berger, I., Fitzgerald, D. J., and Richmond, T. J. (2004). Baculovirus expression system for heterologous multiprotein complexes. *Nature biotechnology*, 22(12):1583–1587.

Bettencourt-Dias, M. and Glover, D. M. (2007). Centrosome biogenesis and function: centrosomics brings new understanding. *Nature Reviews Molecular Cell Biology*, 8(6):451–463.

Bökel, C., Prokop, A., and Brown, N. H. (2005). Papillote and Piopio: Drosophila ZP-domain proteins required for cell adhesion to the apical extracellular matrix and microtubule organization. *Journal of cell science*, 118(3):633–642.

Bonaccorsi, S., Giansanti, M. G., and Gatti, M. (2000). Spindle assembly in Drosophila neuroblasts and ganglion mother cells. *Nature cell biology*, 2(1):54–56.

Bosher, J. M., Hahn, B.-S., Legouis, R., Sookhareea, S., Weimer, R. M., Gansmuller, A., Chisholm, A. D., Rose, A. M., Bessereau, J.-L., and Labouesse, M. (2003). The Caenorhabditis elegans vab-10 spectraplakin isoforms protect the epidermis against internal and external forces. *The Journal of Cell Biology*, 161(4):757–768.

Brodu, V., Baffet, A. D., Le Droguen, P.-M., Casanova, J., and Guichet, A. (2010). A developmentally regulated two-step process generates a noncentrosomal microtubule network in Drosophila tracheal cells. *Developmental cell*, 18(5):790–801.

Browning, H., Hayles, J., Mata, J., Aveline, L., Nurse, P., and McIntosh, J. R. (2000). Tea2p Is a Kinesin-like Protein Required to Generate Polarized Growth in Fission Yeast. *The Journal of Cell Biology*, 151(1):15–28.

Brunner, D. and Nurse, P. (2000). CLIP170-like tip1p Spatially Organizes Microtubular Dynamics in Fission Yeast. *Cell*, 102(5):695–704.

Burton, P. R. and Paige, J. L. (1981). Polarity of axoplasmic microtubules in the olfactory nerve of the frog. *Proceedings of the National Academy of Sciences of the United States of America*, 78(5):3269–3273.

Chang, F. (2001). Establishment of a cellular axis in fission yeast. *Trends in Genetics*, 17(5):273–278.

Chisholm, A. D. and Hsiao, T. I. (2012). The Caenorhabditis elegans epidermis as a model skin. I: development, patterning, and growth. *Wiley Interdisciplinary Reviews: Developmental Biology*, 1(6):861–878.

Ciarletta, P., Ben Amar, M., and Labouesse, M. (2009). Continuum model of epithelial morphogenesis during Caenorhabditis elegans embryonic elongation. *Philosophical transactions. Series A, Mathematical, physical, and engineering sciences*, 367(1902):3379–400.

Costa, M., Draper, B. W., and Priess, J. R. (1997). The role of actin filaments in patterning the Caenorhabditis elegans cuticle. *Developmental biology*, 184(2):373–384.

Costa, M., Raich, W., Agbunag, C., Leung, B., Hardin, J., and Priess, J. R. (1998). A Putative Catenin-Cadherin System Mediates Morphogenesis of the Caenorhabditis elegans Embryo. *The Journal of Cell Biology*, 141(1):297–308.

Dammermann, A., Desai, A., and Oegema, K. (2003). The minus end in sight. *Current Biology*, 13(15):R614–R624.

Dammermann, A. and Merdes, A. (2002). Assembly of centrosomal proteins and microtubule organization depends on PCM-1. *The Journal of Cell Biology*, 159(2):255–266.

Delgehyr, N., Sillibourne, J., and Bornens, M. (2005). Microtubule nucleation and anchoring at the centrosome are independent processes linked by ninein function. *Journal of cell science*, 118(8):1565–1575.

Desai, A. and Mitchison, T. (1997). Microtubule polymerization dynamics. *Annual review of cell and developmental biology*, 13(1):83–117.

Desai, A., Rybina, S., Müller-Reichert, T., Shevchenko, A., Shevchenko, A., Hyman, A., and Oegema, K. (2003). KNL-1 directs assembly of the microtubule-binding interface of the kinetochore in C. elegans. *Genes & development*, 17(19):2421–2435.

Diogon, M., Wissler, F., Quintin, S., Nagamatsu, Y., Sookhareea, S., Landmann, F., Hutter, H., Vitale, N., and Labouesse, M. (2007). The RhoGAP RGA-2 and LET-502/ROCK achieve a balance of actomyosin-dependent forces in C. elegans epidermis to control morphogenesis. *Development*, 134(13):2469–2479.

Dixit, R., Chang, E., and Cyr, R. (2006). Establishment of polarity during organization of the acentrosomal plant cortical microtubule array. *Molecular biology of the cell*, 17(3):1298–1305.

Drummond, D. R. and Cross, R. A. (2000). Dynamics of interphase microtubules in Schizosaccharomyces pombe. *Current Biology*, 10(13):766–775.

Ehrhardt, D. W. and Shaw, S. L. (2006). Microtubule dynamics and organization in the plant cortical array. *Annual review of plant biology*, 57(1):859–875.

Errico, A., Ballabio, A., and Rugarli, E. I. (2002). Spastin, the protein mutated in autosomal dominant hereditary spastic paraplegia, is involved in microtubule dynamics. *Human Molecular Genetics*, 11(2):153–163.

Feldman, J. L. and Priess, J. R. (2012). A role for the centrosome and PAR-3 in the hand-off of MTOC function during epithelial polarization. *Current Biology*, 22(7):575–582.

Flory, M. R. and Davis, T. N. (2003). The centrosomal proteins pericentrin and kendrin are encoded by alternatively spliced products of one gene. *Genomics*, 82(3):401–405.

Fridolfsson, H. N. and Starr, D. A. (2010). Kinesin-1 and dynein at the nuclear envelope mediate the bidirectional migrations of nuclei. *The Journal of Cell Biology*, 191(1):115–128.

Frøkjær-Jensen, C., Davis, M. W., Hollopeter, G., Taylor, J., Harris, T. W., Nix, P., Lofgren, R., Prestgard-Duke, M., Bastiani, M., Moerman, D. G., and Jorgensen, E. M. (2010). Targeted gene deletions in C. elegans using transposon excision. *Nature methods*, 7(6):451–453.

Frøkjær-Jensen, C., Davis, M. W., Hopkins, C. E., Newman, B. J., Thummel, J. M., Olesen, S. r.-P., Grunnet, M., and Jorgensen, E. M. (2008). Single-copy insertion of transgenes in Caenorhabditis elegans. *Nature genetics*, 40(11):1375–1383.

Fygenson, D. K. and Flyvbjerg, H. (1995). Spontaneous nucleation of microtubules. *Physical Review E*, 51(5):5058–5063.

Gally, C., Wissler, F., Zahreddine, H., Quintin, S., Landmann, F., and Labouesse, M. (2009). Myosin II regulation during C. elegans embryonic elongation: LET-502/ROCK, MRCK-1 and PAK-1, three kinases with different roles. *Development*, 136(18):3109–3119.

Gibson, D. G., Young, L., Chuang, R.-Y., Venter, J. C., Hutchison, C. A., and Smith, H. O. (2009). Enzymatic assembly of DNA molecules up to several hundred kilobases. *Nature methods*, 6(5):343–345.

Gittes, F., Mickey, B., Nettleton, J., and Howard, J. (1993). Flexural rigidity of microtubules and actin filaments measured from thermal fluctuations in shape. *The Journal of Cell Biology*, 120(4):923–934.

Goodwin, S. S. and Vale, R. D. (2010). Patronin regulates the microtubule network by protecting microtubule minus ends. *Cell*, 143(2):263–274.

Goshima, G., Mayer, M., Zhang, N., Stuurman, N., and Vale, R. D. (2008). Augmin: a protein complex required for centrosome-independent microtubule generation within the spindle. *The Journal of Cell Biology*, 181(3):421–429.

Goshima, G., Wollman, R., Goodwin, S. S., Zhang, N., Scholey, J. M., Vale, R. D., and Stuurman, N. (2007). Genes required for mitotic spindle assembly in Drosophila S2 cells. *Science*, 316(5823):417–421.

Green, P. B. (1962). Mechanism for Plant Cellular Morphogenesis. *Science*, 138(3548):1404–1405.

Green, R. A., Kao, H.-L., Audhya, A., Arur, S., Mayers, J. R., Fridolfsson, H. N., Schulman, M., Schloissnig, S., Niessen, S., Laband, K., Wang, S., Starr, D. A., Hyman, A. A., Schedl, T., Desai, A., Piano, F., Gunsalus, K. C., and Oegema, K. (2011). A high-resolution C. elegans essential gene network based on phenotypic profiling of a complex tissue. *Cell*, 145(3):470–482.

Grindstaff, K. K., Bacallao, R. L., and Nelson, W. J. (1998). Apiconuclear Organization of Microtubules Does Not Specify Protein Delivery from the Trans-Golgi Network to Different Membrane Domains in Polarized Epithelial Cells. *Molecular Biology of the Cell*, 9(3):685–699.

Guo, J., Yang, Z., Song, W., Chen, Q., Wang, F., Zhang, Q., and Zhu, X. (2006). Nudel Contributes to Microtubule Anchoring at the Mother Centriole and Is Involved in Both Dynein- dependent and -independent Centrosomal Protein Assembly. *Molecular biology of the cell*, 17(2):680–689.

Hagan, I. (1998). The fission yeast microtubule cytoskeleton. *Journal of cell science*, 111(12):1603–1612.

Hamill, D. R., Severson, A. F., Carter, J. C., and Bowerman, B. (2002). Centrosome maturation and mitotic spindle assembly in C. elegans require SPD-5, a protein with multiple coiled-coil domains. *Developmental cell*, 3(5):673–684.

Hannak, E., Oegema, K., Kirkham, M., Gönczy, P., Habermann, B., and Hyman, A. A. (2002). The kinetically dominant assembly pathway for centrosomal asters in Caenorhabditis elegans is gamma-tubulin dependent. *The Journal of Cell Biology*, 157(4):591–602.

Haren, L., Remy, M.-H., Bazin, I., Callebaut, I., Wright, M., and Merdes, A. (2006). NEDD1-dependent recruitment of the gamma-tubulin ring complex to the centrosome is necessary for centriole duplication and spindle assembly. *The Journal of Cell Biology*, 172(4):505–515.

Hazan, J., Fonknechten, N., Mavel, D., Paternotte, C., Samson, D., Artiguenave, F., Davoine, C. S., Cruaud, C., Dürr, a., Wincker, P., Brottier, P., Cattolico, L., Barbe, V., Burgunder, J. M., Prud'homme, J. F., Brice, a., Fontaine, B., Heilig, B., and Weissenbach, J. (1999). Spastin, a new AAA protein, is altered in the most frequent form of autosomal dominant spastic paraplegia. *Nature genetics*, 23(3):296–303.

Heidemann, S. and McIntosh, J. (1980). Visualization of the structural polarity of microtubules. *Nature*, 286(5772):517–519.

Heidemann, S. R., Landers, J. M., and Hamborg, M. A. (1981). Polarity orientation of axonal microtubules. *The Journal of Cell Biology*, 91(3):661–665.

Heitz, M. J., Petersen, J., Valovin, S., and Hagan, I. M. (2001). MTOC formation during mitotic exit in fission yeast. *Journal of cell science*, 114(24):4521–4532.

Hendershott, M. C. and Vale, R. D. (2014). Regulation of microtubule minus-end dynamics by CAMSAPs and Patronin. *Proceedings of the National Academy of Sciences of the United States of America*, 111(16):5860–5865.

Hirokawa, N., Funakoshi, S. T., and Takeda, S. (1997). Slow axonal transport: the subunit transport model. *Trends in cell biology*, 7(10):384–388.

Hirokawa, N. and Takemura, R. (2005). Molecular motors and mechanisms of directional transport in neurons. *Nature Reviews Neuroscience*, 6(3):201–214.

Holy, T. E. and Leibler, S. (1994). Dynamic instability of microtubules as an efficient way to search in space. *Proceedings of the National Academy of Sciences of the United States of America*, 91(12):5682–5685.

Jana, S. C., Marteil, G., and Bettencourt-Dias, M. (2014). Mapping molecules to structure: unveiling secrets of centriole and cilia assembly with near-atomic resolution. *Current opinion in cell biology*, 26:96–106.

Jankovics, F. and Brunner, D. (2006). Transiently reorganized microtubules are essential for zippering during dorsal closure in Drosophila melanogaster. *Developmental cell*, 11(3):375–385.

Jaulin, F., Xue, X., Rodriguez-Boulan, E., and Kreitzer, G. (2007). Polarization-dependent selective transport to the apical membrane by KIF5B in MDCK cells. *Developmental cell*, 13(4):511–522.

Jiang, K., Hua, S., Mohan, R., Grigoriev, I., Yau, K. W., Liu, Q., Katrukha, E. a., Altelaar, a. F. M., Heck, A. J. R., Hoogenraad, C. C., and Akhmanova, A. (2014). Microtubule Minus-End Stabilization by Polymerization-Driven CAMSAP Deposition. *Developmental cell*, 28(3):295–309.

Kawaguchi, S.-i. and Zheng, Y. (2004). Characterization of a Drosophila centrosome protein CP309 that shares homology with Kendrin and CG-NAP. *Molecular biology of the cell*, 15(1):37–45.

Kellogg, D. R., Field, C. M., and Alberts, B. M. (1989). Identification of microtubule-associated proteins in the centrosome, spindle, and kinetochore of the early Drosophila embryo. *The Journal of Cell Biology*, 109(6):2977–2991.

Khodjakov, A., Cole, R. W., Oakley, B. R., and Rieder, C. L. (2000). Centrosome-independent mitotic spindle formation in vertebrates. *Current Biology*, 10(2):59–67.

Kikkawa, M., Ishikawa, T., Nakata, T., Wakabayashi, T., and Hirokawa, N. (1994). Direct visualization of the microtubule lattice seam both in vitro and in vivo. *The Journal of Cell Biology*, 127(6):1965–1971.

Kim, J. C., Badano, J. L., Sibold, S., Esmail, M. A., Hill, J., Hoskins, B. E., Leitch, C. C., Venner, K., Ansley, S. J., Ross, A. J., Leroux, M. R., Katsanis, N., and Beales, P. L. (2004). The Bardet-Biedl protein BBS4 targets cargo to the pericentriolar region and is required for microtubule anchoring and cell cycle progression. *Nature genetics*, 36(5):462–470.

King, M. D. A., Phillips, G. W., Bignone, P. A., Hayes, N. V. L., Pinder, J. C., and Baines, A. J. (2014). A conserved sequence in calmodulin regulated spectrin-associated protein 1 links its interaction with spectrin and calmodulin to neurite outgrowth. *Journal of neurochemistry*, 128(3):391–402.

Kollman, J. M., Merdes, A., Mourey, L., and Agard, D. a. (2011). Microtubule nucleation by γ-tubulin complexes. *Nature Reviews Molecular Cell Biology*, 12(11):709–721.

Kollman, J. M., Polka, J. K., Zelter, A., Davis, T. N., and Agard, D. a. (2010). Microtubule nucleating gamma-TuSC assembles structures with 13-fold microtubule-like symmetry. *Nature*, 466(7308):879–882.

Labouesse, M. (2006). Epithelial junctions and attachments. *WormBook*.

Lafont, F., Burkhardt, J., and Kai, S. (1994). Involvement of microtubule motors in basolateral and apical transport in kidney cells. *Nature*, 372(6508):801–803.

Lechler, T. and Fuchs, E. (2007). Desmoplakin: an unexpected regulator of microtubule organization in the epidermis. *The Journal of Cell Biology*, 176(2):147–154.

Ledbetter, M. C. (1963). A "MICROTUBULE" IN PLANT CELL FINE STRUCTURE. *The Journal of Cell Biology*, 19(1):239–250.

Lindeboom, J. J., Lioutas, A., Deinum, E. E., Tindemans, S. H., Ehrhardt, D. W., Emons, A. M. C., Vos, J. W., and Mulder, B. M. (2013a). Cortical microtubule arrays are initiated from a nonrandom prepattern driven by atypical microtubule initiation. *Plant physiology*, 161(3):1189–1201.

Lindeboom, J. J., Nakamura, M., Hibbel, A., Shundyak, K., Gutierrez, R., Ketelaar, T., Emons, A. M. C., Mulder, B. M., Kirik, V., and Ehrhardt, D. W. (2013b). A mechanism for reorientation of cortical microtubule arrays driven by microtubule severing. *Science*, 342(6163):1245533.

Little, M., Krauhs, E., and Ponstingl, H. (1981). Tubulin sequence conservation. *Biosystems*, 14(3):239–246.

Lüders, J., Patel, U. K., and Stearns, T. (2006). GCP-WD is a gamma-tubulin targeting factor required for centrosomal and chromatin-mediated microtubule nucleation. *Nature cell biology*, 8(2):137–147.

Mahoney, N. M., Goshima, G., Douglass, A. D., and Vale, R. D. (2006). Making microtubules and mitotic spindles in cells without functional centrosomes. *Current Biology*, 16(6):564–569.

Mandelkow, E., Schultheiss, R., Rapp, R., Muller, M., and Mandelkow, E. (1986). On the surface lattice of microtubules: helix starts, protofilament number, seam, and handedness. *The Journal of Cell Biology*, 102(3):1067–1073.

Manning, J. A., Shalini, S., Risk, J. M., Day, C. L., and Kumar, S. (2010). A direct interaction with NEDD1 regulates gamma-tubulin recruitment to the centrosome. *PloS ONE*, 5(3).

Marcette, J., Chen, J., and Nonet, M. (2014). The Caenorhabditis elegans microtubule minus-end binding homolog PTRN-1 stabilizes synapses and neurites. *eLife*, 3.

Mata, J. and Nurse, P. (1997). tea1 and the Microtubular Cytoskeleton Are Important for Generating Global Spatial Order within the Fission Yeast Cell. *Cell*, 89(6):939–949.

Matsushita-Ishiodori, Y., Yamanaka, K., and Ogura, T. (2007). The C. elegans homologue of the spastic paraplegia protein, spastin, disassembles microtubules. *Biochemical and biophysical research communications*, 359(1):157–162.

McNally, K., Audhya, A., Oegema, K., and McNally, F. J. (2006). Katanin controls mitotic and meiotic spindle length. *The Journal of Cell Biology*, 175(6):881–891.

Meads, T. and Schroer, T. A. (1995). Polarity and nucleation of microtubules in polarized epithelial cells. *Cell motility and the cytoskeleton*, 32(4):273–288.

Megraw, T. L., Kao, L.-R., and Kaufman, T. C. (2001). Zygotic development without functional mitotic centrosomes. *Current Biology*, 11(2):116–120.

Megraw, T. L., Li, K., Kao, L. R., and Kaufman, T. C. (1999). The centrosomin protein is required for centrosome assembly and function during cleavage in Drosophila. *Development*, 126(13):2829–2839.

Meng, W., Mushika, Y., Ichii, T., and Takeichi, M. (2008). Anchorage of microtubule minus ends to adherens junctions regulates epithelial cell-cell contacts. *Cell*, 135(5):948–959.

Meunier, S. and Vernos, I. (2012). Microtubule assembly during mitosis - from distinct origins to distinct functions? *Journal of cell science*, 125(12):2805–2814.

Mitchison, T. and Kirschner, M. (1984). Dynamic instability of microtubule growth. *Nature*, 312(5991):237–242.

Mogensen, M. M., Malik, A., Piel, M., Bouckson-Castaing, V., and Bornens, M. (2000). Microtubule minus-end anchorage at centrosomal and non-centrosomal sites: the role of ninein. *Journal of cell science*, 113(17):3013–3023.

Mogensen, M. M., Tucker, J. B., and Stebbings, H. (1989). Microtubule polarities indicate that nucleation and capture of microtubules occurs at cell surfaces in Drosophila. *The Journal of Cell Biology*, 108(4):1445–1452.

Moribe, H., Yochem, J., Yamada, H., Tabuse, Y., Fujimoto, T., and Mekada, E. (2004). Tetraspanin protein (TSP-15) is required for epidermal integrity in Caenorhabditis elegans. *Journal of cell science*, 117(22):5209–5220.

Moss, D. K., Bellett, G., Carter, J. M., Liovic, M., Keynton, J., Prescott, A. R., Lane, E. B., and Mogensen, M. M. (2007). Ninein is released from the centrosome and moves bi-directionally along microtubules. *Journal of cell science*, 120(17):3064–3074.

Murata, T., Sonobe, S., Baskin, T. I., Hyodo, S., Hasezawa, S., Nagata, T., Horio, T., and Hasebe, M. (2005). Microtubule-dependent microtubule nucleation based on recruitment of gamma-tubulin in higher plants. *Nature Cell Biology*, 7(10):961–968.

Müsch, A. (2004). Microtubule organization and function in epithelial cells. *Traffic*, 5(1):1–9.

Nelson, W. and Yeaman, C. (2001). Protein trafficking in the exocytic pathway of polarized epithelial cells. *Trends in Cell Biology*, 11(12):483–486.

Noda, Y., Okada, Y., Saito, N., Setou, M., Xu, Y., Zhang, Z., and Hirokawa, N. (2001). KIFC3, a microtubule minus end-directed motor for the apical transport of annexin XIIIb-associated Triton-insoluble membranes. *The Journal of Cell Biology*, 155(1):77–88.

Oakley, B. R. and Morris, N. R. (1981). A β-tubulin mutation in Aspergillus nidulans that blocks microtubule function without blocking assembly. *Cell*, 24(3):837–845.

Oakley, C. E. and Oakley, B. R. (1989). Identification of gamma-tubulin, a new member of the tubulin superfamily encoded by mipA gene of Aspergillus nidulans. *Nature*, 338(6217):662–664.

Oegema, K., Wiese, C., Martin, O. C., Milligan, R. A., Iwamatsu, A., Mitchison, T. J., and Zheng, Y. (1999). Characterization of two related Drosophila γ-tubulin complexes that differ in their ability to nucleate microtubules. *The Journal of Cell Biology*, 144(4):721–733.

Ohta, T., Essner, R., Ryu, J.-H., Palazzo, R. E., Uetake, Y., and Kuriyama, R. (2002). Characterization of Cep135, a novel coiled-coil centrosomal protein involved in microtubule organization in mammalian cells. *The Journal of Cell Biology*, 156(1):87–99.

Ori-McKenney, K. M., Jan, L. Y., and Jan, Y.-N. (2012). Golgi outposts shape dendrite morphology by functioning as sites of acentrosomal microtubule nucleation in neurons. *Neuron*, 76(5):921–930.

Page, A. P. and Johnstone, I. L. (2007). The cuticle. *WormBook*.

Paredez, A. R., Somerville, C. R., and Ehrhardt, D. W. (2006). Visualization of cellulose synthase demonstrates functional association with microtubules. *Science*, 312(5779):1491–1495.

Piekny, A. J., Johnson, J.-L. F., Cham, G. D., and Mains, P. E. (2003). The Caenorhabditis elegans nonmuscle myosin genes nmy-1 and nmy-2 function as redundant components of the let-502/Rho-binding kinase and mel-11/myosin phosphatase pathway during embryonic morphogenesis. *Development*, 130(23):5695–5704.

Piekny, A. J., Wissmann, A., and Mains, P. E. (2000). Embryonic Morphogenesis in Caenorhabditis elegans Integrates the Activity of LET-502 Rho-Binding Kinase, MEL-11 Myosin Phosphatase, DAF-2 insulin receptor and FEM-2 PP2c phosphatase. *Genetics*, 156(4):1671–1689.

Pizon, V., Gerbal, F., Diaz, C. C., and Karsenti, E. (2005). Microtubule-dependent transport and organization of sarcomeric myosin during skeletal muscle differentiation. *The EMBO journal*, 24(21):3781–3792.

Priess, J. R. and Hirsh, D. I. (1986). Caenorhabditis elegans morphogenesis: the role of the cytoskeleton in elongation of the embryo. *Developmental biology*, 117(1):156–173.

Quintyne, N. J., Gill, S. R., Eckley, D. M., Crego, C. L., Compton, D. A., and Schroer, T. a. (1999). Dynactin is required for microtubule anchoring at centrosomes. *The Journal of Cell Biology*, 147(2):321–334.

Redenbach, D. M. and Vogl, A. W. (1991). Microtubule polarity in Sertoli cells: a model for microtubule-based spermatid transport. *European journal of cell biology*, 54(2):277–290.

Ren, J., Wen, L., Gao, X., Jin, C., Xue, Y., and Yao, X. (2008). CSS-Palm 2.0: an updated software for palmitoylation sites prediction. *Protein engineering, design & selection*, 21(11):639–644.

Richardson, C., Spilker, K., and Cueva, J. (2014). PTRN-1, a microtubule minus end-binding CAMSAP homolog, promotes microtubule function in Caenorhabditis elegans neurons. *eLife*, 3.

Roll-Mecak, A. and McNally, F. J. (2010). Microtubule-severing enzymes. *Current opinion in cell biology*, 22(1):96–103.

Roll-Mecak, A. and Vale, R. D. (2005). The Drosophila homologue of the hereditary spastic paraplegia protein, spastin, severs and disassembles microtubules. *Current Biology*, 15(7):650–655.

Roll-Mecak, A. and Vale, R. D. (2006). Making more microtubules by severing: a common theme of noncentrosomal microtubule arrays? *The Journal of Cell Biology*, 175(6):849–851.

Roll-Mecak, A. and Vale, R. D. (2008). Structural basis of microtubule severing by the hereditary spastic paraplegia protein spastin. *Nature*, 451(7176):363–367.

Samejima, I., Miller, V. J., Groocock, L. M., and Sawin, K. E. (2008). Two distinct regions of Mto1 are required for normal microtubule nucleation and efficient association with the gamma-tubulin complex in vivo. *Journal of cell science*, 121(23):3971–3980.

Sawin, K., Lourenco, P., and Snaith, H. (2004). Microtubule nucleation at non-spindle pole body microtubule-organizing centers requires fission yeast centrosomin-related protein mod20p. *Current Biology*, 14(9):763–775.

Sherwood, N. T., Sun, Q., Xue, M., Zhang, B., and Zinn, K. (2004). Drosophila spastin regulates synaptic microtubule networks and is required for normal motor function. *PLoS biology*, 2(12).

Siegel, L. and Monty, K. (1966). Determination of molecular weights and frictional ratios of proteins in impure systems by use of gel filtration and density gradient centrifugation. Application to crude preparations of sulfite and hydroxylamine. *Biochimica et Biophysica Acta (BBA)-Biophysics including Photosynthesis*, 112(2):346–362.

Simon, J. R., Parsons, S. F., and Salmon, E. D. (1992). Buffer conditions and non-tubulin factors critically affect the microtubule dynamic instability of sea urchin egg tubulin. *Cell motility and the cytoskeleton*, 21(1):1–14.

Song, Y. and Mandelkow, E. (1995). The anatomy of flagellar microtubules: polarity, seam, junctions, and lattice. *The Journal of Cell Biology*, 128(January):81–94.

Song, Y. H. and Mandelkow, E. (1993). Recombinant kinesin motor domain binds to beta-tubulin and decorates microtubules with a B surface lattice. *Proceedings of the National Academy of Sciences of the United States of America*, 90(5):1671–1675.

Srayko, M., Kaya, A., Stamford, J., and Hyman, A. A. (2005). Identification and characterization of factors required for microtubule growth and nucleation in the early C. elegans embryo. *Developmental cell*, 9(2):223–236.

Stepanova, T., Slemmer, J., Hoogenraad, C. C., Lansbergen, G., Dortland, B., De Zeeuw, C. I., Grosveld, F., van Cappellen, G., Akhmanova, A., and Galjart, N. (2003). Visualization of microtubule growth in cultured neurons via the use of EB3-GFP (end-binding protein 3-green fluorescent protein). *The Journal of neuroscience*, 23(7):2655–2664.

Stiess, M., Maghelli, N., Kapitein, L. C., Gomis-Rüth, S., Wilsch-Bräuninger, M., Hoogenraad, C. C., Tolić-Nø rrelykke, I. M., and Bradke, F. (2010). Axon extension occurs independently of centrosomal microtubule nucleation. *Science*, 327(5966):704–707.

Stone, M. C., Roegiers, F., and Rolls, M. M. (2008). Microtubules Have Opposite Orientation in Axons and Dendrites of Drosophila Neurons. *Molecular biology of the cell*, 19(10):4122–4129.

Sugimoto, K., Williamson, R. E., and Wasteneys, G. O. (2000). New techniques enable comparative analysis of microtubule orientation, wall texture, and growth rate in intact roots of Arabidopsis. *Plant physiology*, 124(4):1493–1506.

Sulston, J. E., Schierenberg, E., White, J. G., and Thomson, J. N. (1983). The embryonic cell lineage of the nematode Caenorhabditis elegans. *Developmental biology*, 100(1):64–119.

Sumigray, K. D., Foote, H. P., and Lechler, T. (2012). Noncentrosomal microtubules and type II myosins potentiate epidermal cell adhesion and barrier formation. *The Journal of Cell Biology*, 199(3):513–525.

Tai, A. W., Chuang, J.-Z., Bode, C., Wolfrum, U., and Sung, C.-H. (1999). Rhodopsins Carboxy-Terminal Cytoplasmic Tail Acts as a Membrane Receptor for Cytoplasmic Dynein by Binding to the Dynein Light Chain Tctex-1. *Cell*, 97(7):877–887.

Takahashi, M., Yamagiwa, A., Tamako, N., Mukai, H., and Ono, Y. (2002). Centrosomal proteins CG-NAP and kendrin provide microtubule nucleation sites by anchoring γ-tubulin ring complex. *Molecular biology of the cell*, 13(9):3235–3245.

Tassin, A. M., Maro, B., and Bornens, M. (1985). Fate of microtubule-organizing centers during myogenesis in vitro. *The Journal of Cell Biology*, 100(1):35–46.

Terada, S., Kinjo, M., and Hirokawa, N. (2000). Oligomeric Tubulin in Large Transporting Complex Is Transported via Kinesin in Squid Giant Axons. *Cell*, 103(1):141–155.

Terada, Y., Uetake, Y., and Kuriyama, R. (2003). Interaction of Aurora-A and centrosomin at the microtubule-nucleating site in Drosophila and mammalian cells. *The Journal of Cell Biology*, 162(5):757–763.

Tran, P. T., Marsh, L., Doye, V., Inoué, S., and Chang, F. (2001). A mechanism for nuclear positioning in fission yeast based on microtubule pushing. *The Journal of Cell Biology*, 153(2):397–411.

Trotta, N., Orso, G., Rossetto, M. G., Daga, A., and Broadie, K. (2004). The hereditary spastic paraplegia gene, spastin, regulates microtubule stability to modulate synaptic structure and function. *Current Biology*, 14(13):1135–1147.

Troutt, L. L. and Burnside, B. (1988). The unusual microtubule polarity in teleost retinal pigment epithelial cells. *The Journal of Cell Biology*, 107(4):1461–1464.

Venkatram, S., Tasto, J. J., Feoktistova, A., Jennings, J. L., Link, A. J., and Gould, K. L. (2004). Identification and characterization of two novel proteins affecting fission yeast γ-tubulin complex function. *Molecular biology of the cell*, 15(5):2287–2301.

Vorobjev, I. A., Svitkina, T. M., and Borisy, G. G. (1997). Cytoplasmic assembly of microtubules in cultured cells. *Journal of cell science*, 110(21):2635–2645.

Wang, H., Brust-Mascher, I., Civelekoglu-Scholey, G., and Scholey, J. M. (2013). Patronin mediates a switch from kinesin-13-dependent poleward flux to anaphase B spindle elongation. *The Journal of cell biology*, 203(1):35–46.

Waterman-Storer, C. M. and Salmon, E. D. (1997). Actomyosin-based retrograde flow of microtubules in the lamella of migrating epithelial cells influences microtubule dynamic instability and turnover and is associated with microtubule breakage and treadmilling. *The Journal of Cell Biology*, 139(2):417–434.

Weisenberg, R. C., Borisy, G. G., and Taylor, E. W. (1968). The colchicine-binding protein of mammalian brain and its relation to microtubules. *Biochemistry*, 7(12):4466–4479.

Weisenberg, R. C., Deery, W. J., and Dickinson, P. J. (1976). Tubulin-nucleotide interactions during the polymerization and depolymerization of microtubules. *Biochemistry*, 15(19):4248–4254.

Williams, B. D. and Waterston, R. H. (1994). Genes critical for muscle development and function in Caenorhabditis elegans identified through lethal mutations. *The Journal of Cell Biology*, 124(4):475–490.

Wissmann, A., Ingles, J., and Mains, P. E. (1999). The Caenorhabditis elegans mel-11 myosin phosphatase regulatory subunit affects tissue contraction in the somatic gonad and the embryonic epidermis and genetically interacts with the Rac signaling pathway. *Developmental biology*, 209(1):111–127.

Wissmann, A., McGhee, J. D., and Mains, P. E. (1997). Caenorhabditis elegans LET-502 is related to Rho-binding kinases and human myotonic dystrophy kinase and interacts genetically with a homolog of the regulatory subunit of smooth muscle myosin phosphatase to affect cell shape. *Genes & Development*, 11(4):409–422.

Woo, W.-M., Goncharov, A., Jin, Y., and Chisholm, A. D. (2004). Intermediate filaments are required for C. elegans epidermal elongation. *Developmental biology*, 267(1):216–229.

Xiang, X., Beckwith, S. M., and Morris, N. R. (1994). Cytoplasmic dynein is involved in nuclear migration in Aspergillus nidulans. *Proceedings of the National Academy of Sciences of the United States of America*, 91(6):2100–2104.

Yu, W., Qiang, L., Solowska, J., Karabay, A., Korulu, S., and Baas, P. W. (2008). The microtubule-severing proteins spastin and katanin participate differently in the formation of axonal branches. *Molecular biology of the cell*, 19(4):1485–1498.

Yuan, M., Shaw, P. J., Warn, R. M., and Lloyd, C. W. (1994). Dynamic reorientation of cortical microtubules, from transverse to longitudinal, in living plant cells. *Proceedings of the National Academy of Sciences of the United States of America*, 91(13):6050–6053.

Yvon, A. M. and Wadsworth, P. (1997). Non-centrosomal microtubule formation and measurement of minus end microtubule dynamics in A498 cells. *Journal of cell science*, 110(1):2391–2401.

Zanic, M., Widlund, P. O., Hyman, A. A., and Howard, J. (2013). Synergy between XMAP215 and EB1 increases microtubule growth rates to physiological levels. *Nature cell biology*, 15(6):688–693.

Zanin, E., Dumont, J., Gassmann, R., Cheeseman, I., Maddox, P., Bahmanyar, S., Carvalho, A., Niessen, S., Yates, J. R., Oegema, K., and Desai, A. (2011). Affinity purification of protein complexes in C. elegans. *Methods in cell biology*, 106:289–322.

Zhang, H., Landmann, F., Zahreddine, H., Rodriguez, D., Koch, M., and Labouesse, M. (2011). A tension-induced mechanotransduction pathway promotes epithelial morphogenesis. *Nature*, 471(7336):99–103.

Zheng, Y., Wong, M. L., Alberts, B., and Mitchison, T. (1995). Nucleation of microtubule assembly by a gamam-tubulin-containing ring complex. *Nature*, 378(6557):578–583.

Zhou, K., Rolls, M. M., Hall, D. H., Malone, C. J., and Hanna-Rose, W. (2009). A ZYG-12-dynein interaction at the nuclear envelope defines cytoskeletal architecture in the C. elegans gonad. *The Journal of Cell Biology*, 186(2):229–241.

Zimmerman, S., Tran, P., Daga, R. R., Niwa, O., and Chang, F. (2004a). Rsp1p, a J Domain Protein Required for Disassembly and Assembly of Microtubule Organizing Centers during the Fission Yeast Cell Cycle. *Developmental Cell*, 6(4):497–509.

Zimmerman, W., Sillibourne, J., Jack, R., and Doxsey, S. J. (2004b). Mitosis-specific anchoring of γ tubulin complexes by pericentrin controls spindle organization and mitotic entry. *Molecular biology of the cell*, 15(8):3642–3657.